A NOVEL FLOW SYSTEM UTILIZING AN EXPLANTED PORCINE HEART TO DETERMINE THE EFFICACY OF CAVAL VALVE IMPLANTATION

Karthic Anbalakan

B.Eng. (Hons), National University of Singapore

A THESIS SUBMITTED
FOR THE DEGREE OF MASTER OF ENGINEERING

DEPARTMENT OF BIOMEDICAL ENGINEERING
NATIONAL UNIVERSITY OF SINGAPORE

2016

DECLARATION

I hereby declare that the thesis is my original work and it has been written by me in its entirety. I have duly acknowledged all the sources of information which have been used in the thesis.

This thesis has also not been submitted for any degree in any university previously.

(Sign here)

Karthic Anbalakan

(insert date)

Thanks to

Dr Leo Hwa Liang, Dr Yap Choon Hwai, Tan Guo Dong Sean, Munirah Ismail and Chan Zhi Wei Kenneth for their encouragement, support and guidance.

Special thanks to

Mabel Nguyen Ngoc and Ong Chi Wei for making this possible.

Author: Karthic Anbalakan

Student ID: A0086381Y

Department of BioMedical Engineering, National University of Singapore

Session: 2015/2016

TABLE OF CONTENTS

ABSTRACT

Tricuspid regurgitation (TR) is a neglected entity and often occurs secondary to left sided heart disease. For that reason TR is treated concomitantly with left sided heart diseases, like mitral regurgitation, since a second surgery carries too great a risk. In addition, the treatment methods for TR, which include repair and replacement, are open surgical procedures which also carry a high operative mortality. Therefore, TR is often left untreated in patients where the risks outweighed the benefits.

To exacerbate this further, TR was found to be progressive and could potentially worsen in 2 grades within 5 years. This leads to several other comorbidities which include, right heart congestive failure, hepatosplenomegaly, peripheral edema and ascites. Severe tricuspid regurgitation (STR) is associated to a 50% mortality rate at 5 year follow up, which highlights the importance of a potentially new therapeutic procedure that could enable the treatment of STR.

To address this, a new percutaneous transcatheter technique known as Caval Valve Implantation (CAVI) was introduced. It involves the heterotopic implantation of caval valves in the vena cava in the hopes of alleviating the detrimental effects of STR.

In this study, the efficacy of this procedure is tested through the development of a novel flow system which utilizes an explanted porcine heart. The system is meant to be physiologically representative and TR is to be quantified through flow, pressure and echocardiographic parameters.

The results reported in this study allude to the efficacy of CAVI as a potential therapeutic technique; cardiac output was found to be 2.22 times greater after CAVI, the Jugular Venous Pressure (JVP) waveform was restored along with a significant decrease in the central venous pressure and the effective regurgitant orifice area was reduced by a factor of 2.42.

LIST OF TABLES

LIST OF FIGURES

LIST OF ABBREVIATIONS

TV	Tricuspid Valve
TR	Tricuspid Regurgitation
TA	Tricuspid Annulus
MR	Mitral Regurgitation
SVC	Superior Vena Cava
IVC	Inferior Vena Cava
STR	Severe Tricuspid Regurgitation
EROA	Effective Regurgitant Orifice Area
RV	Right Ventricle
LV	Left Ventricle
RT3DE	Real Time Three Dimensional Echocardiography
PISA	Proximal Iso-Velocity Surface Area
PISAr	Proximal Iso-Velocity Surface Area Radius
LHD	Left Heart Disease
MV	Mitral Valve
PAPs	Pulmonary Artery Pressures

ESC	European Society of Cardiology
AP-4CV	Apical Four Chamber View
sysTA	Systolic Dimension of the Tricuspid Annulus
CO	Cardiac Output
JVP	Jugular Venous Pressure
PIs	Performance Indexes
CAVI	Caval Valve Implantation
CMR	Cardiac Magnetic Resonance
PRF	Pulse Repetition Frequency

Chapter 1:

INTRODUCTION

Tricuspid regurgitation (TR) has long been an underestimated entity. TR being secondary to several diseases, like mitral regurgitation (MR), has been assumed to improve when the primary disease is treated. This misconception has resulted in TR being neglected and often overlooked in both clinical and surgical settings.[23]

Recently, various studies have demonstrated that in addition to TR being secondary to several diseases, it is also progressive, and it may in turn potentially cause the onset of other diseases.[23, 25, 60] TR is also an important determinant in the long term prognosis as well as the survival rates of patients. [23, 52, 60]

The current methods for treatment are either to repair the tricuspid valve (TV) or to replace it. However, these methods are only performed if the benefits outweigh the risks, noting also that TV repair or replacement is often done concomitantly with surgeries intended to treat the left sided heart disease (LHD), which only serves to exacerbate the risks of the surgery.[23, 48] Resulting in many patients left untreated.

This elucidates the benefits of a transcatheter approach in treating TR, since a percutaneous valve replacement would carry much less risk when compared to an open surgical approach. However, no such transcatheter approach is yet clinically available.[23, 48] Moreover, experiments aimed at testing the feasibility of this approach, have yet to address the problem of fixation of the prosthetic valve in the highly dynamic and plastic tricuspid annulus (TA).[5, 7]

1.1 Hypothesis

In this study, it is hypothesized that utilizing an explanted porcine heart within an in-vitro flow system would allow for a greater physiological representation; which could potentially serve as an intermediary step before animal studies and preclinical trials to determine the efficacy of Caval Valve Implantation (CAVI).

1.2 Aim of Study

Therefore, the objective in this study is to analyze the effects of percutaneous heterotopic implantation of heart valves in the vena cava – CAVI.

1) The physiological representation of the in-vitro flow system would be assessed on its ability to reproduce results from previous studies involving CAVI. These studies have demonstrated that the heterotopic implantation of valves in the superior vena cava (SVC) and inferior vena cava (IVC) would alleviate the detrimental effects of STR; by reducing the central venous pressure and increasing the cardiac output.

2) Following which, the efficacy of CAVI will be further explored with this in-vitro flow system, through quantitative flow, pressure and echocardiographic assessments. Additionally, the reduction in regurgitation is to be quantified through the determination of the effective regurgitant orifice area; thereby expanding on the previous study.

1.3 Thesis Organization

The following chapter will provide background into the tricuspid valve and the disease, specifically focusing on the pathophysiology, geometric changes and progression of the disease; in a bid to highlight the severity of the disease as well as the need for new therapeutic interventions. It will also address the current treatment methods and the limitations of these methods so as to demonstrate how Caval Valve Implantation could potentially address these shortcomings.

In chapter 3 the discussion will address how the in-vitro experimental set up was established. It will outline how the porcine heart was processed and prepared for the experimentation. The specifications of the caval valve will also be highlighted along with the equipment used – to extract the relevant results.

Chapter 4 will encompass the results for the volumetric flow profile, pressure waveforms and the echocardiographic investigations. Subsequently, chapter 5 will review the results and address the inherent limitations of the study.

Chapter 6 will explore potential improvements and future works pertaining to this study. It will also highlight why some previously explored ideas are not feasible in this in-vitro investigation.

Chapter 2:

BACKGROUND

2.1 Tricuspid Valve

The TV has a complex morphology that involves 3 leaflets in a non-planar, elliptical saddle shaped annulus. It comprises of four primary elements: the valve leaflets, the valve annulus, papillary muscles and the chordae tendineae. The largest of the leaflets is the anterior leaflet, followed by the posterior leaflet and the septal leaflet. The posterior leaflet extends from the posterior margin of the TA, from the septum to the infero-lateral wall, while the septal leaflet arises directly from the TA above the inter-ventricular septum, as seen in figure 2-1.[23, 80, 85]

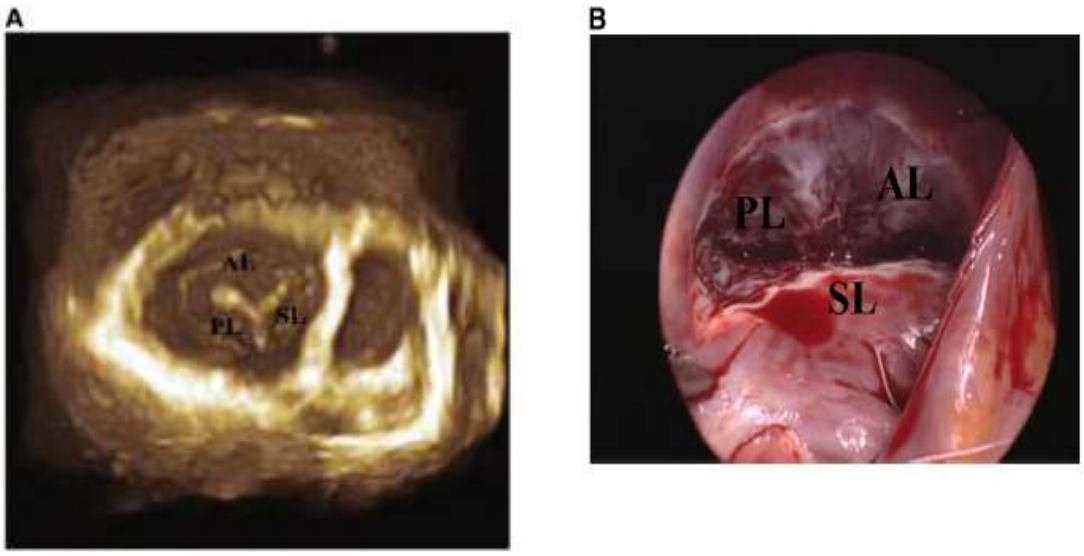

Figure 2-1: 3 dimensional transthoracic echocardiography (a) and intraoperative echocardiographic view (b) of the tricuspid valve. SL = septal leaflet, AL = anterior leaflet, and PL posterior leaflet. Image from [23]

The TA is non-planar, with the highest point at the antero-septal portion and the lowest at the postero-septal portion, as seen in figure 2-2. The area of the TA ranges from 3.9cm^2 to 5.6cm^2, with an approximate percentage change of 30% during the cardiac cycle.[34] Although

identifiable, the ‘fibrous’ TA along the parietal attachment of the leaflets is difficult to define. In addition, the TA is encircled by the right coronary artery which often lies in close contiguity.[78]

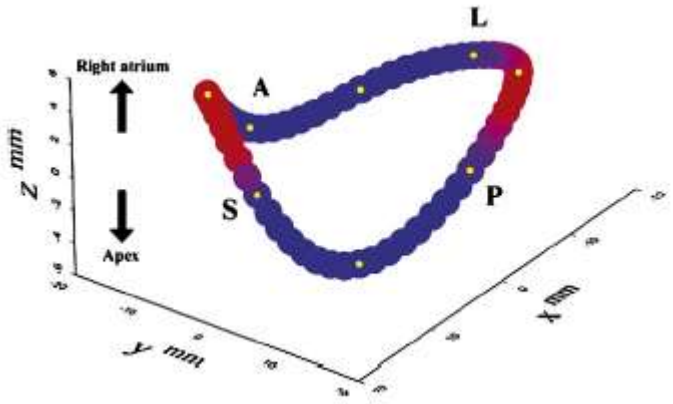

Figure 2-2: The tricuspid annulus has a complex geometry with the postero-septal portion being the lowest and the antero-septal portion being the highest. Image from [80]

The chordae tendineae stem from each of the papillary muscles (usually three) and branch into several insertion areas on the leaflets. The marginal chordae refer to those which attach onto the tip of the free leaflet edge. These usually tend to be thinner than the basal chordae which attach onto the basal region close to the annulus. The marginal chordae help to keep the leaflets stationary while the basal chordae take on a more supportive role. The papillary muscles prevent the TV from prolapsing into the atrium during ventricular systole.[85]

These four components work in tandem to ensure proper functioning of the TV. In a healthy heart, no flow is observed through the TV during systole, while a biphasic flow profile is observed during diastole. The first peak is called the ‘E wave’ and occurs due to ventricular relaxation. During isovolumic relaxation, the right atrial pressure exceeds that of the right ventricle causing the TV to open and the blood to flow through – passive ventricular filling. Following ventricular relaxation the atrium contracts, accelerating the blood into the ventricle

once more and accounting for the second peak called the 'A wave'.[85] The flow profile of the mitral valve is similar to the TV; however the flow velocities of the TV are smaller due to the larger valve orifice.[62, 71, 86]

2.2 Tricuspid Regurgitation

TR is a complex valvular lesion in which the TV leaks – resulting in the retrograde flow of blood into the atrium, instead of the pulmonary artery, during systole. TR is characterized as either organic or functional. Organic TR is a result of structural abnormalities of the TV, which may either be acquired or congenital in nature. Organic TR accounts for 8-10% of all STR.

Functional TR on the other hand, is due to the deformation of the TV apparatus – dilation and geometric changes to the TA – and accounts for more than 90% of all STR.[4, 58] TR can result from a number of comorbidities such as right ventricle (RV) enlargement due to left-sided heart valve disease, LV or RV dysfunction, pulmonic stenosis or regurgitation, pulmonary hypertension, and dilated cardiomyopathy.[23] Table 1 illustrates a more comprehensive list of the aetiology for both functional and organic (structurally abnormal) TR.

In this study, no distinction is made between organic and functional TR (with the exception 2.2.1) since CAVI is a heterotopic implantation and does not address the native leaflets directly.

2.2.1 Pathophysiology of Functional Tricuspid Regurgitation

RV enlargement and dysfunction may be primary or secondary to LHD; which may lead to pulmonary hypertension. Functional TR that arises due to this ventricular deformation is often a result of valve tenting. In contrast, functional TR that occurs in the absence of pulmonary hypertension is predominantly due to annular enlargement, as seen in figure 2-3. This explains

why despite the association between pulmonary hypertension and TR, not all patients with pulmonary hypertension develop significant TR.[4, 57, 81] This was further exemplified in an echocardiographic study, where mild TR was observed in 65% of patients with pulmonary artery pressures (PAPs) between 50 and 65 mmHg and only 46% in patients with PAPs above 70mmHg [23, 58]. This indicates that other factors such as atrial fibrillation, pacemaker leads, and RV remodeling are also significant determinants in the onset of TR.[4, 23, 81]

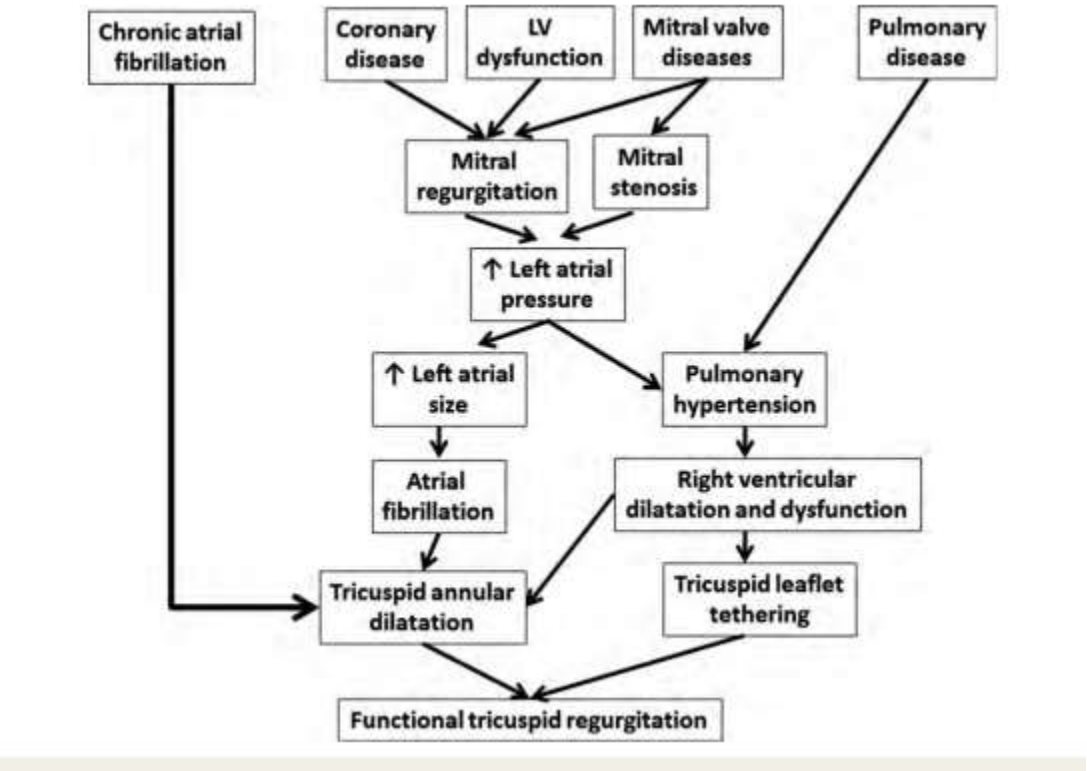

Figure 2-3: Pathophysiology of Functional Tricuspid Regurgitation. Image from [4]

TR results in chronic RV volume overload, which causes right sided congestive heart failure. Patients usually demonstrate signs of liver congestion, peripheral edema and ascites. When TR occurs secondary to LV dysfunction, patients may present with dyspnea, orthopnea and

paroxysmal nocturnal dyspnea.[23, 48] Therefore the natural history of TR is poor, even more so with severe tricuspid regurgitation (STR) where the patients are highly symptomatic.

In a study, Nath et al. [60] looked into the prognostic significance of TR in a group of 5223 patients undergoing echocardiography. This revealed, at a 4 year follow up, that more that 70% of patients with mild or less TR were still alive while less than 50% of patients with STR survived. Moreover, despite pulmonary hypertension being one of the primary indicators for surgical intervention [8], TR is associated with higher mortality regardless of the presence of pulmonary hypertension.[60] Similarly, while LV dysfunction is a well-established risk factor for early mortality in patients, STR is associated with worse survival regardless of LV ejection fraction; in both healthy individuals and in patients undergoing left heart valve surgery.[10, 60]

Table 2-1: Aetiology of Tricuspid Regurgitation. Image from [4]

- Functional (morphological normal leaflets with annular dilatation)
  - Left heart diseases (LV dysfunction or valve diseases) resulting in pulmonary hypertension
  - Primary pulmonary hypertension
  - Secondary pulmonary hypertension (e.g. chronic lung disease, pulmonary thrombo-embolism, left-to-right shunt)
  - Right ventricular dysfunction from any cause (e.g. myocardial diseases, ischaemic heart disease)
  - Atrial fibrillation
  - Cardiac tumours (particularly right atrial myxomas)
- Structural abnormality of the tricuspid valve
  - Rheumatic
  - Prolapse
  - Congenital
    - Ebstein anomaly
    - Tricuspid valve dysplasia
    - Tricuspid valve hypoplasia
    - Tricuspid valve cleft
    - Double orifice tricuspid valve
    - Unguarded tricuspid valve orifice
  - Endocarditis
  - Endomyocardial fibrosis
  - Carcinoid disease
  - Traumatic (blunt chest injury, laceration)
  - Iatrogenic
    - Pace-maker/defibrillator lead interference
    - Right ventricular biopsy
    - Drugs (e.g. exposureto fenfluramine-phentermine, or methysergide)
    - Radiation

2.2.1.1 Geometric Changes of Functional Tricuspid Regurgitation

The introduction of real time three-dimensional echocardiography (RT3DE) has provided new insights into the pathophysiological mechanisms of TR.[3, 73] In TR, the leaflets of the TV fail to coapt due to the geometrical changes in the TA. The annulus tends to dilate in the anterior and posterior directions, causing it to assume a more circular shape as shown in figure 2-4. This is evidenced by the decrease in the medial-lateral/antero-posterior ratio from 1.32 ± 0.09 to 1.11 ± 0.09, $p < 0.001$.[80] Moreover, both the maximum and minimum TA areas were significantly larger in patients with TR.[34] Annular dilation may become irreversible over time. This is observed in patients with chronic thromboembolic pulmonary hypertension, in whom there were no significant changes in the annular dimensions after successful thromboendarterectomy.[69]

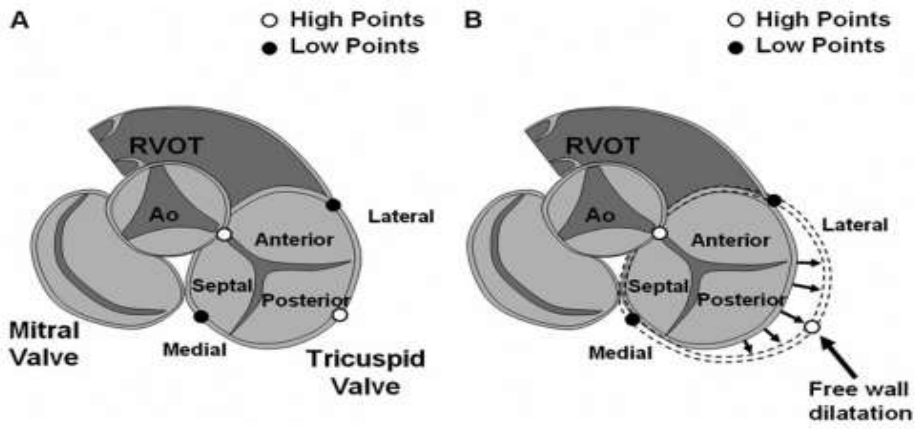

Figure 2-4: A) The TV of a healthy heart viewed from the atrium. B) Dilation of TV in a heart with TR, viewed from the atrium. Image from [80]

Furthermore, through RT3DE studies , TR has been shown to cause a decrease in the TA contraction, especially in severe cases, from 29.6% to 14.6%.[34] In addition, annular flattening has also been observed in TR which results in the loss of the biomodal shape of the TA.[80]

2.2.1.2 Progression of Functional Tricuspid Regurgitation

The development of functional TR is often illustrated in three stages, as seen in figure 2-5.[26, 78] The first stage is described as the initial annular dilation of the TV. At this stage, TR is still to be considered mild or moderate. In the stage that follows, the annular dilation increases thereby preventing the normal coaption of the tricuspid leaflets; causing the TR to become significant and RV to begin dilating. The final stage reflects the RV dilation and its subsequent dysfunction. This results in papillary muscle displacement and increased tethering forces leading to further leaflet malcoaption.[23, 33] As the dilation of the RV increases, so does the RV diastolic pressure, which in turn causes further leftward septal displacement and LV compression. This would result in an increase in the LV diastolic pressure and pulmonary artery pressure which ultimately begets more TR.[33]

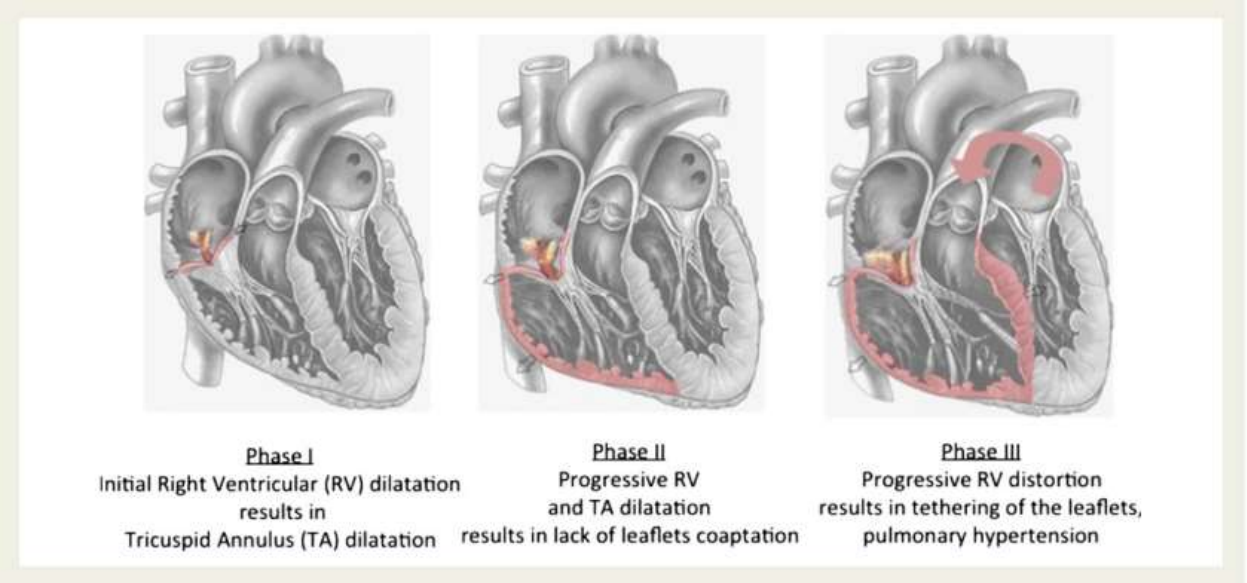

Figure 2-5: Progression of TR in 3 phases. Image from [78]

Similarly, other studies have also indicated that TR is a progressive disease and leaving it untreated, at the time of MV surgery, begets more regurgitation at follow-up.[19, 23, 25] In one such

study, the progression of moderate to mild TR in 174 patients, undergoing isolated MV surgery, was analyzed. At a follow-up of 8.2 years TR had evolved into moderate to severe in 16% of the patients.[53] Through multivariate analysis, uncorrected moderate TR, atrial fibrillation, and huge left atrium, were identified as statistically significant factors in predicting progression of TR after surgery.[23] De Bonis et al. further demonstrated, that if the presence of moderate to severe TR at follow-up was considered together with the worsening of the TR by 2 grades, at a mean follow-up of 1.8 years, the likelihood of progression of TR reaches 18.6%.[19]

Furthermore, Dreyfus et al. [25] showed that TR worsened by more than 2 grades in 48% of patients undergoing isolated mitral valve (MV) repair and only 2 % in patients who were undergoing both MV and TV repair. Patients with moderate to severe TR, undergoing isolated MV annuloplasty, have been observed to have a significantly lower 5 year survival rate and possibility of being alive in the NYHA classes 1-2 as compared to those with mild or less TR.[24]

These studies suggest that TR may not resolve after treating the primary LHD. Desai R.R et al. [21] concluded that in patients with both mitral valve disease and STR, isolated mitral valve repair improved TR and RV function; however this was incomplete and only temporary. However, reported that concomitant TV repair, conversely, eliminated STR and improved RV function, significantly reducing the likelihood of worsening TR and improved the survival rate.[21]

The progressive nature of TR could potentially be due to further RV enlargement and dysfunction, resulting in increased annular dilation and papillary muscles displacement with leaflet tethering.[19] This vicious cycle could elucidate the prognostic significance of untreated moderate to severe TR. Since persistent or worsening TR is associated with elevated pulmonary

artery pressures; which induces congestive hepatopathy with liver fibrosis, atrophy of hepatocytes, and potentially cirrhosis.[23, 48]

Ultimately, the natural history of TR is unfavorable; considering it is a progressive disease and one that is often left untreated due to the high risk associated with the treatment procedures. Aside from it being secondary to LHD, persistent and worsening TR leads to increased pulmonary pressures and reduced cardiac output, which in turn leads to other comorbidities.[48]

2.3 Current Treatment Methods

Surgical repair and replacement are the only corrective therapies, currently available to treat TR, and they are associated with a high operative mortality of 22%.[1, 48] Although transcatheter valve therapy is clinically available for the treatment of aortic, mitral and pulmonary valve diseases no similar method is yet available for TR.[16, 27, 41, 83] Since a transcatheter technique is associated with fewer complications and lower mortality, it would be a great asset in treating TR. To this end, new therapeutic methods are being developed.[78]

However, it is important to analyze the current surgical methods and their respective shortcomings to ensure the success of the newer therapies. Another concern is *when* should the repair/replacement of the TV be performed, in relation to surgery intended for the LHD?

2.3.1 Surgical Decision Making

TV repair is often done concomitantly with left sided heart surgery and the decision to perform repair is often left to the surgeon's discretion.[10, 32] Pre-operative echocardiographic parameters and intraoperative findings have recently been gaining increasing importance for decision making. Aside from the severity of TR other factors such as annular diameter, have to also be

considered. This was observed in a study by Dreyfus et al. [25], where TV annuloplasty was only performed when the TA diameter was greater than twice the normal size (>70mm), regardless of severity of regurgitation. According to the ESC (European Society of Cardiology) guidelines, TV annuloplasty should only be considered in patients with moderate TR with a dilated annulus (>40mm from the AP-4CV) undergoing left sided valve surgery.[58]

In a study by Chopra et al. [15], patients with non-severe TR were found with maximal diastolic tricuspid annular diameter that was within the normal range; implying that TR may occur without annular dilation and is not the sole criteria for surgical decision making.

The decision to perform TV annuloplasty could also be based on the preoperative echocardiographic systolic dimensions of the tricuspid annulus (sysTA). To this end, Calafiore et al. [11] determined the normal reference values by studying twenty healthy volunteers; median sysTA of 24mm and maximum sysTA of 28mm were established accordingly. TV annuloplasty was recommended for patients with moderate to severe TR and in those with mild TR if sysTA was found to be greater than 24mm. Patients with sysTA less than 24mm who underwent MV surgery without TV repair showed no worsening of TR at midterm. Whereas untreated patients with sysTA greater than 24mm developed moderate to severe TR at follow-up; still maintaining a normal sysTA.[11]

Therefore, while the decision to treat the TV during left sided heart surgery is still ultimately left to the discretion of the surgeon, there are several preoperative echocardiographic parameters that could potentially aid in the discerning the appropriate course of treatment.

2.3.2 Tricuspid Valve Repair

TV repair is usually prophylactic and is directed at reshaping the annulus through either suture or ring annuloplasty.[23] This surgery is often directed at patients with lesser degrees of preoperative TR but have a dilated annulus. Suture annuloplasty methods aim to reduce the annular size by using a continuous suture to purse string the annulus.[79] Some of the more common suture annuloplasty techniques are the Kay repair, De Vega Repair and the Clover Techniques.[79]

The Kay repair method involves the bicuspidization of the TV. This is accomplished by plicating the annulus along the posterior leaflet thereby obliterating the leaflet when the sutures are tied. This creates a bicuspid valve, as seen in figure 2-6B.[40] The De Vega annuloplasty on the other hand, involves plicating both the anterior and posterior leaflets; using a single suture around the TA while avoiding the atrioventricular node (figure 2-6C).[22] Annuloplasty can also be achieved by suturing a support device like a pericardial strip or a semi-rigid/rigid prosthetic ring to permanently fix the annulus in the systolic position (figure 2-6D).[12, 35] Another example of ring annuloplasty is the Edwards MC3 annuloplasty system [31], as seen in figure 2-7. The clover technique on the other hand, is often used to address the severe tethering and involves the suturing of the free edges of the tricuspid leaflets as seen in figure 2-6E.[18]

In general, the survival curves based on the surgical techniques did not differ significantly across the studies.[43, 55] However, several studies have demonstrated that ring annuloplasty is more durable than suture annuloplasty, and that it is associated with better event free survival in both a 10 year[63] and 15 year[77] follow up.

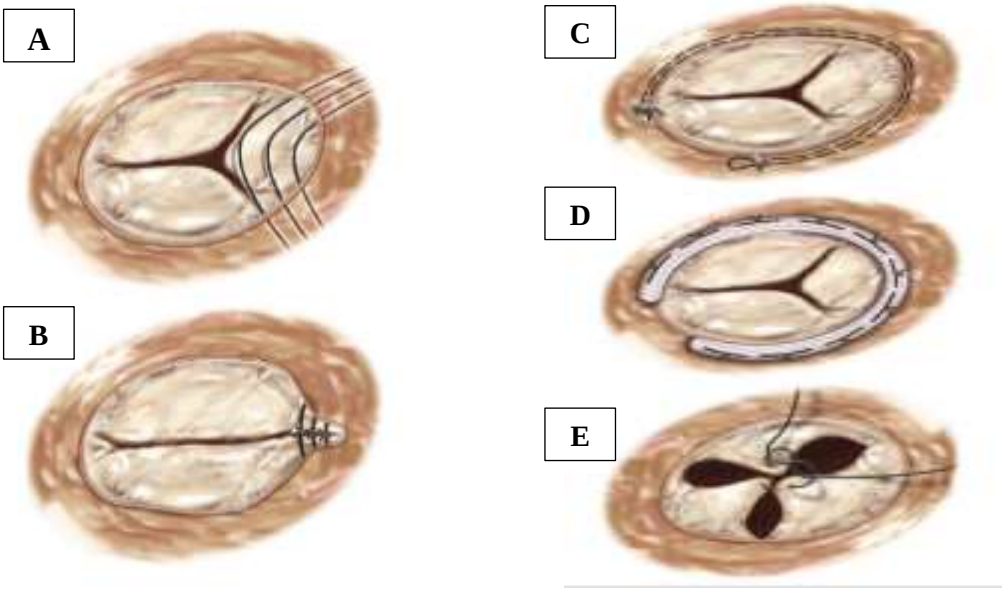

Figure 2-6: Kay Technique (Left): A: Tricuspid Valve bicuspidization is done by plicating the posterior the annulus along the posterior leaflet. B: The sutures are tied obliterating the posterior leaflet, converting the tricuspid valve into a bicuspid valve. Other techniques (Right): C: De Vega repair where a single suture is placed around the tricuspid annulus, avoiding the area of the atrioventricular node. The suture is tied completing the annuloplasty. D: Tricuspid annuloplasty with a rigid prosthetic ring. E: The clover technique: The middle parts of the free edges of the tricuspid annulus are sutured together. Image from [79].

Figure 2-7: Intraoperative view of the Edwards MC3 annuloplasty system. Image from [31]

TV repair however, is still associated with a recurrence rate of 2.5% to 5.5% at a 1 year follow up.[10, 11, 54] In addition, a study by Navia et al. [61] reported that flexible bands and pericardial strips used in ring annuloplasty are associated with a higher TR recurrence at a 5 year follow up. Similarly, McCarthy et al. [55] found that, at a 8 year follow up, rate of repair failure is 17%, 33% and 37% for ring annuloplasty, DeVega technique and pericardial strip annuloplasty, respectively.

Therefore, TV repair continues to be a high risk procedure which is associated with recurrent TR. This further emphasizes the importance for a new potential percutaneous transcatheter technique to treat TR.

2.3.3 Tricuspid Valve Replacement

Patients who exhibit RV dysfunction with RV dilation would not benefit from TV repair – suture or ring annuloplasty – and would present a high risk of failure. These patients instead undergo curative surgery because TV annuloplasty will result in increased tethering of the anterior and posterior leaflets, since the annulus is displaced toward the septum.[23] Therefore, in patients with RV dilation, surgical tethering will result in postoperative TR worsening rather than better leaflet coaption. Hence, the only option clinically available would then be TV replacement, which involves the insertion of a prosthetic valve within the annulus.[23, 48]

The ideal heart valve for TV replacement should: produce minimal pressure drop, have small regurgitant volumes, minimize turbulence, reduce high shear stress and not create stagnation or flow separation within the flow field.[85] Pressure drop across the valve determines the effectiveness of the prosthetic valve. A large drop in pressure would in turn demand a greater systolic pressure in order to drive circulation. Therefore, an effective prosthetic heart valve

would not cause too great a flow resistance and thereby minimize the pressure drop.[72] Similarly, heart valves that induce regions of flow separations and stagnations are less than ideal. They are associated with increased likelihood of thrombus formation, tissue overgrowth and possible calcification.[85] In addition, prosthetic valve designs may also cause high flow velocities, shear stress and excessive turbulence which could result in hemolysis of blood cells and lead to thromboembolic complications.[36, 70] Therefore, factors such as flow velocities, flow fields and flow shear stress should be considered when optimizing a design for prosthetic valves. Moreover, since these factors are used to determine the ideal hemodynamic flow, they are also relevant in determining the effectiveness of various tricuspid valve repair strategies.

2.3.3.1 Mechanical Heart Valves

There were three main designs for the mechanical heart valves: Caged ball design, tilting disc and the bileaflet valve.[85] While the caged ball heart valve had good reliability it was associated with very poor hemodynamic performance and as of 2007 the Starr-Edwards caged ball, the only caged ball design available, was discontinued by Edward Lifesciences.[14] Therefore only the tilting disc and bileaflet mechanical heart valves will be discussed.

Tilting Disc Valve

The Medtronic-Hall mechanical valve is the most commonly used tilting disc valve. As suggested by the name, it has a major and a minor orifice which is divided by a tilting disc. Two nearly symmetrical flow profiles are observed from both the major and minor orifice.[85] However, the major orifice jet is larger and has a slightly higher velocity as compared to its minor counterpart, as seen in figure 2-8A.[84] A region of retrograde flow occurs adjacent to the wall in the minor orifice at peak systole, 2mm from the wall, shown in figure 2-8. Moreover, a

region of flow separation forms next to the wall of the major orifice and flow stagnation is also observed immediately downstream from the minor orifice during the acceleration and deceleration phases.[85] The tilting disc mechanical valve has a slightly smaller regurgitant volume when compared to the bileaflet mechanical heart valve. Moreover, the performance indexes (PIs), which is the ratio of the effective orifice area to the valve sewing area, ranges between 0.40 to 0.65.[85] The PIs help to reflect how well a prosthetic valve design optimizes its total mounting area.

Furthermore, leakage jets are often observed in the gap between the disc and the housing. While these jets might be useful in 'washing' of the gap region, they are also associated with high velocities and turbulent shear stresses. The maximum turbulent shear stress associated with the tilting disc design is between 1200 to 1500 dyne/cm^2, as seen in figure 2-8. Even though this is below the hemolysis threshold of 4000 dyne/cm^2 for the Reynolds's shear stress, the damage mechanism for hemolysis is a complicated process which is affected by the resident time of the blood cells in the affected environment.[70, 85] Therefore, this could potentially still lead to thromboembolic complications.

Bileaflet Mechanical Valve

St. Jude Medical bileaflet mechanical valve is the most commonly used bileaflet valve and has two semicircular leaflets that divide the effective orifice area into 3 regions: 2 lateral regions and a central orifice. Most of the forward flow occurs in the 2 lateral orifices, as seen in figure 2-9.[84] Flow separation occurs adjacent to the flow channel wall where the flow separates from the orifice ring. Small regions of retrograde flow also occur next to the hinge mechanism of the valve. The maximum turbulent shear stress levels are found to be 3000 dyne/cm^2, which is

within the threshold range. Although the bileaflet mechanical valve has a slightly larger regurgitant volume as compared to the tilting disc valve, it has a lower pressure drop comparatively.[85]

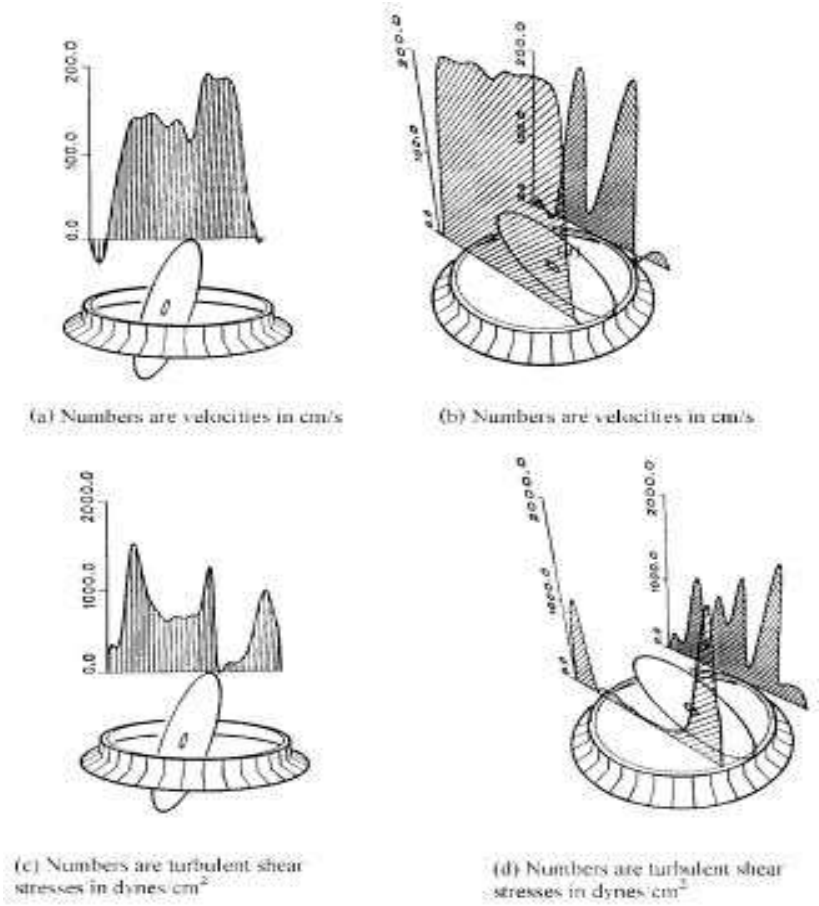

Figure 2-8: Medtronic-Hall tilting disc valve flow profile (A) Velocity profile 15 mm downstream on the centerline across the major and minor orifices (major orifice to theright) at peak systole; (B) velocity profiles 13 mm downstream in the major and minor orifices at peak systole; (C) turbulent shearstress profile 15 mm downstream on the centerline across the major and minor orifices at peak systole; (D) turbulent shear stress profiles 13 mm downstream in the major and minor orifices at peak systole. Image from [84]

Mechanical heart valve designs are optimized through laser doppler velocimetry and computational fluid dynamics. These studies are often aimed at improving the hinge design as well as at minimizing the likelihood of cavitation.[28, 29, 50] Although CAVI involves a stented

valve (caval valve) that is to be deployed percutaneously, advances in the mechanical valve design might lend some insight into optimizing valve design specific to the process of CAVI.

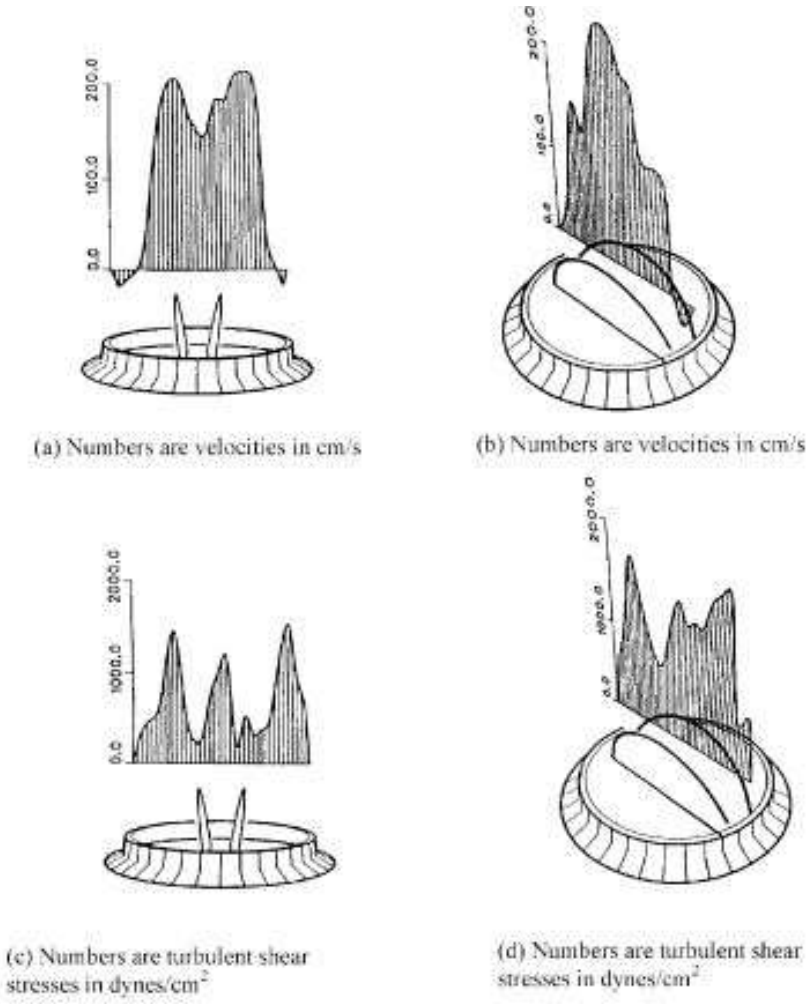

Figure 2-9: Flow profile of St. Jude Medical bileaflet valve (A) Velocity profile 13 mm downstream on the centerline during peak systole; (B) velocity profile 13 mm downstream across the central orifice during peak systole; (C) turbulent shear stress profile 13 mm downstream of the centerline orifice during peak systole; (D) turbulent shear stress profile 13 mm downstream across the central orifice during peak systole. Image from [84]

2.3.3.2 Bioprosthetic Valves

Bioprosthetic valves are usually composed of three biological leaflets made from porcine aortic valve leaflets or bovine pericardium. These tissues are extracted and treated with a gluteraldehyde solution before being sutured onto a metal or polymeric stent.[85] Unlike their mechanical valve counterparts, bioprosthetic valves or tissue valves do not have any occlusion in their central orifice. These valves tend to produce high velocity jet-like forward flow profiles. The flow profiles also tend to be more evenly distributed as compared to the mechanical valves, as seen in figure 2-10. Although no flow separation is usually observed during the systolic period, flow stagnation occurs throughout systole at the annular region between the outflow surface and the flow chamber wall.[84]

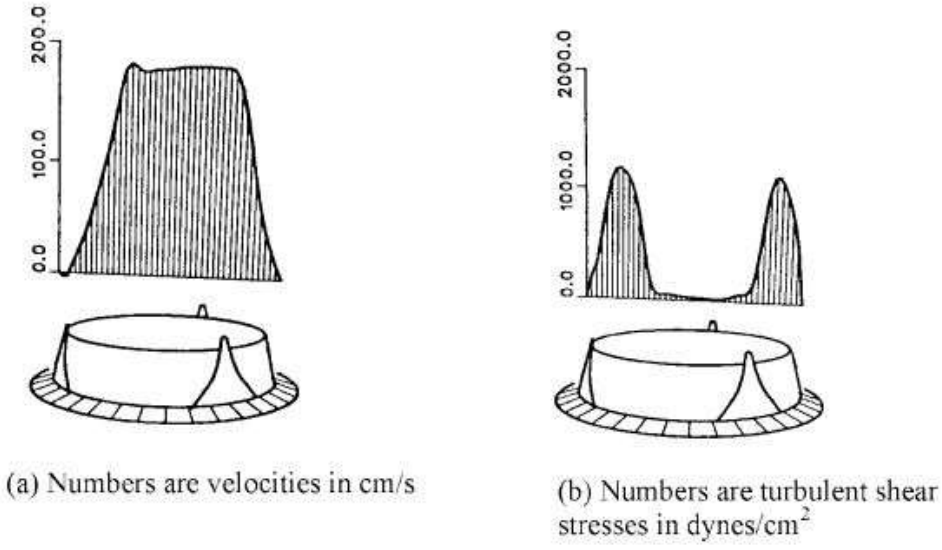

Figure 2-10: Flow profile of Carpentier-Edwards pericardial valve (A) Velocity profile 17 mm downstream on the centerline during peak systole; (B) turbulent shear stress profile 17 mm downstream on the centerline during peak systole

Generally, all tissue valves are mildly stenotic compared to the natural valve. This is due to the stent restriction to leaflet opening, construction of leaflets, stiffness of treated tissue and man-made commissures. As a result, the PIs for bioprosthetic valves usually range between 0.3 to 0.4.[84]

In bioprosthetic valves, high turbulent shear stresses usually occur at the edge of the central jet and range between 1000 to 4500 dynes/cm^2.[84] The flow profile of the Carpentier-Edwards pericardial valve at peak systole is shown in figure 2-10.[85]

Mechanical or Bioprosthetic heart valve

The choice between a mechanical valve and a bioprosthetic valve has been controversial topic. Some researchers have reported that mechanical valves are superior to bioprosthetic valves,[39, 67] while others have reported that bioprosthetic valves are in fact superior.[13, 17, 56] However, in a more recent study, [30] the long term survival of patients was found to be similar regardless of prosthesis used. This was further supported by a meta-analysis of 11 studies conducted by Rizzoli et al.[68] which reported no significant difference in early mortality, late survival or reoperations.

2.3.3.3 Limitation of Tricuspid Replacement

Although mechanical and bioprosthetic heart valves have their respective advantages and disadvantages, the inherent problems associated with heart valves have yet to be eliminated.[85] Thromboembolic complications, anticoagulant-related hemorrhage, tissue overgrowth and paravalvular leakage owing to healing effects are some of these problems.

In fact, TV replacement is associated with high mortality rate and is only considered as a therapeutic option when TV repair is no longer viable. [64] In a study by Ratnatunga et al.[66] the early mortality rate associated with tricuspid valve replacement was reported to be 22%. The long term survival of TV replacement was found to be 50% at a 10 year follow up in a subsequent study.[30]

Ultimately, the current treatment modalities of TV repair and replacement still carry too great an operative risk. This is reflected by the significant number of people with STR who are left untreated due to said risks.[78] Therefore, a transcatheter approach would be ideal for treating patients with TR since it is associated with significantly lower mortality and complications. However, while transcatheter therapy has bolstered the therapeutic options for patients with aortic, mitral and pulmonary valve diseases no trans-catheter technique is currently available to treat TR.[48]

Hence in this study, the efficacy of the heterotopic implantation of valves in the vena cava is investigated as a potential therapeutic solution to TR.

2.4 Novel Therapeutic Concepts

Even though percutaneous procedures are an ideal treatment modality for TR, there are still none that are clinically available. However, several novel percutaneous transcatheter based techniques are under evaluation and in preliminary clinical research trials.[78] Despite the limitation in data and the preliminary nature of the current investigations, these ideas are worth exploring.

2.4.1 Mitralign System

The Mitralign device (Mitralign, Inc. Tewsbury, USA) was initially intended to treat mitral regurgitation but has recently been used to treat TR as well.[75] Mitralign system treats TR by performing a transcatheter bicuspidization of the TV through the transvenous jugular approach.[74] A steerable catheter is inserted into the RV across the TV and positioned with echocardiographic imaging. Following which, a radiofrequency wire is advanced from the base of the leaflet and within the annulus and guided toward the right atrium; where it is positioned adjacent to the anteroposterior commissure. After the wire is through the annulus, a pledget delivery catheter is moved over the wire from the right atrium across the TV to the RV. This process is repeated opposite to the anteroposterior commissure. A dedicated plication lock device is then used to bring the pledgeted sutures together, plicating the annulus and converting it into a bicuspid valve, as seen in figure 2-11.[78]

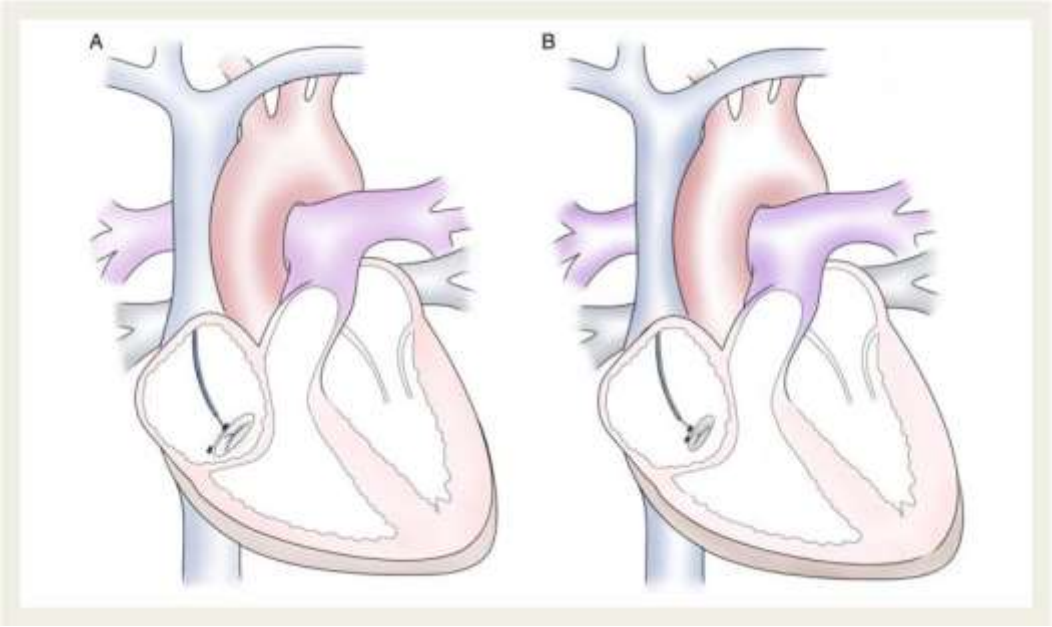

Figure 2-11: The Mitralign concept. (A)The pledget delivery catheter is advanced over the wire from the right atrium. (B) Plication of the annulus and reduction of its dimension. Image from [78]

2.4.2 TriCinch Device

The TriCinch (4Tech Cardio, Galway, Ireland) device, as the name suggests, aims to reduce anteroseptal annular dimension and TR by cinching the TA. To achieve this, a steerable catheter is introduced in the femoral vein and advanced to the TA.[45] The catheter is placed between the anteroposterior commissure and the mid anterior annulus. Following this, a corkscrew is implanted adjacent to the mid part of the anterior TA, as seen in figure 2-12. Right coronary artery angiography is performed to ensure no coronary damage. After the corkscrew is secured, the delivery system is extracted. A self-expandable Nitinol stent is then introduced over the wire and coupled to the implant. Tension is used to reshape the TV by cinching the annulus to increase leaflet coaption. Finally, a stent is deployed in the IVC to maintain the tension, as shown in figure 2-12.[78]

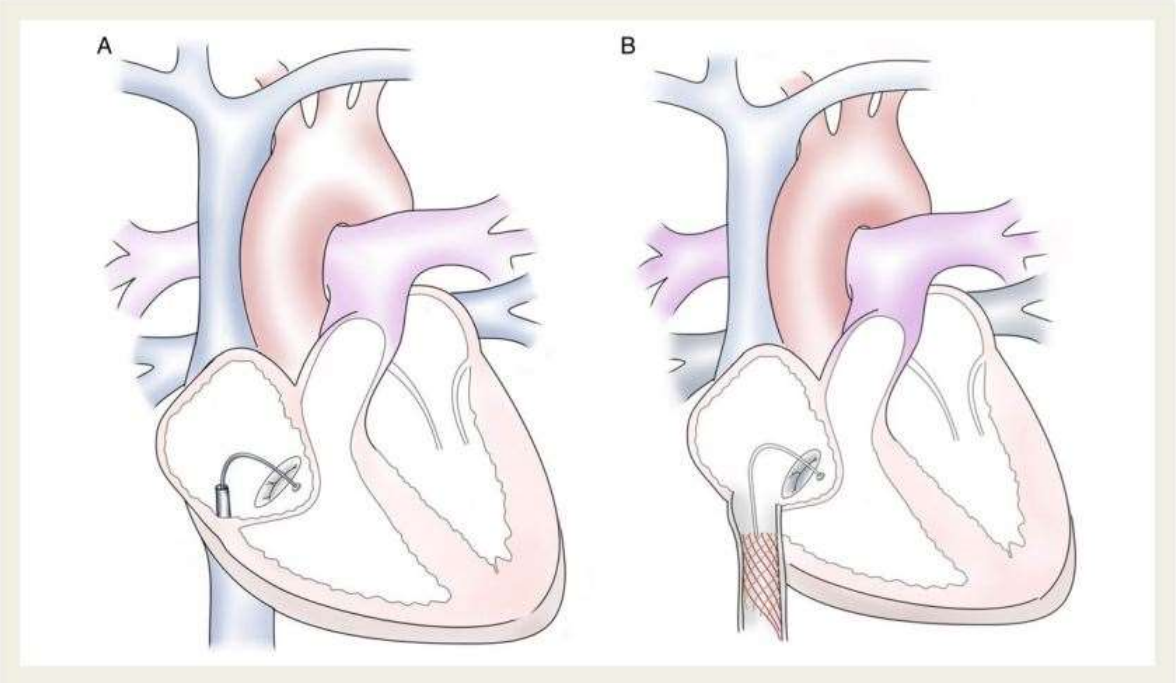

Figure 2-12: The TriCinch concept. (A) The corkscrew is implanted in the target zone. (B) The system is tensioned to reshape the annulus. The stent is deployed in the IVC to maintain the tension. Image from [78]

2.5 Caval Valve Implantation

2.5.1 Motivation for study

Like the Mitralign system and the TriCinich device, Caval Valve Implantation (CAVI) is also a new transcatheter therapeutic technique with limited data to support any evidence of its clinical efficacy. Therefore, this study aims to develop a physiologically representative in-vitro flow system that would be able to lend some insight into the efficacy of CAVI.

This study focuses on CAVI over the Mitralign system and the TriCinich device due to their inherent limitations. The Mitralign system, while a promising technique which is based on a proven surgical background,[35, 61, 78] is technically challenging and requires an advanced 3D echocardiography imaging system.[78] The TriCinch device similarly, requires advanced imaging and is only applicable to patients who do not present with significant RV dysfunction.[78] CAVI on the other hand, is technically very easy to perform and is not restricted by the same complexities as the other techniques.[78] Therefore, it would be feasible for an in-vitro flow system, utilizing an explanted porcine heart, to be sufficiently physiologically representative to study CAVI. Furthermore, 2D color doppler echocardiography would be able to quantify the efficacy of CAVI within the proposed flow system.

2.5.2 The concept of Caval Valve Implantation

Boudjemline et al. [9] experimented with a catheter based approach to treat TR by implanting a double disc nitinol stent with a semilunar valve into the tricuspid annulus. While the technicality of the process was proven to be feasible, several shortcomings such as the lack of fixation of the self-expanding valve in the highly plastic TA were not resolved.[9, 48] This was further supported

by a subsequent study, in which the authors claimed that percutaneous valve replacement for TR, by means of orthotopic valve implantation, proves to be extremely challenging with the currently available materials and methods.[5, 48, 49] However, CAVI leverages on the benefits of a transcatheter approach whilst avoiding the problem of fixation faced by an orthotopic implantation; thereby alluding to its potential to be a new therapeutic procedure capable of treating STR, especially in patients considered to be inoperable.

CAVI is described as the heterotopic implantation of caval valves into the SVC and IVC to reduce venous regurgitation and congestion; caused by STR,[48, 49, 78] as seen in figure 2-13. For this reason it is said to 'ventricularize' the right atrium. By reducing the hepatic, abdominal and peripheral venous congestion, CAVI aims to ameliorate right heart failure.[78] Since the implantation is at a low pressure site, patients would probably require lifelong anticoagulants. However, since TR is often found secondary to LHD, most patients would already be subjected to the same anticoagulant therapy.[78]

The feasibility of this procedure was demonstrated by Lauten et al. [49] through experimental study in animals. In said study, a significant reduction of the v-wave and y-descent was reported in the IVC along with an increase in the cardiac output (CO); alleviating the deleterious effects of TR.[48, 49] Moreover, strong fixation of the valves to the venous wall by fibrous covering implied that device migration would be highly improbable. CAVI however, does not address the damaged native tricuspid valve, therefore atrial overloading and increased atrial pressures within the right atrium were observed in this study, as seen in table 2. A subsequent study was done in a patient who was deemed inoperable due to previous open-heart surgeries and significant comorbidities. CAVI was performed as a 'compassionate treatment' and a decrease in IVC

regurgitation and symptoms pertaining to IVC congestion were observed, further bolstering the feasibility of this CAVI.[48]

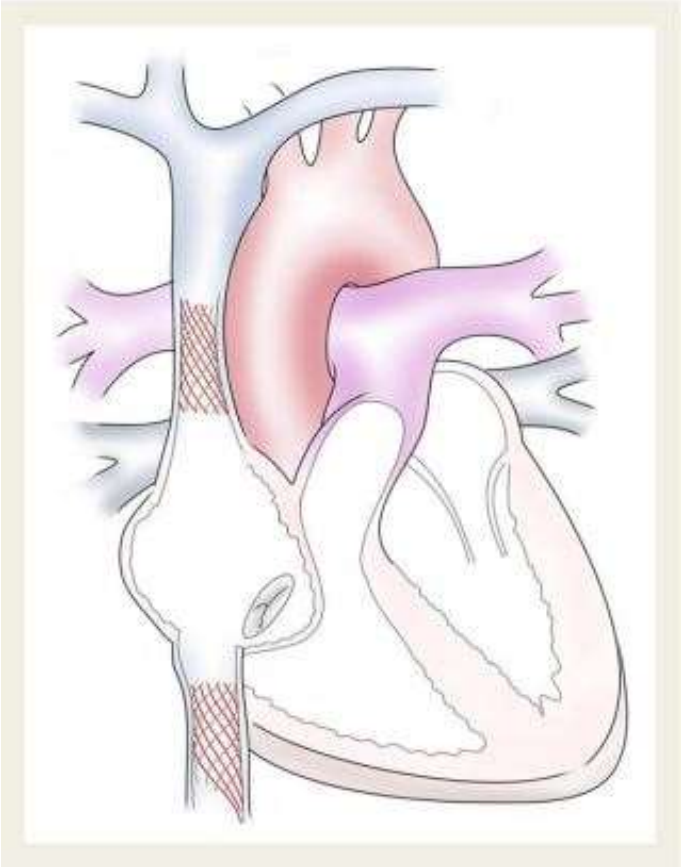

Figure 2-13: CAVI; Heterotopic valve implantation at the SVC and IVC. Image from [78]

Table 2-2: Hemodynamic parameters during implantation and follow up in chronic group as retrieved from [49]

	Baseline	with TR	After device implantation	End of chronic observation
HR (b.p.m.)	87.7 (5.51)	105.0 (12.15)	97.3 (13.63)	83.4 (17.10)
RA-V (mmHg)	9.8 (0.95)	14.8 (2.06)	15.3 (1.71)	15.0 (1.41)
RA-Y (mmHg)	6.5 (0.58)	8.8 (0.50)	7.9 (2.51)	9.5 (1.29)
RAP mean (mmHg)	8.0 (0.81)	12.9 (1.14)	11.7 (2.08)	11.5 (1.29)
IVC-V (mmHg)	10.0 (0.82)	14.9 (1.71)	12.7 (1.15)	12.0 (0.82)
IVC-Y (mmHg)	7.3 (0.95)	9.5 (0.58)	10.8 (1.53)	10.0 (1.41)
IVCP mean (mmHg)	9.0 (0.81)	12.25 (0.96)	11.7 (1.15)	10.8 (1.50)
CO (L/min)	5.8 (0.96)	4.1 (1.10)	5.4 (0.67)	5.2 (1.00)

Presented are mean (± SD) of four sheep. HR, heart rate; RA-V, right atrial v-wave; RA-Y, right atrial y-descent; RAP mean, right atrial mean pressure; IVC-V, inferior vena cava v-wave; IVC-Y, inferior vena cava y-descent; IVCP mean, inferior vena cava mean pressure; CO, cardiac output.

However, Lauten et al. [49] addresses some limitations within the animal study, stating that in human patients, TR is usually observed secondary to annular dilation. Therefore, substantially higher venous pressures are expected, compared to those reported in the animal study. Furthermore, the echocardiographic parameters were not reported and the alleviation of TR was based solely on the reduction of the central venous pressure and the increment of the CO.[49]

In order to address these limitations and expand on this work, a novel flow system utilizing an explanted porcine heart was established in this study; in an attempt to determine the efficacy of CAVI through more quantitative means.

Additionally, in the study that involved the 'compassionate treatment' of TR in a patient through CAVI, only one valve was implanted in the IVC due to several technical complications.[48] However, there are no data available as to whether a single valve approach or a dual valve approach would be more ideal.[46, 47] Similarly, there are also no data available on the ideal CAVI prosthesis.[45, 47] Here, 'ideal' refers to both the design of the prosthesis as well as the location of the heterotopic implantation (IVC, SVC or both) to optimize the alleviation of the detrimental effects of TR; in regards to CO, JVP waveform and EROA.

The primary aim of this study is to establish a physiologically representative in-vitro flow system capable of reproducing the results from previous studies involving CAVI; through quantitative flow, pressure and echocardiographic assessments. However, in doing so this experimental set-up could then be used to determine the ideal treatment (single vs dual valve) as well as an optimal CAVI prosthesis. Although this is not to be done in this preliminary study, it aids in reflecting the potential value of this study.

2.6 Imaging and Flow Systems

Cardiac Catheterization

In the past, the presence and severity of TR was confirmed through cardiac catheterization. The diagnosis of TR proved to be very challenging since selective angiography into the RV would often distort the TV and the position of the catheter was difficult to maintain within the RV. However, with the introduction of 2D echocardiography and Doppler echocardiography, cardiac catheterization is rarely used for diagnosis or quantification of TR.[4]

Chest X-Ray

Chest radiograph is limited in its usefulness. While it may be able to distinguish prominent right heart borders associated with cardiomegaly, there are no specific findings which suggest a diagnosis of TR.[4]

Cardiac Magnetic Resonance

Cardiac Magnetic Resonance (CMR) is used when the echocardiographic investigations are limited due to suboptimal acoustic window, the findings are equivocal or if 3-dimensional echocardiography is unavailable. Unlike echocardiography, CMR is not restricted by acoustic windows and is able to image the entire heart in any plane to provide accurate myocardial definition.[4] CMR is currently, the best imaging modality to study RV morphology and function, and has also been used to assess the anatomy of the TA.[2]

Echocardiography

2D echocardiography together with spectral and color flow Doppler is currently the most commonly used means of detecting and quantifying TR.[44] TR is often identified through

echocardiography by TA dilation (> 40mm) and tethering of leaflets (tenting distance >8mm).[4] Color flow Doppler is very responsive to regurgitation and therefore provides reliable semi-quantitative assessment of its severity.[44] Parasternal, apical or subcostal acoustic windows, as shown in figure 2-14, are often the primary planes through which TR is studied.

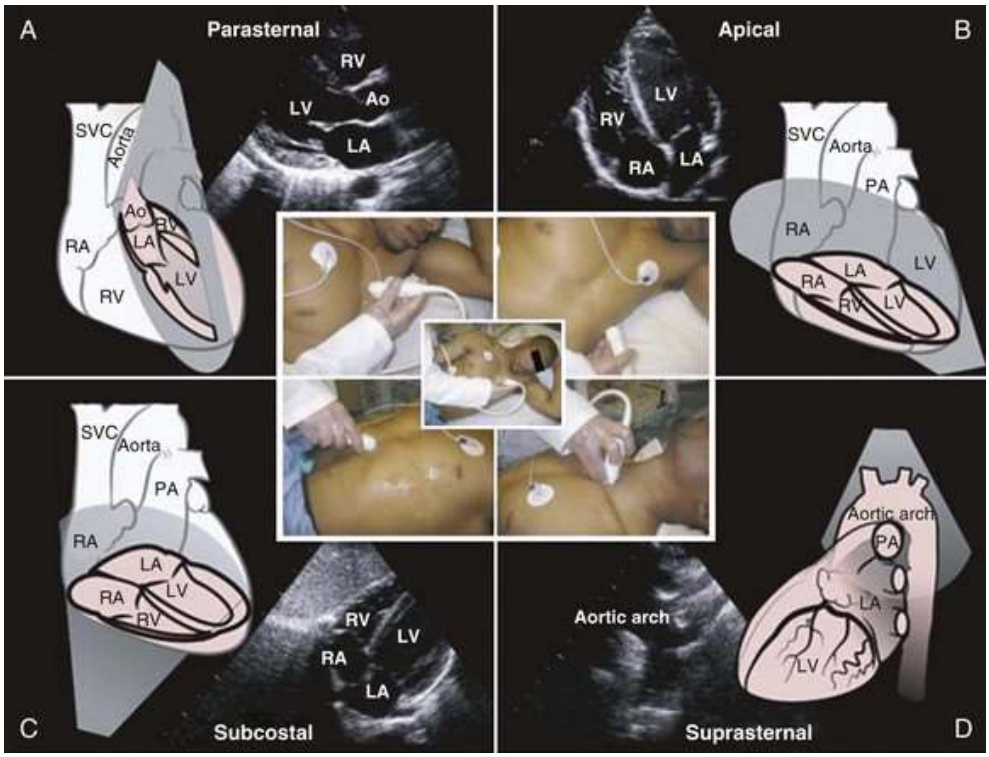

Figure 2-14: Schematic representation of several planes of imaging commonly used in echocardiography studies. (A) 4-chamber parasternal view (B) 4-chamber apical view (C) 4-chamber subcostal view and (D) suprasternal view. Image from http://clinicalgate.com/echocardiography-5

A more quantitative measurement of TR severity is provided by the vena contracta and the proximal isovelocity surface area (PISA). The vena contracta reflects the cross-sectional area of the narrowest point in a stream (regurgitant orifice) where the maximum flow velocity is observed.[4] An inherent limitation of measuring the vena contracta is that the regurgitant orifice has a complex geometry and not an idealized 'pinhole'. Despite this, the vena contracta is used to

determine the regurgitant orifice area and the PISA radius which is widely accepted as a good quantitative indicator of the severity of regurgitation.[4, 82]

In-vitro flow systems

In-vitro flow systems are a cheaper alternative to animal models and are able to produce reliable data for a wide range of studies. To this end in-vitro flow systems have been used to study chemical mechanisms, micro-fluidic flow patterns, versatility of imaging systems and even the effectiveness and feasibility of medical devices.

In a study by Jesty et al.[38], platelet activation was explored through circulatory experiments that were performed in a flow loop. In another study, the utility of quantitative 3D-power Doppler angiography was analyzed using an in-vitro flow system.[65] These studies help to illustrate the convenience afforded by flow systems, which can potentially be used as a platform for analysis. Moreover, Tan et al.[76] further demonstrated the utility of flow systems by analyzing the left ventricular flow patterns, within such a system, to determine the efficacy of a bioprosthesis. Therefore, in-vitro experimental flow set-ups are an efficient means to streamline design and optimize flow studies.

Similarly, in this study, an in-vitro flow system, utilizing an explanted porcine heart is established to determine the efficacy of a potential therapeutic transcather technique; CAVI.

Chapter 3:

METHODOLOGY

3.1 In-Vitro Flow Loop Set-Up

A flow system, utilizing an explanted porcine heart, was established to emulate the venous flow within the right side of the heart. Physiologically, after distributing oxygen, blood is collected as deoxygenated blood into the SVC and IVC and directed into the right atrium of the heart. The blood is then pumped into the right ventricle, through the tricuspid valve, during atrial systole. Following which, the blood is pumped, during ventricular systole, through the pulmonary valve, to the pulmonary artery which carries the deoxygenated blood to the pulmonary vasculature (lungs) to be oxygenated. The newly oxygenated blood is then collected through the pulmonary vein and directed into the left atrium. During atrial systole, the oxygenated blood is pumped into the left ventricle through the mitral valve. The blood is then pumped through aortic valve into the aorta and to the rest of the body during ventricular systole. The flow system was designed to mimic this flow, however choosing to focus only on the right side of the heart in an effort to simplify the set up.

A reservoir was used to direct the flow of the working solution (meant to represent deoxygenated blood) into the vena cava and ultimately into the right atrium of the explanted porcine heart. The hydrostatic pressure within the reservoir, due to the elevation of the working solution, ensured its continuous flow into the explanted heart. A pulsatile pump *(SuperPump AR series, ViVitro Labs Inc., Victoria, BC, Canada)* was used to generate the ventricular pressure to simulate ventricular systole of the cardiac cycle. The pump was attached to the ventricle of the explanted heart through a silicone tube. A schematic representation of the flow system is shown in figure 3-1A.

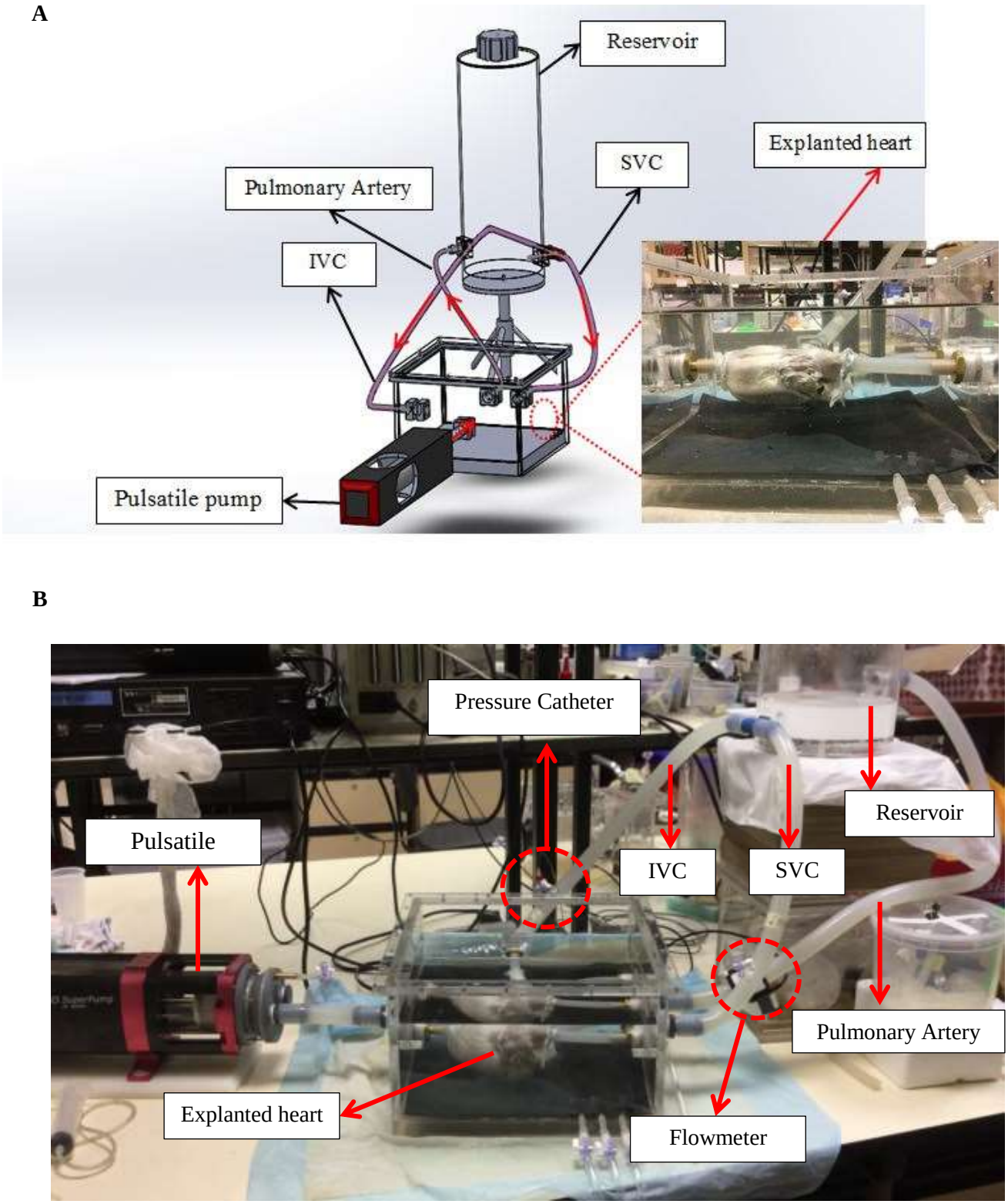

Figure 3-1: In-Vitro Flow system. (A) Schematic representation of the flow system. (B) Lateral view of the flow system with the explanted porcine heart.

A pressure catheter system *(Mikro-Tip SPR-340S, Millar Instruments Inc., Houston, TX, USA)* was used to capture the pressure within the vena cava by inserting the catheter through the silicone tubes; which were meant to represent the SVC and IVC. The cardiac output was measured in the silicone tube representing the pulmonary artery of the explanted porcine heart using a flowmeter *(ME16PXL, Transonic Systems Inc., Ithaca, NY, USA)*. The pulmonary artery (silicone tube) emptied out into the reservoir during the simulated cardiac cycle, thereby forming a closed flow circuit. The length of the tubes and height of the reservoir were optimized to produce pressures within the desired range. Figure 3-1B shows the lateral view of the entire flow system with the explanted porcine heart.

3.2 Explanted Porcine Heart

The explanted porcine heart was sourced from a local abattoir *(Primary Industries Pte Ltd, Singapore)* and had to be processed before being used as part of the flow system. The excess fat and tissue were removed carefully and the heart was subsequently flushed with water to remove any blood clots that might obstruct the flow and impede valve functionality. The SVC and IVC were subsequently cut, making sure to leave sufficient tissue for the placement of the caval valves, for CAVI. In order to incorporate the explanted heart into the flow system 4 silicone tubes had to be 'fixed' to the heart at the SVC, IVC, pulmonary artery and right ventricle. To accomplish this, 4 silicone rings were made using a 2 part silicone mix (*EasyMold Silicone Rubber)*. The silicone rubber was added to a complementary cavity to be molded into the desired shape and thickness, as seen in figure 3-2. The silicone rings were then adhered to the silicone tubes using a neutral silicon sealant.

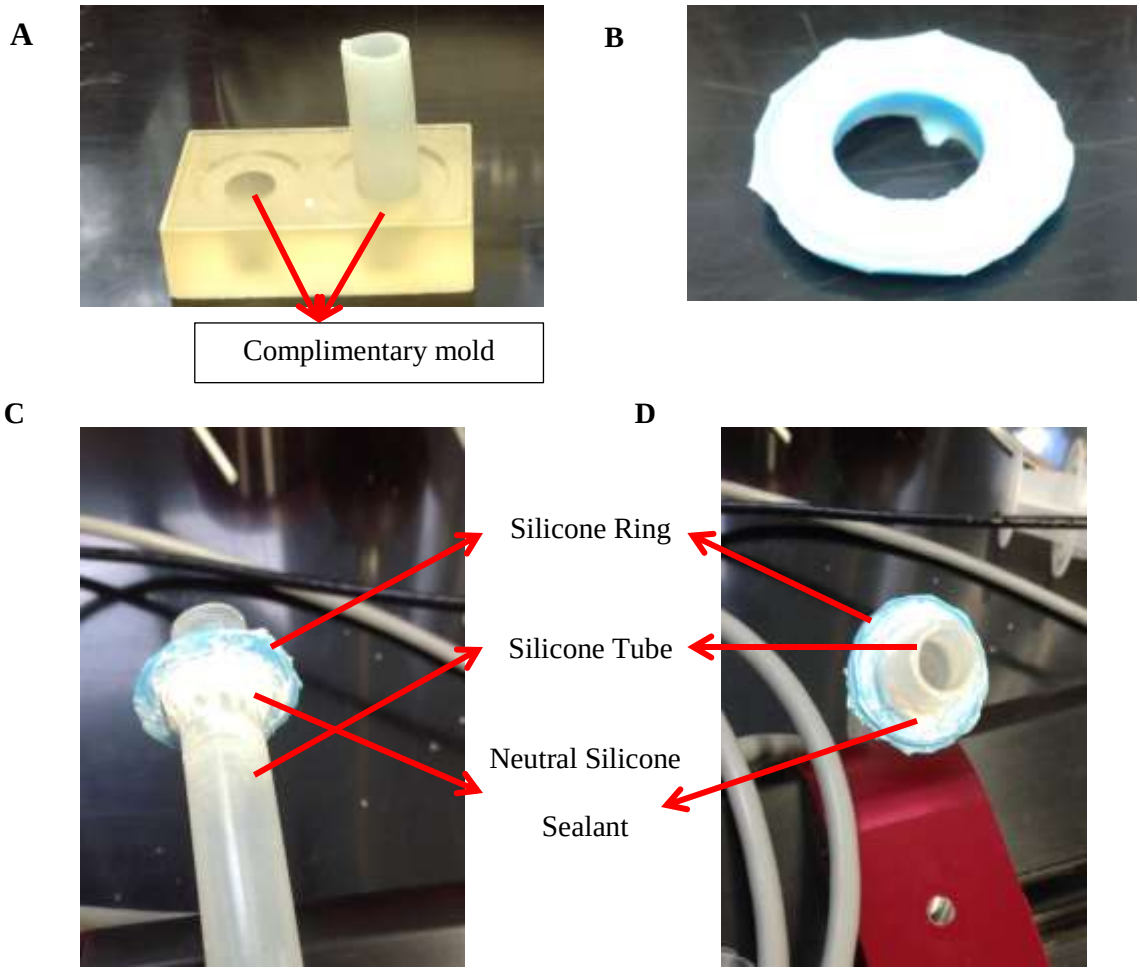

Figure 3-2: (A) Complementary cavity used to create the (B) silicone rings which are adhered to silicone tubing through silicone sealant as shown in (C) and (D)

A scalpel was then used to make a small insertion into the right ventricle. This was done as close to the apex as possible so as to not damage the tricuspid valve, chordae tendineae or the papillary muscles. The silicone tubes with the rings were then attached to the heart at the SVC, IVC, pulmonary artery and the ventricle by placing several interrupted sutures between the rings and the heart tissue, as shown in figure 3-3.

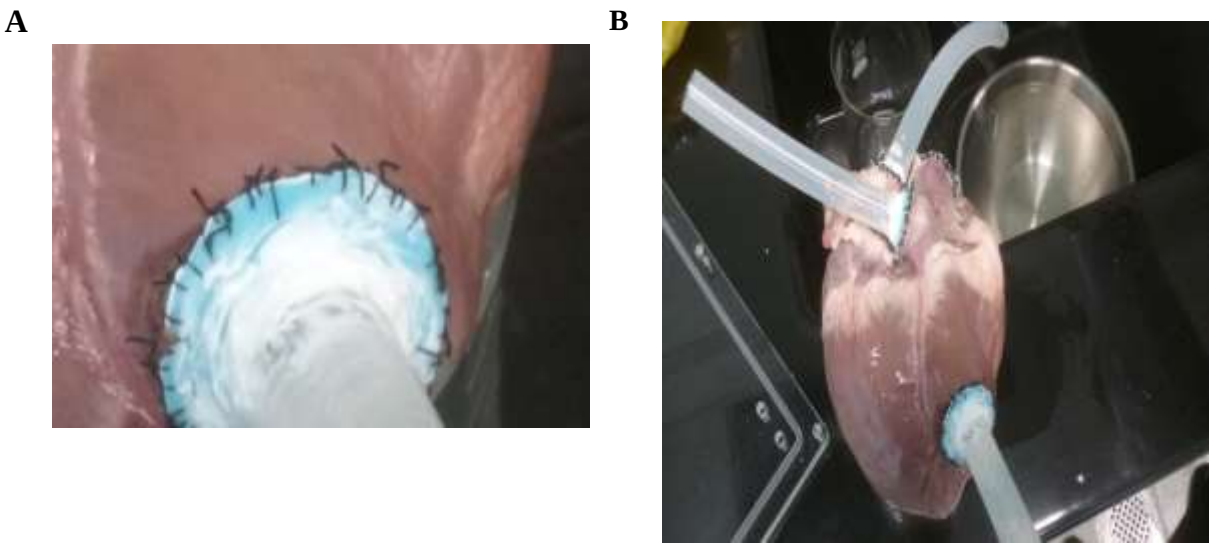

Figure 3-3: (A) The interrupted sutures used to attach the silicone tubes to the heart. (B) All four tubes are attached to the heart

Pericardium was then glued over the silicone ring and attached to the tissue to provide an additional seal for the tubing. This pericardial seal was done to ensure that no leaks would occur at the attachments to the heart. Subsequently, the heart was incorporated into the flow system and the data for the regurgitant model were extracted accordingly.

After CAVI, where the caval valves were incorporated into SVC and IVC of the explanted heart, the data for the ventricularized state (referring to post CAVI) was extracted. Figure 3-4 shows the ventricularized model incorporated within the flow system. Echocardiography was used to ensure the heterotopic implantation of the valves were performed at the right location and deployed successfully, as seen in figure 3-5.

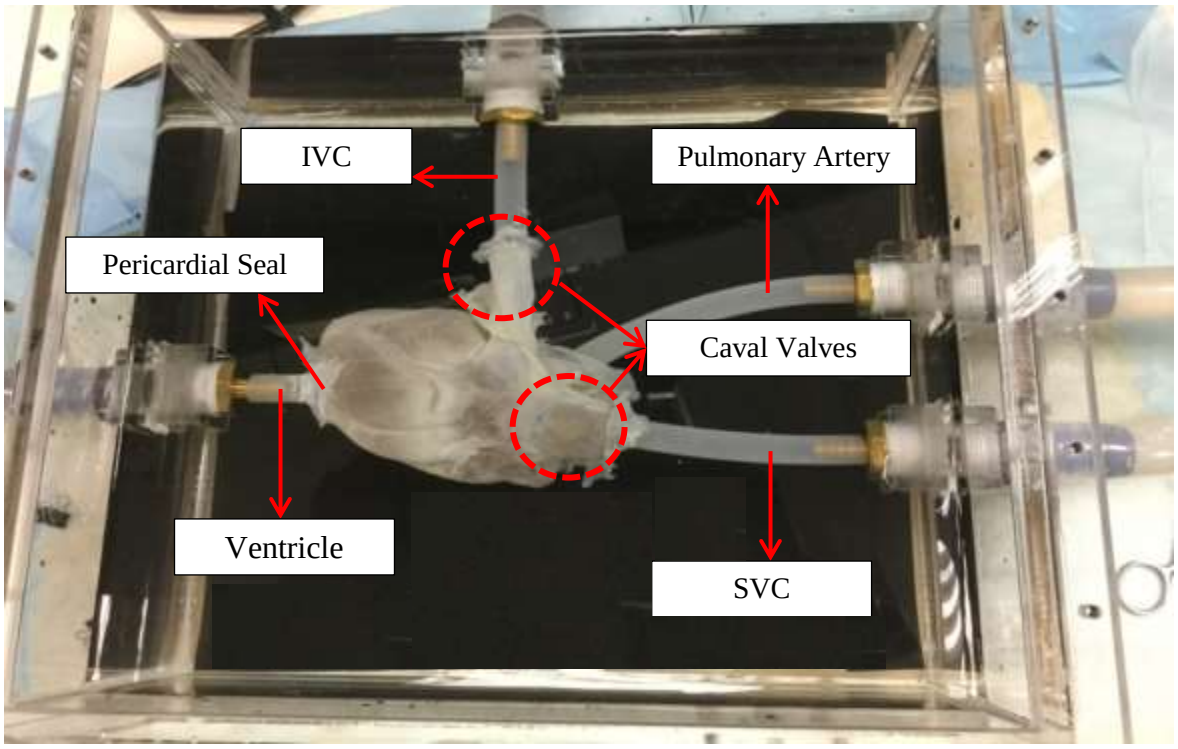

Figure 3-4: The incorporation of the processed porcine heart into flow system

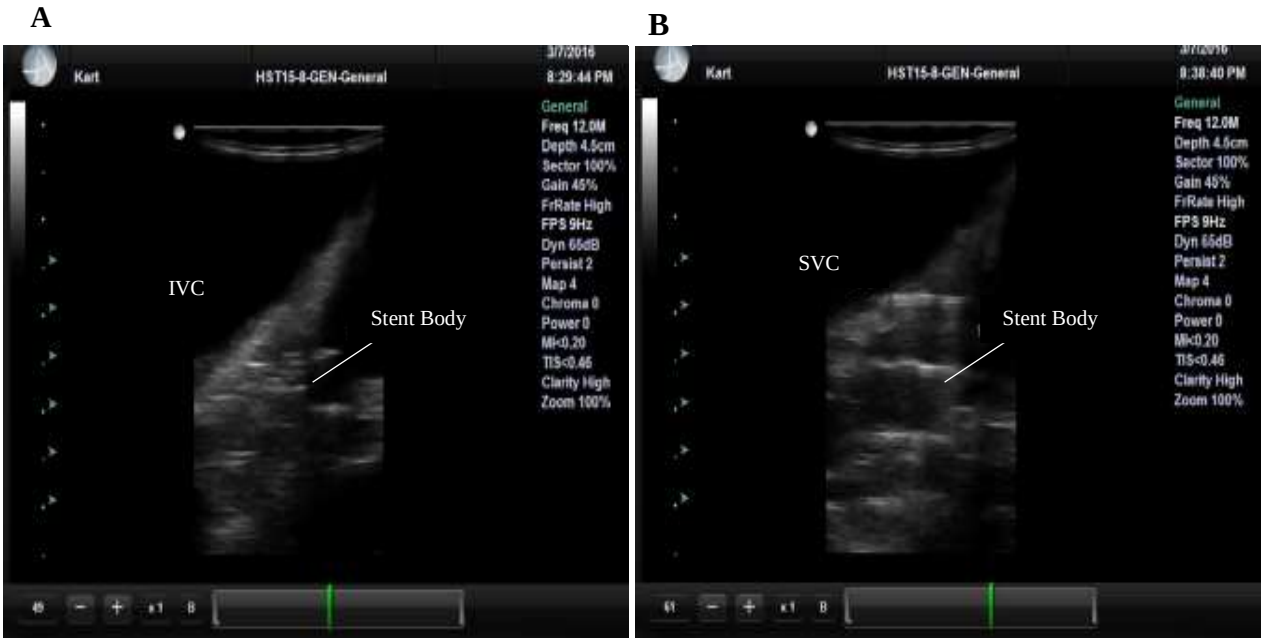

Figure 3-5: Echocardiographic images showing the successful deployment of the caval valves IVC (A) and SVC (B)

3.3 Caval Valves

The stented valves used in this study comprised of two balloon-expandable, tubular, stainless steel (304 stainless steel), and bare stents with diamond-shaped cells. The diamond closed-cell configuration ensured the crimpability of the stent. The stents were designed and fabricated (diameter 25mm, length 20mm, Meko, Hannover, Germany) (see figure 3-6) with nine crowns to accommodate a tri-leaflet valve. The strut was made to be 0.4mm thick to allow for the valves to be crimped to a smaller diameter and therefore a smaller catheter size for the deployment of the stented valves. Because the cyclic mechanical stresses acting on the valves in the Vena Cava are significantly smaller than those in the left side of the heart, the strut diameter can be reduced without compromising on the structural integrity.

The bare metal stent was dip-coated with five coating layers of polyurethane (ChronoFlex AR, AdvanSource Biomaterials Corporation, Wilmington, MA, USA). This was done to minimize the paravalvular leakage of the transcatheter valve. The porcine pericardium was harvested from a local abattoir (Primary Industries Pte Ltd, Singapore) and placed between two leaflet molds: of a tri-leaflet configuration of the human aortic leaflets. The pericardium was then treated for 20 minutes in buffered glutaraldehyde (0.5%) at room temperature and pressure. The porcine pericardial leaflets were sutured onto the coated stent using 5-0 Mersilk sutures (Ethicon Endo-Surgery, San Francisco, CA, USA). Single point attached commissure method was used to create the transcatheter valve.

The optimization of the caval valve design was based on the study done by Ismail et al.[37]

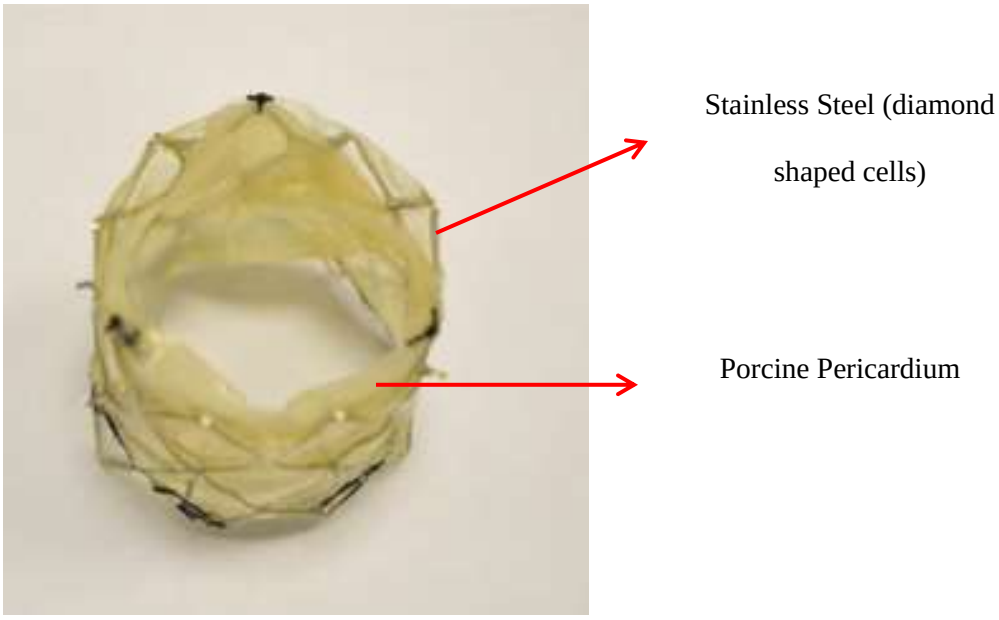

Figure 3-6: The transcatheter caval valves for the heterotopic implantation into the SVC and IVC. Image from[37]

3.4 Echocardiographic Investigation

The echocardiographic investigations were done using an ultrasonic transducer *(SonixTablet, BK Ultrasound Inc., Peabody, Massachusetts, USA)* capable of pulse-wave color Doppler echocardiography. Since the explanted porcine heart was submerged in water no coupling medium had to be used. Echocardiography was used to view the malcoaption of the tricuspid valve leaflets, which was a result of the dilated annulus of the regurgitant heart model. The regurgitant model was established by subjecting the heart to elevated pulmonary pressures, with the reservoir, within the flow system. Echocardiographic imaging was also used to ensure the proper implantation of the caval valves in the SVC and IVC for the Ventricularized heart model, as shown in figure 3-5.

Corn starch was used as the seeding particles for echocardiographic analysis, to determine the PISAr and for Doppler investigations. This was done for both the regurgitant and ventricularized heart models.

3.4.1 Posterior 2-Chamber Long Axis Apical View

Generally, TR is observed and quantified through either a 4 chamber apical view or a parasternal long axis right chamber view.[4, 20] However, in this in-vitro experimental flow system only the right side of the heart is connected to a closed flow circuit. Therefore, to optimize the echocardiographic imaging window the posterior section of the heart was exposed while the anterior section was hidden, as seen in figure 3-4. The echocardiographic investigation is based on the Doppler equation:

$$f_a = \frac{2f\cos\theta}{c}$$

Where f_a is the frequency-shift; f is the source frequency, c is speed of ultrasound in the medium (soft tissue) and θ represents the angle between the ultrasound scan line and the flow of the seeding particles (working solution). Ideally the scan lines should be parallel to the flow of the solution; however this is not possible in both the clinical and this experimental setting due to the technical limitations since the transducer cannot be placed perfectly parallel to the flow profile through the TV such that $\theta = 0$. Nevertheless, the generally accepted range of less than 60 degrees was adhered to in this experiment. In addition, this experiment involves the comparative analysis between the regurgitant state and the ventricularized state, thus any errors associated to the angle, while still within the accepted accuracy range, can be negated.

To achieve the optimal acoustic window, and the smallest angle between the scan lines and flow, a posterior 2 chamber long axis apical view was adopted, as shown in figure 3-7.

A B

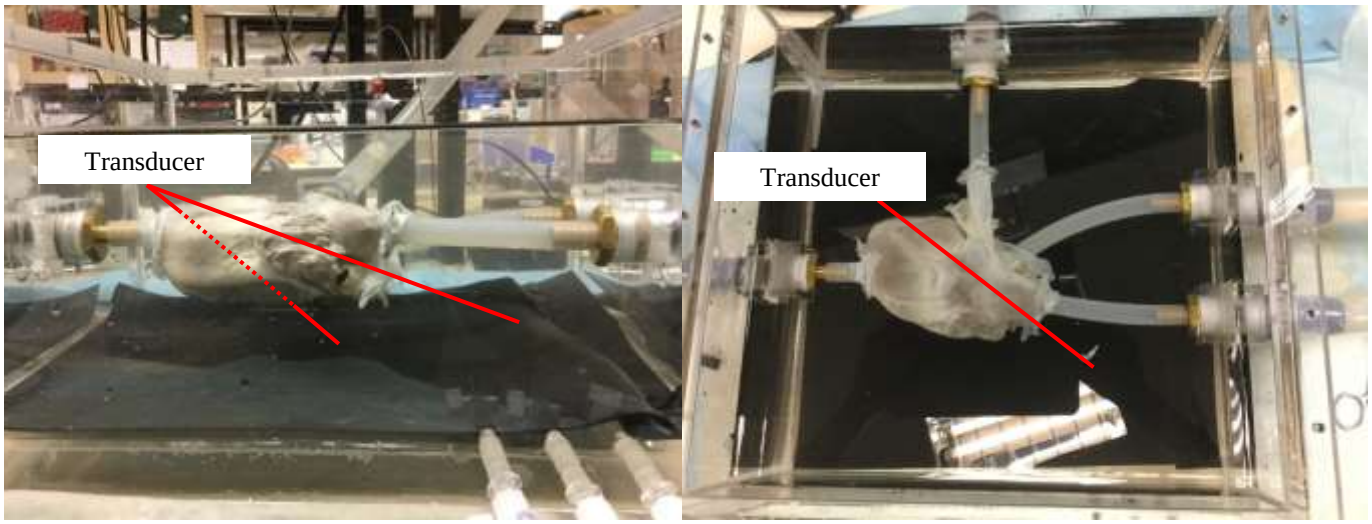

Figure 3-7: Posterior 2 chamber long axis apical view. (A) Lateral view of the scan lines (B) Superior view of the posterior section of the heart

3.4.1 Quantification

In this study the level of regurgitation was determined both qualitatively, through pressure and flow waveforms with echocardiographic images of the malcoaption of the leaflets, and quantitatively, through echocardiographic investigations to determine the PISAr and effective regurgitant orifice area (EROA).

Tricuspid regurgitation was quantified via 2D colour Doppler Proximal Isovelocity Surface Area (PISA) measurements as is the clinical standard, through non-invasive imaging. This method is based on the principal of conservation of mass: as blood approaches the regurgitant orifice, velocity increases, forming concentric shells of increasing velocity and decreasing surface area.[51]

From the conservation theory, it follows that the volumetric flow rates on either side of the tricuspid valve must be equal. This is represented by:

$$Q_1 = Q_2$$

Where Q represents the volumetric flow rate which is defined as:

$$Q = Area * Velocity$$

From this it follows that:

$$Area_1 * Velocity_1 = Area_2 * Velocity_2$$

The area proximal to the regurgitant orifice area, at the right ventricle, can be estimated through 2D color Doppler echocardiography to be a hemispherical distribution of velocity vectors. It can therefore be represented by:

$$Area_1 = 2\pi R^2$$

The radius can be determined through the 2D color echocardiographic investigations as the radial distance from the regurgitant orifice area to the isovelocity surface area. This surface area is dependent upon the aliasing velocity that has been defined. This would then imply:

$$Velocity_1 = Aliasing\ Velocity$$

The area of the flow on the other side, in the right atrium, is referred to as the Effective Regurgitant Orifice Area (EROA) and it is one of the key determinants of the severity of the TR. The EROA is the cross sectional area of the vena contracta and therefore is also the point of the maximum velocity. From this, it follows:

$$Velocity_2 = Maximum\ Velocity$$

$$2\pi R^2 * Aliasing\ velocity = EROA * Maximum\ Velocity$$

Hence,

$$EROA = \frac{2\pi R^2 * Aliasing\ Velocity}{Maximum\ Velocity}$$

The maximum velocity can be determined through continuous wave color Doppler or pulse wave Doppler, measured at the central axis of the regurgitant jet. Figure 3-8 illustrates the 2D color Doppler echocardiographic method described.

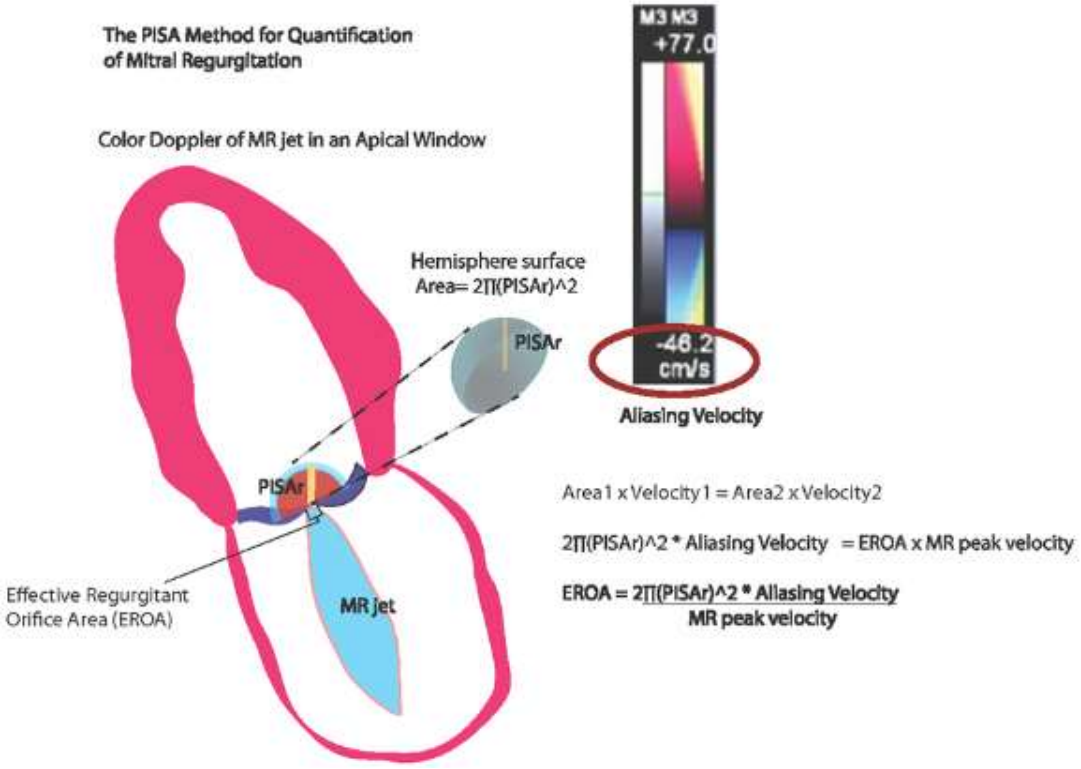

Figure 3-8: 2D color Doppler echocardiography method used to determine the effective regurgitant orifice area

While this method is the clinical standard it is not without its assumptions and limitations. The hemispherical flow convergence is based on the assumption that the regurgitant area is small and a perfectly round orifice. This is one of the limiting factors since the regurgitant area often has a complex shape and is dependent upon causality of TR such as annular dilation, leaflet calcification and RV enlargement.

Another limitation is the Doppler ultrasound's ability to only detect velocity components aligned with the direction of the ultrasound beam. Inability of the ultrasound to detect the velocity perpendicular to the scan lines means the velocities observed are a projection of the actual velocity. However, the true value can be modulated with the cosine of the angle between ultrasound scan line and the direction of the velocity.

Chapter 4:

RESULTS

4.1 Preliminary Echocardiographic Imaging

After the regurgitant model was established, the annular dilation was observed through echocardiographic investigations. This was done to ensure that the regurgitation was due to annular dilation, right ventricular dilation and papillary muscle displacement rather than a leak within the flow system. Figure 4-1 shows the coaption of the Tricuspid valve over a single cardiac cycle at various points in time. As seen in the images, the leaflets fail to coapt due to the tethering of the leaflets which are a result of the papillary muscles displacement brought about by the annular and ventricular dilation. While the regurgitant orifice area is observable, more quantitative measures are required to demonstrate the efficacy of CAVI.

Therefore, the relevant data for the flow, pressure and echocardiographic parameters (PISAr and EROA) were extracted. The successful deployment of the caval valves into the SVC and IVC established the ventricularized model. This was confirmed through echocardiography as well, as seen in figure 3-5. After CAVI, the native leaflets were observed for any notable changes over a single cardiac cycle, as shown in figure 4-2. The leaflets demonstrated better coaption; and a smaller regurgitant orifice area was observed. However, while this qualitative means of measurement is useful in reflecting the utility of the flow system, more quantitative measures were required to determine the efficacy of the therapeutic procedure.

The images show in figures 4-1 and 4-2 were extracted using Matlab 2013b.

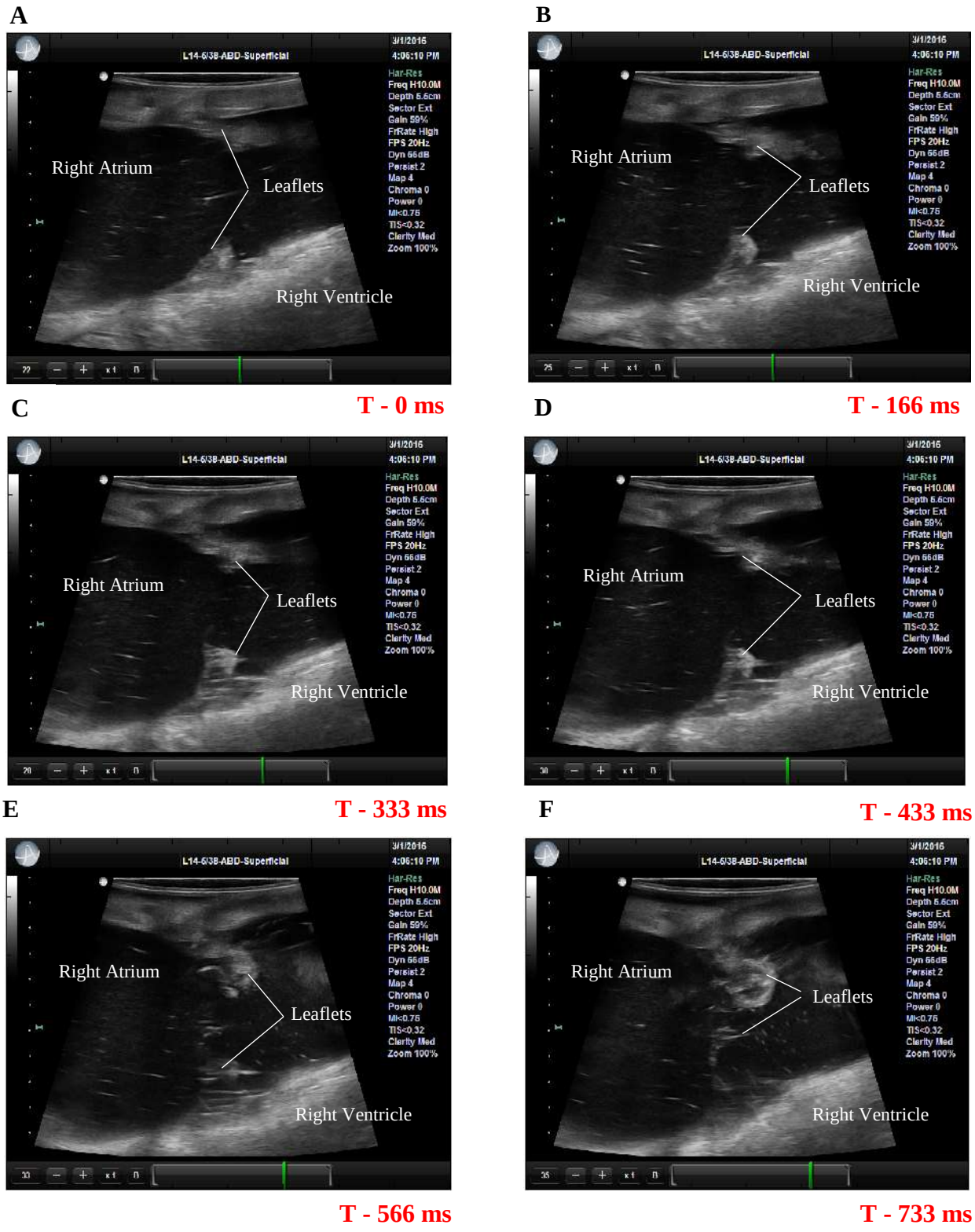

Figure 4-1: Regurgitant Tricuspid Valve Mechanics (A) The opening of the tricuspid valve in the regurgitant model. (F) The malcoaption of the tricuspid valve during systole due to papillary muscle displacement

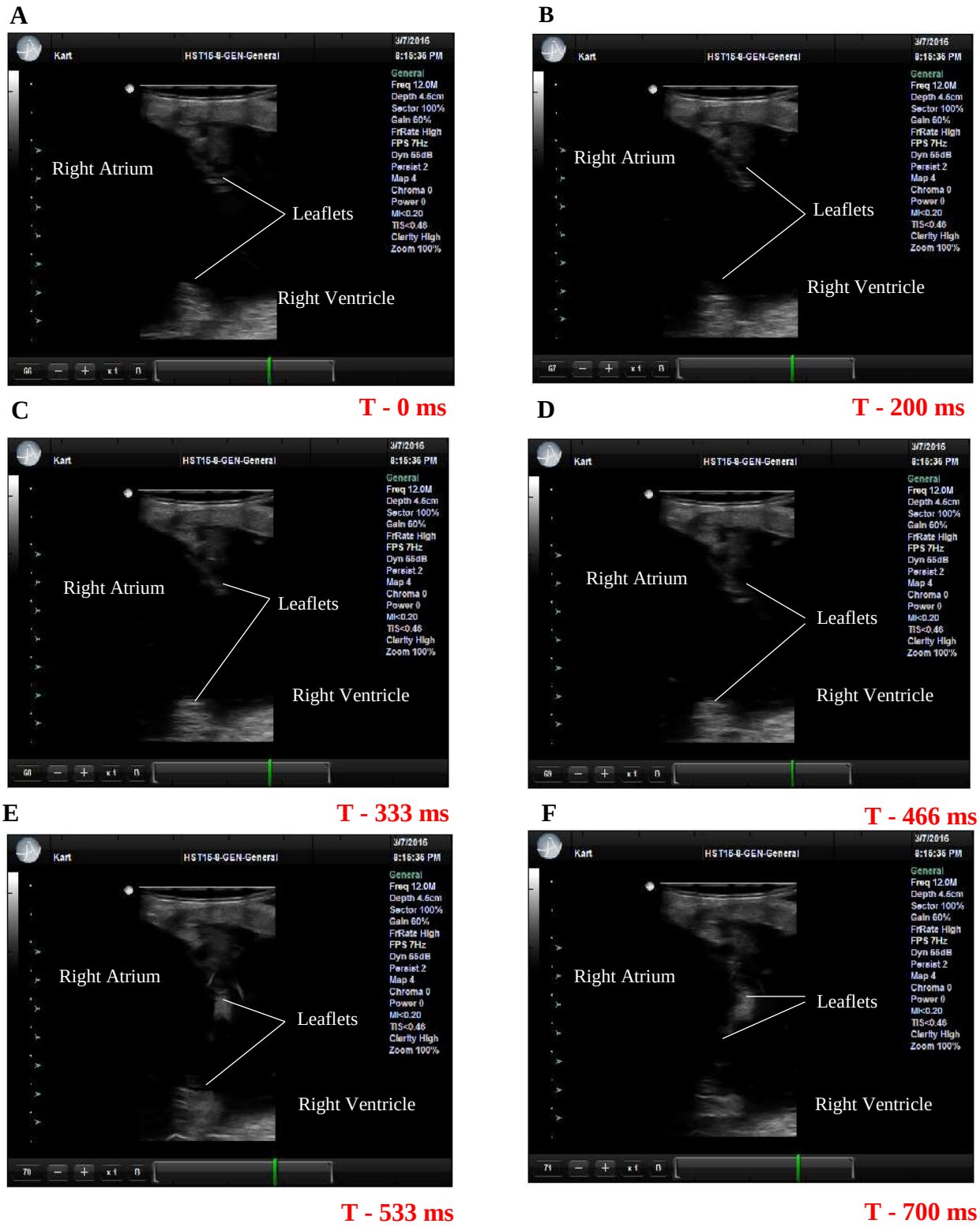

Figure 14-2: Ventricularized Tricuspid Valve Mechanics (A) Opening of the tricuspid valve in the Ventricularized model. (F) Improved coaption of the tricuspid valve during systole after CAVI

The pressure profiles of the regurgitant and post-CAVI (ventricularized) state were plotted parallel to the time stamps of the echocardiographic images, as shown in figure 4-3.

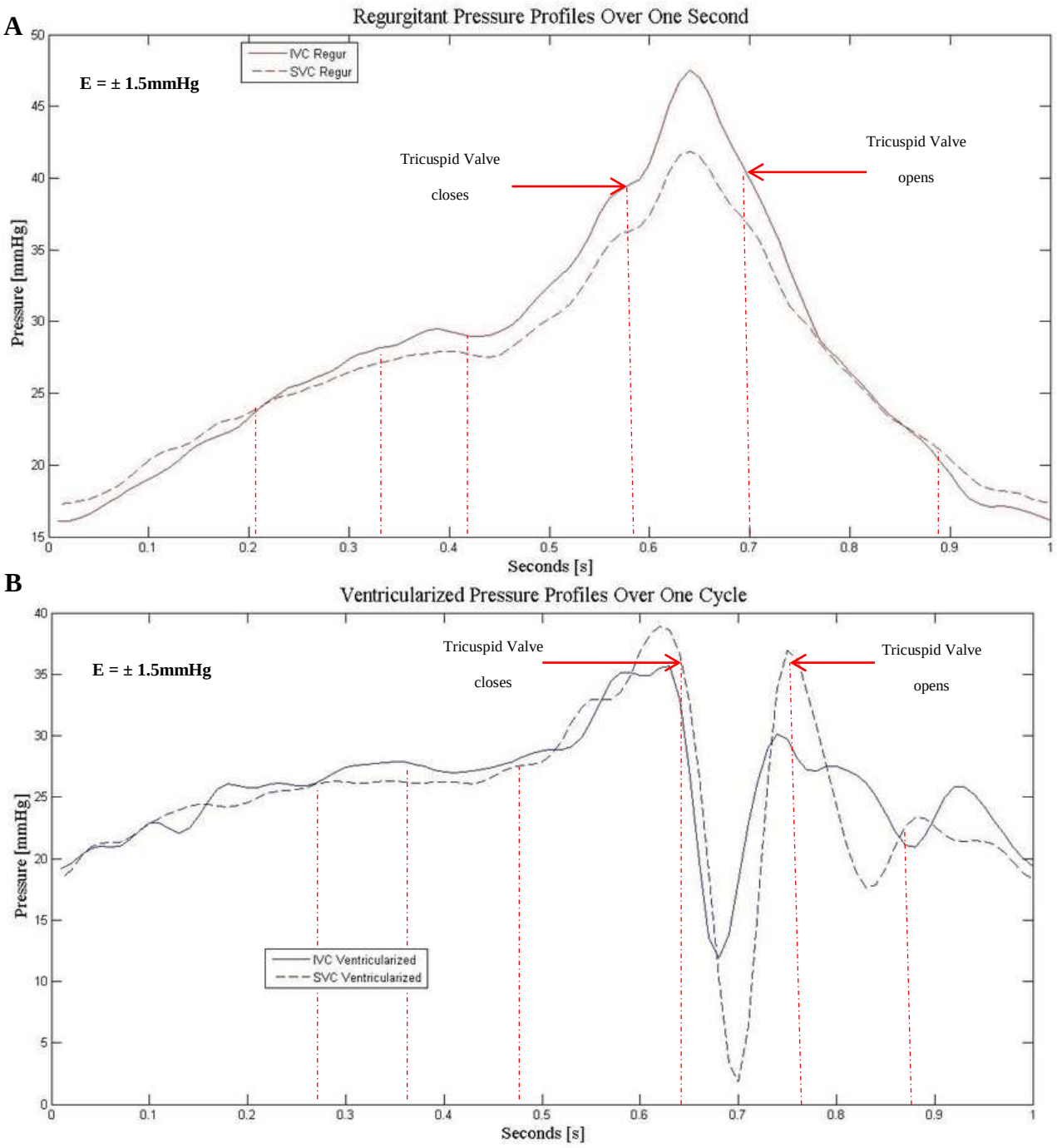

Figure 4-3: Pressure Profiles of (A) Regurgitant state and (B) Ventricularized state and the corresponding time points in the echocardiographic findings

4.2 Cardiac Output

The cardiac output in the pulmonary artery was recorded in both the regurgitant model and the Ventricularized model. Pulsatile flow was observed in both models since a pulsatile pump (attached to the right ventricle) was programmed to mimic the ventricular systole of the cardiac cycle. The sinusoidal flow waveform, shown in figure 4-4A, corresponds to the CO over 4 seconds. There is a notable difference in the CO between the regurgitant model and the Ventricularized model, with the latter being greater than the former.

The integral of the CO was taken over one minute, as reflected in figure 4-4B, the CO for the regurgitant model was determined to be 0.87206 liters per minute while the CO for the ventricularized model was found to be 1.9373 liters per minute. Therefore the CO increased by a factor of 2.22 after CAVI. This is similar to the findings reported by Lauten et al. [49] in their animal study; where the regurgitant CO decreased by a factor of 1.78. While this result is consistent with the expected trend (CAVI improves CO) the difference in magnitude can be attributed to a number of reasons such as the size of heart, difference in artificial introduction of regurgitation and the state of the soft tissue. Note: Matlab 2013b was used to determine the integral of the flow data.

Negative flow was also observed within the pulmonary artery, as seen in figure 4-4A, in both the regurgitant and the ventricularized model.

Ultimately, these observations allude to the efficacy of CAVI and further bolster the preliminary echocardiographic findings. Still, the pressure profiles of the JVP, PISAr and the EROA were required to establish a more quantitative means of analysis.

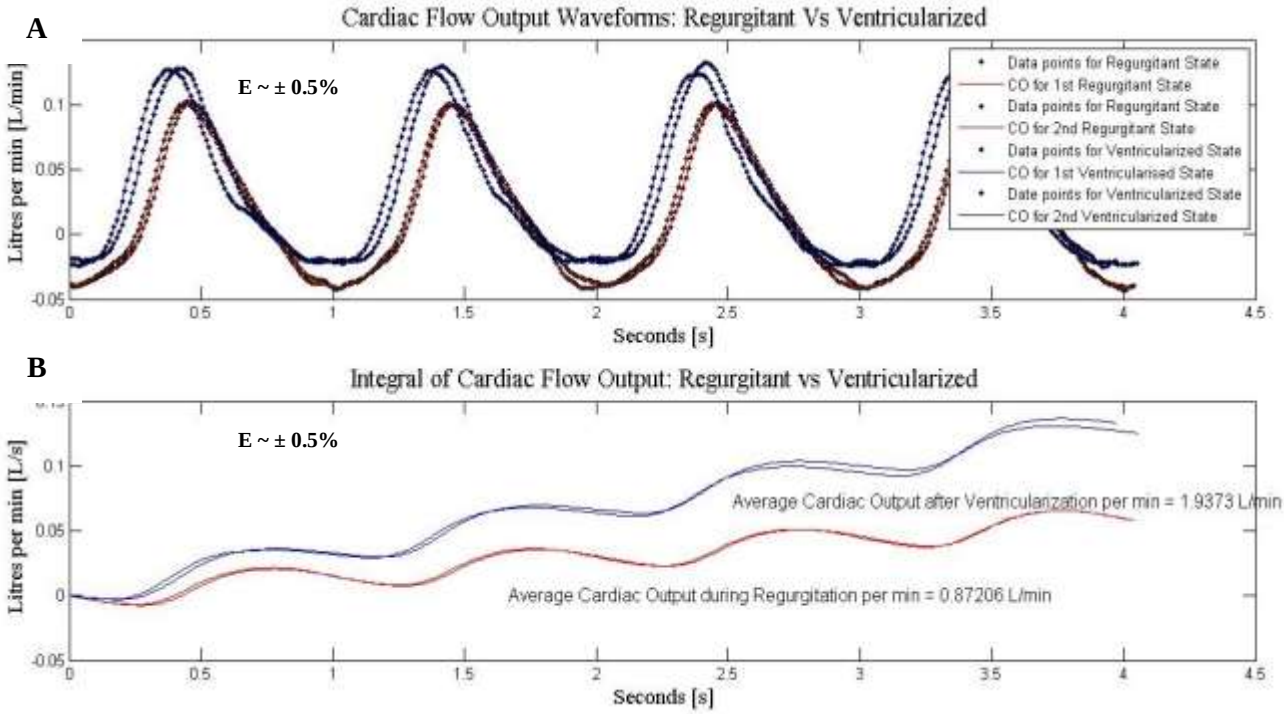

Figure 4-4: (A) The pulsatile cardiac output flow waveform over 4 seconds. (B) The integral of the flow waveform illustrating the volumetric flow

4.3 Jugular Venous Pressure Profiles

Under physiological conditions the Jugular Venous Pressure (JVP) waveform is characterized by the ‘a’, ‘c’ and ‘v’ wave and the ‘x’ and ‘y’ decent, as illustrated in the figure 4-5. The shape of the JVP coincides with the activity of the heart during the cardiac cycle. The ‘a’ wave corresponds to the atrial contraction which causes the pressure to increase and subsequently fall as the contraction slows. When the tricuspid valve closes there is a small increase in the pressure which is representative of the ‘c’ wave. The ‘x’ decent occurs during ventricular systole, where the atrium expands and relaxes. The rising ‘v’ wave follows the ‘x’ decent and occurs during systole due to the rapid filling of the atrium. As the pressure in the atrium becomes greater than

the ventricle, the tricuspid valve opens, and the passive filling of the ventricle occurs resulting in the ‘y’ decent.

With tricuspid regurgitation, an abnormal JVP with an absent ‘x’ decent and a dominant ‘v’ wave would be observed. This is due to the malcoaption of the tricuspid valve leaflets causing the rising pressure in the right ventricle, during systole, to be distributed in the atrium as well.

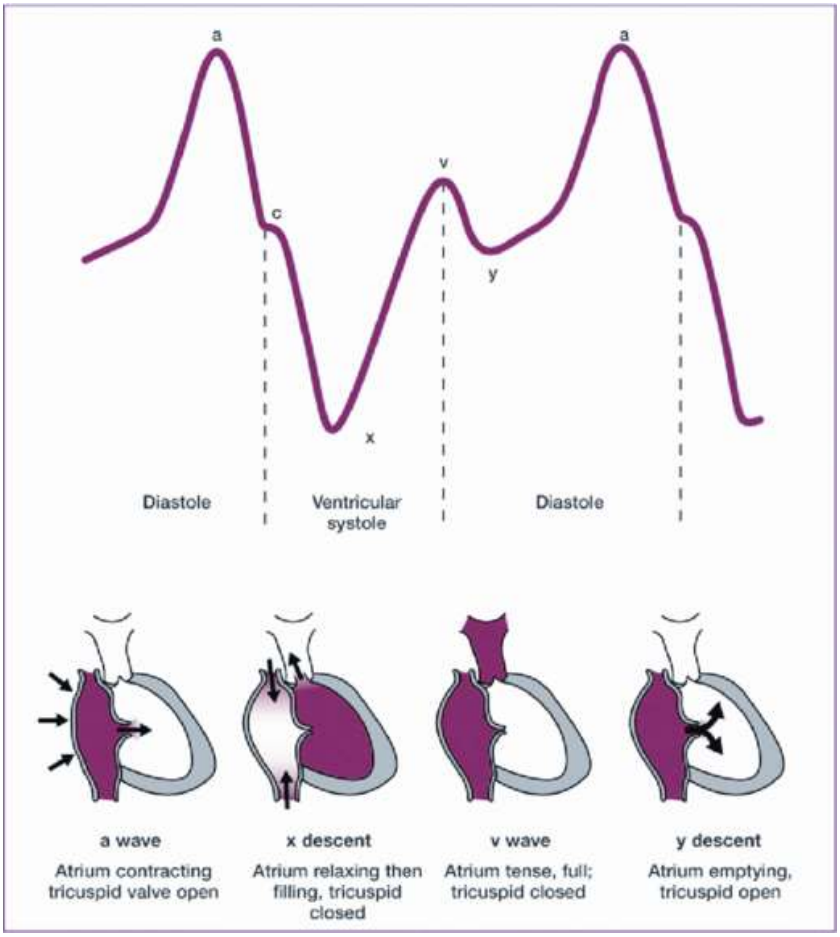

Figure 4-5: Illustration of the JVP. Image from [42]

The pressure profiles for both the regurgitant and ventricularized model were captured using the pressure catheter placed in the SVC and IVC. The pressure waveform recorded for the

regurgitant model had a dominant ‘v’ wave and an absent ‘x’ descend – features representative of tricuspid regurgitation in the JVP. The peak pressure for the regurgitant pressure profile is 47.52mmHg and 42.26mmHg for the IVC and SVC, respectively.

In the ventricularized heart model, the pressure profile had a restored ‘x’ descend and the ‘v’ wave was no longer dominant. The maximum pressure observed was that of the ‘a’ wave and was recorded as 36.29mmHg and 39.12mmHg for the IVC and the SVC respectively.

The pressure profiles for both heart models are represented in figure 4-6. The central venous pressure was reduced after CAVI and the results are parallel to those presented by Lauten et al.[48]

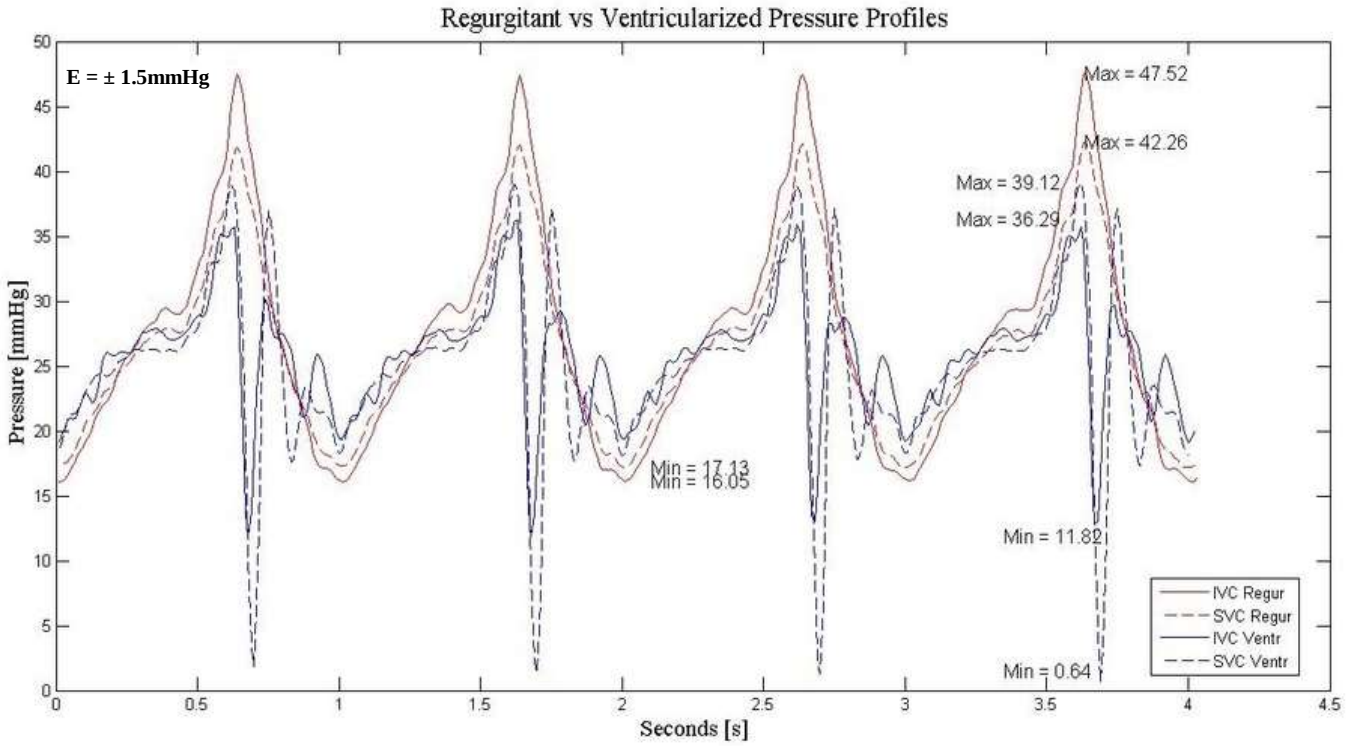

Figure 4-6: The pressure profile observed in the SVC and IVC for both the regurgitant (red) and Ventricularized (blue) heart model.

4.4 Echocardiographic Investigation

The echocardiographic parameters were important in quantifying regurgitation for both the regurgitant and the ventricularized model, in order to determine the efficacy of the treatment method. The PISAr, the radial distance from the regurgitant orifice area to the isovelocity surface area, was measured using 2D color Doppler echocardiography.

The isovelocity surface area was calculated by taking the radial distance parallel to the beam formation, as seen in figure 4-7. The parallel radial distance was used as the PISAr measurements, to prevent errors associated to angular adjustments, in determining the EROA; which was measured to be 6.73mm and 4.81mm for the regurgitant state and the ventricularized state, respectively. The aliasing velocity for the regurgitant state was found to be 52cm/s, and 51cm/s for the Ventricularized state.

The maximum velocity was determined using a pulse wave Doppler echocardiography along several points on the central axis of the regurgitant jet. The maximum velocity for the regurgitant model was 68.0cm/s while the maximum velocity for the ventricularized model was 82.2cm/s. The Doppler echocardiography for both the regurgitant and ventricularized model can be seen in figure 4-8.

Pulse wave systems have an intrinsic limitation; that at a given sampling frequency, pulse repetition frequency (PRF), the maximum Doppler frequency that can be measured without aliasing is half that of the PRF. Low velocities are examined using low PRF since a longer interval between pulses allows the scanner to better identify slow flow. Conversely, high pulse frequencies are used to determine high velocities. Therefore, to determine the maximum velocity in both the regurgitant and ventricularized model a PRF of 12.5 kHz (maximum) was used.

A

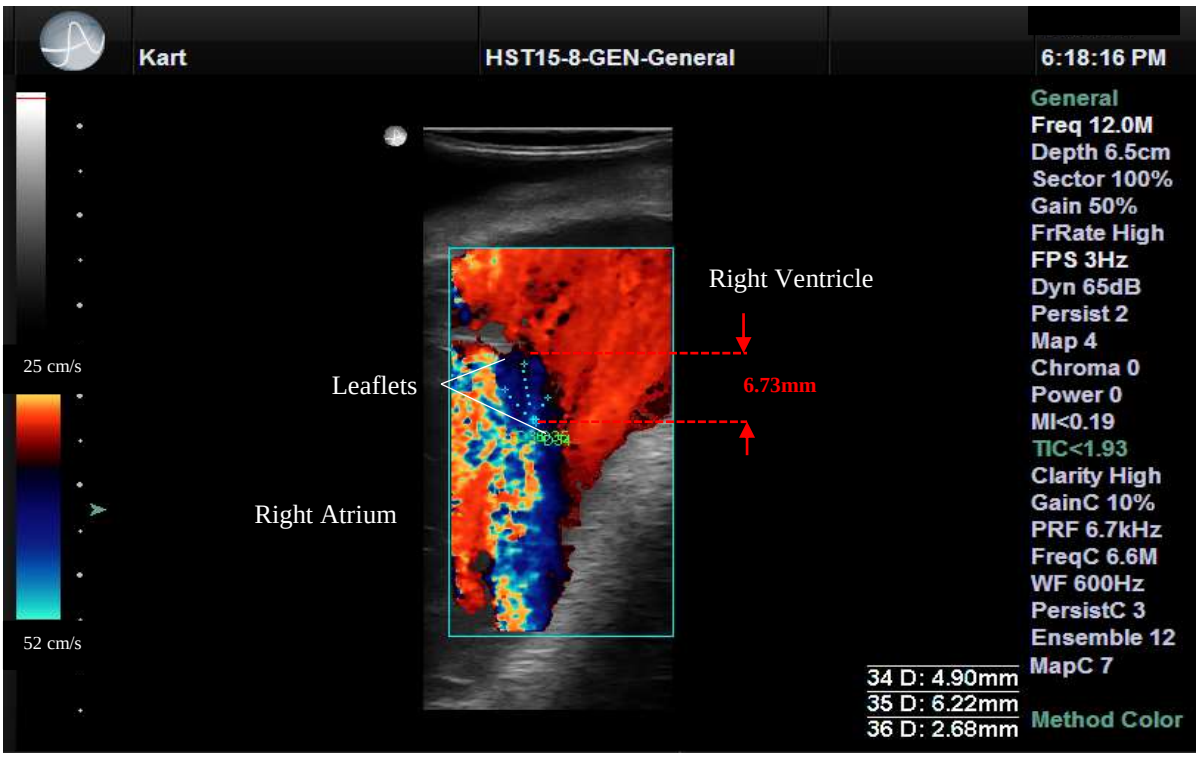

B

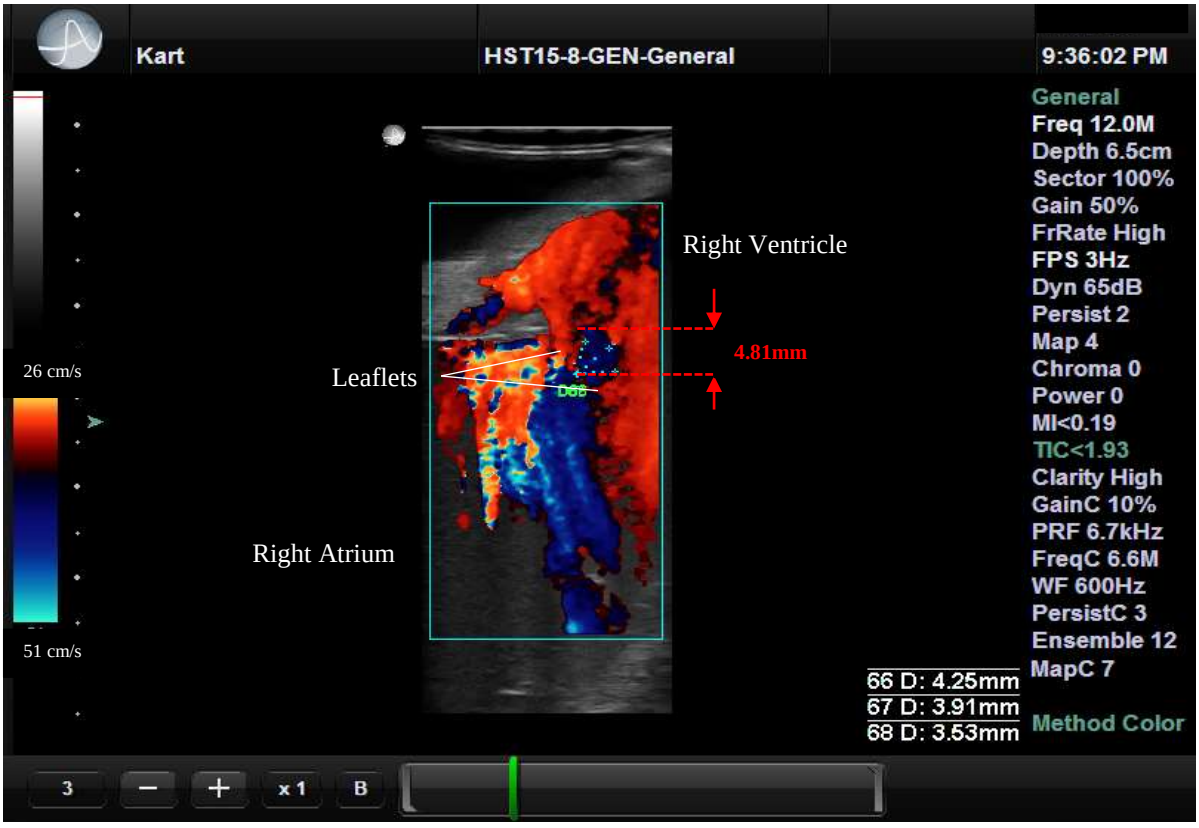

Figure 4-7: The echocardiographic study to determine the PISAr for (A) Regurgitant model and (B) Ventricularized model.

However, using a high PRF might result in lower velocities going undetected. For this reason the PRF used in the color Doppler, to determine the PISAr, was 6.7 kHz.

Similarly, other factors like the depth, gain and baseline were optimized to best extract the relevant data.

EROA was determined as:

$$EROA = \frac{2\pi R^2 * Aliasing\ Velocity}{Maximum\ Velocity}$$

EROA is based on the principal of conservation of mass. The results of the echocardiographic study, summarized in table 3, demonstrate that CAVI had successfully reduced the EROA by a factor of 2.42.

Table 4-1: Summary of the echocardiographic results

	PISAr [mm]	Surface Area [mm^2]	Aliasing Velocity [cm/s]	Maximum Velocity [cm/s]	EROA [cm^2]
Regurgitant	6.73	284.58	52	68.0	2.18
Ventricularized	4.81	145.37	51	82.2	0.90

A

B

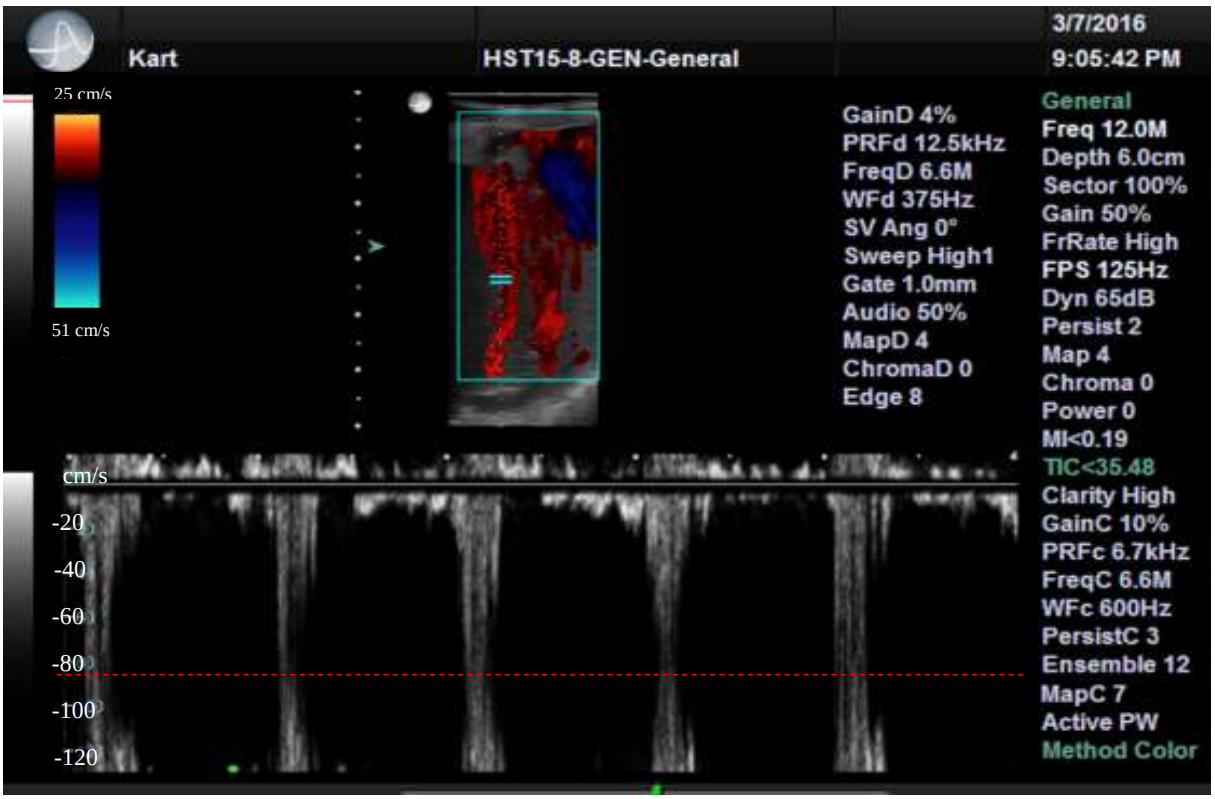

Figure 4-8: Doppler echocardiography to determine the maximum velocity in (A) the regurgitant model and (B) Ventricularized model.

Chapter 5:

DISCUSSION

In this study the efficacy of CAVI – the percutaneous heterotopic implantation of caval valves in the vena cava– is analyzed as a potential therapeutic treatment for tricuspid regurgitation. To do this, a novel flow system with an explanted porcine heart was designed to capture the pathophysiological representation of TR. The explanted heart was processed and made into a regurgitant model by inducing annular and ventricular dilation through hydrostatic pressure. The cardiac output, central venous pressure and the relevant echocardiographic parameters to quantify regurgitation were extracted. 2 caval valves were then placed into the vena cava to create the ventricularized model and the quantitative parameters were again extracted, and studied against that of the regurgitant model.

The annular dilation and tethering of the leaflets were observed in the regurgitant model through echocardiography, as seen in figure 4-1. The opening and closing of the leaflets, in the ventricularized model, were also observed, as seen in figure 4-2, to qualitatively visualize the improvement in the coaption of the leaflet. This demonstrates that the increase in atrial pressure due to CAVI is able to suppress the regurgitation during systole, as a smaller regurgitant area is observed. However, this would only be a qualitative assertion and not a quantitative one. Moreover, some extent of acoustic shadowing is observed which urges the need for a more quantitative determination of the efficacy of the procedure.

Dr Lauten et al.[49] reported, in his animal study, an increase in cardiac output with CAVI and concluded that the procedure alleviated the detrimental effects of STR by doing so. With tricuspid regurgitation, a reduction of the cardiac output is expected due to the retrograde flow of blood into the atrium instead of the ventricular outflow tract. Similar to Dr Lauten's findings,

this study reports a significant improvement of the CO in the ventricularized model when compared with the CO of the regurgitant model, as seen in figure 4-4.

Furthermore, from the figure 4-4A, the pulsatile nature of the flow is appropriately captured which lends credibility to the flow system being physiologically representative. Figure 4-4B, reflects the integration of the outflow over one minute, indicating the significant improvement in the volumetric flow through the pulmonary artery in the ventricularized model as opposed to the regurgitant model. While this demonstrates the efficacy of the procedure there are certain limitations of the flow system that must be addressed.

One of the limitations is magnitude of the volumetric flow in both diseased and treated model. Physiologically, the CO in a healthy individual is about 4.5 liters per minute and less in patients with TR – depending on severity. However, in this study the CO reported for the regurgitant model is 0.87206 l/min and 1.9373 l/min for the treated (ventricularized) model. This is due to the loss of the muscular recoil of the porcine heart and the manner in which ventricular systole is mimicked – pulsatile pump connected to the ventricle. Due to this, the stroke volume is not increased to the physiological range to prevent the pump from creating a strong jet within the ventricle during systole. This jet could potentially impede the natural functionality of the tricuspid leaflets and affect their coaption, which would compromise the results. Therefore, the stroke rate was optimized such that CAVI showed a marked improvement in the CO without affecting the functionality of the leaflets; which was confirmed through echocardiography.

Another drawback is the negative flow observed in the pulmonary artery. This can be attributed to the piston pump used to simulate the ventricular systole. When the piston draws back it creates a negative pressure (vacuum) that results in recirculation and backflow. Despite this limitation,

the flow is largely positive and pulsatile, and the CO has been shown to improve significantly with CAVI which supports its validity as a therapeutic solution to TR. This negative flow could have been mitigated further by adding an additional dampening component directly after the pump and before connecting to the heart. The reason why this was not implemented in the final set-up was due to the trade-off between mitigating the negative flow and maintaining the physiological pressure profiles; the latter being more pertinent to the overall analysis.

With TR the central venous pressure is heightened which in turn results in several comorbidities such as hepatosplenomegaly, peripheral edema and ascites. This was also reported in the animal study done by Dr Lauten et al.[49] In a healthy heart, the jugular venous pressure waveform – represents the pressure in the right atrium and vena cava – is characterized by the 'a' wave, 'x' descend, 'v' wave and the 'y' descend, as seen in figure 4-5. Each of these features corresponding to a part of the cardiac cycle; 'a' wave the atrial contraction, 'x' descend the ventricular systole, 'v' wave the rapid passive filling of the atrium and the 'y' descend the opening of the tricuspid valve.

However, with TR the JVP is modified and a single large peak is formed, as seen in figure 4-6. This is because the 'x' descend which used to indicate a drop in pressure, during ventricular systole, as the atrium relaxed and expands, is absent. The absence is a result of the regurgitant jet in the right atrium which instead increases the pressure within the atrium. This is further exacerbated by the rapid passive filling of the atrium which results in a single dominant 'v' wave, having merged with the 'a' wave. This was observed in the pressure profiles extracted from both the SVC and IVC in the regurgitant model of the flow system.

Moreover, with the ventricularized model the JVP was returned to the physiological state in both the SVC and IVC, as seen in figure 4-6. The ‘x’ descend was restored and the ‘v’ wave was no longer dominant with the peak pressures reported from the ‘a’ wave. The central venous pressure was also significantly lower. These results support the observations of Dr Lauten’s animal study and the effectiveness of CAVI as a therapeutic procedure.

Furthermore, in the animal study the peak pressures were reported without the JVP waveforms and STR was introduced via deliberate damage to the leaflet using a 0.07 inch wire blade. Therefore, the regurgitation reported occurred without annular dilation and was significantly lower than the physiological pressures expected. These limitations, highlighted by Lauten et al. [48], were addressed in this novel flow system using an explanted porcine heart. Therefore, adding credibility to the flow system in highlighting the efficacy of CAVI as a potential new therapeutic method.

The echocardiographic parameters extracted from this study also support the efficacy of CAVI. The proximal isovelocity surface area radius was found to be significantly smaller in the treated (ventricularized) model than in the regurgitant model; 4.81mm in treated and 6.73mm in the regurgitant. CAVI contains the elevated pressure within the right atrium; which reduces the amount of regurgitation, since the heightened pressure would ‘flatten’ the pressure gradient from the ventricle to the atrium, during systole.

After the aliasing velocities for each of the models were determined, the maximum velocity of the regurgitant jet was analyzed using pulse wave Doppler color echocardiography. The maximum velocity for the treated model, 82.2 cm/s, was much higher than the regurgitant model, 68.0cm/s. This was as expected since the echocardiographic method, for quantification, is based

on the principal of conservation of volumetric flow. Hence, the maximum velocity was observed for the ventricularized model which has the smaller PISAr.

With the PISAr, aliasing velocities, and the maximum velocities the effective regurgitant orifice area was determined, for both the treated and diseased model. The results demonstrate that CAVI could potentially be an effective transcatheter therapeutic technique to treat STR; since the EROA for the treated model was 2.42 times smaller than the regurgitant model.

However, there are some limitations that must be addressed in this study. Firstly, pulse wave color Doppler echocardiography was used to determine the maximum velocity. While this is possible, it is limited to point based analysis of the central axis of the regurgitant jet, which might be subjected to human error. Ideally the maximum velocity is determined using continuous wave Doppler color echocardiography which mitigates the possibility of human error.

Secondly, despite the encouraging flow, pressure and echocardiographic results, the EROA for the treated model is $0.50cm^2$. While this is 2.42 times smaller than the EROA in the regurgitant model it is still considered severe. TR is considered to be severe when the EROA is greater than $0.4cm^2$. However, this is explained by the inherent limitations in this study.

Finally, it is important to note that this study was done with an explanted porcine heart and therefore there are certain intrinsic limitations. The heart model, while processed to be complementary to the flow system, is still unable to produce any muscular recoil or recovery. Still, using an explanted porcine heart provided an extremely physiologically, and pathophysiologically, representative model. STR was introduced through deliberate accentuated hydrostatic pressure which resulted in annular dilation. While the model was able to demonstrate how CAVI would be able to reduce the EROA – by containing the elevated pressure within the

right atrium – it is unable to emulate the muscular activity and recoil. This is reflected by the still severe EROA in the treated model; although significantly improved.

Aside from the limitations of the flow system, the potential drawbacks of the technique must also be discussed. CAVI, being a heterotopic implantation, does not affect the native tricuspid leaflets and 'contains' the elevated pressures within the atrium. While this reduces the central venous pressure and improves the cardiac output it may pose long term detrimental effects on the right atrium. The right atrium being subjected to persistent elevated pressures might undergo remodeling and potentially develop atrial fibrillation. More studies have to be done to determine the likelihood as well as the possible predictors (parameters) that might lend insight into this investigation.

Ultimately, having acknowledged the potential limitations of the both the flow system and the technique, CAVI has proven to be a very promising transcatheter therapeutic procedure that could potentially expand the available techniques to treat tricuspid regurgitation. The flow system developed in this study was able to demonstrate the benefits of techniques that were highlighted by Lauten et al. [48] and additionally provided quantitative assessment on the technique; through echocardiography.

Chapter 6:

CONCLUSION

6.1 Future Works

The flow system was optimized after several iterations, through the use of several hearts, to ensure that the results obtained were not compromised due to random error. Having incorporated an explanted porcine heart, the complex morphology of the tricuspid valve, annulus and sub apparatus like the papillary muscles and chordae tendineae were 'captured' in the flow system. This further bolsters the novelty as well as the physiological representation of both the diseased and treated state. However, with further iteration an even greater degree of complexity could potentially be introduced to achieve an even more representative model.

One possible complexity would be the introduction of a pericardial membrane around the heart designed to prevent its excessive excursion during the simulated cardiac cycle. This would be useful in circumventing the lack of muscular recoil which tends to dilate the heart progressively throughout the study. This pericardial fold however, should not impede the ability to carry out echocardiographic assessments on the explanted heart. Therefore it could be a potential development in making the flow system even more representative.

Moreover, the flow system with the explanted heart could be used to study the effectiveness of various medical procedures and devices. It could also likely be used to expedite research by serving as an initial test for the relevant procedures and devices before animal study; potentially increasing the success rates.

Devices with unique means of anchorage and fixation could be studied in the flow system, by leveraging on the complexity of the explanted heart, without having to conduct animal studies

initially; which are often time consuming and expensive. It could also be used to demonstrate the feasibility of a procedure and predict the likelihood of success.

In addition, the flow system could be used in research where cardiology is concerned. A phantom silicone model could be established in conjunction with the explanted heart model and particle image velocimetery could be used to ascertain the flow profile within the heart. A simulatory study could also be established to reflect the data extracted from the flow system and could potentially be used as a predictive template for various devices and procedures. These methods could help to provide a more holistic interpretation of a medical device or procedure.

Langendoff Preparation

The mammalian heart perfusion method conceptualized by Oscar Langendoff in 1985 might lead to some very interesting and potentially significant developments. The Langendoff preparation of a heart model has been used to study basic heart physiology, myocardial function and various human diseased states such as hypertension, ischemia and reperfusion injury.[6] In this study, the efficacy of heterotopic implantation of caval valves in the vena cava was investigated as a potential solution to TR and therefore the Langendoff method is not entirely applicable. This is because the Langendoff heart model is perfused in a retrograde fashion through the aorta which forces the aortic valve to close; forcing the solution into the coronary vessels which normally supply the heart tissue with blood. This method keeps the heart beating for several hours where crucial data is extracted. Figure 5-1 illustrates a working model of the Langendoff heart established in a study done by R.M. Bell et al.[6]

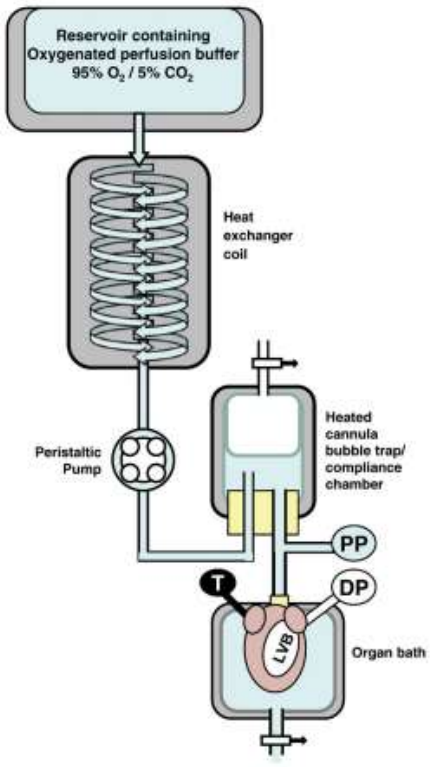

Figure 6-1: Schematic representation of a working Langendoff heart model done by R.M. Bell et al.[6]

Despite not being directly applicable, some aspects of the Langendoff model could increase the physiological representation of our explanted heart flow system. For example, the Krebs Henseleit Buffer could be used as the perfusing solution instead of a starch solution. However, the feasibility of echocardiographic analysis must not be compromised and therefore further investigations would be required. On the other hand, whole blood perfusion could be considered as well. The temperature could be modulated and controlled as done in the study by R.M. Bell et al.[6]

There have also been studies that have attempted to use electrical stimulation together with image analysis to study other comorbidities such as ventricular fibrillation with some success.[59] While this would be an interesting and useful idea to incorporate into our own model, it would not be feasible at this stage. One of the primary reasons is the need to immobilize the tissue using

uncoupling drugs which have significant effect on the cell electrophysiology.[59] Moreover, the cardiac movement incited by electrical stimulation has to be coordinated very precisely to emulate a successful cardiac cycle. The time limitation should also be taken into consideration since electrical simulation would only be effective for a small window post explantation. Furthermore, the induced cardiac cycle has to be strong enough to create the physiological pressure waveforms; which based on current studies are not sufficient.

Therefore, while the current flow system does produce favorable results and is sufficiently representative of the physiological state, there are still several methods to be studied that could potentially advance the complexity of this novel flow system even further.

Ultimately in this study, the effectiveness of CAVI, as a percutaneous transcatheter treatment for tricuspid regurgitation, was analyzed. This was done through a novel flow system that utilized an explanted porcine heart. Through the incorporation of the heart, the complexities associated with the morphology of the tricuspid valve, annulus, papillary muscle and chordae tendineae were introduced into the flow system, allowing a more physiological representation.

The diseased model of the heart was made by deliberately exposing the right atrium to elevated hydrostatic pressure resulting in annular dilation and severe tricuspid regurgitation. The ventricularized model was made by heterotopic implantation of 2 caval valves into the superior and inferior vena cava of the diseased model.

The corresponding results of the study were supportive of a previous animal study done on this procedure. There was a significant increase the cardiac output and decrease in the central venous pressure which was similarly reported in the previous study. However, unlike the previous study,

tricuspid regurgitation was introduced with annular dilation and the jugular venous waveforms were reported in full, addressing the limitations of the previous study.

Moreover, echocardiographic assessments were made to quantify the levels of regurgitation in both the diseased and treated model. These results again were favorable, lending further viability to CAVI as a potential therapeutic procedure.

While there are several intrinsic limitations of using an explanted porcine heart, it still adds to the complexity of the flow system and increases its physiological representation of the diseased model. It also provides unique insight to the potential shortcomings of CAVI which warrants more study.

In conclusion, CAVI increases the cardiac output, reduces the central venous pressure and reduces the effective regurgitant orifice area, thereby alleviating the detrimental effects of severe tricuspid regurgitation. Although more research is required to comprehend the long term effects of the heterotopic implantation of the caval valves in the vena cava, CAVI could potentially expand the transcatheter therapeutics for treating tricuspid regurgitation percutaneously.

References:

1. Antunes, M. J. and J. B. Barlow. Management of tricuspid valve regurgitation. Heart. 93:271-276, 2007.

2. Anwar, A. M., O. I. I. Soliman, A. Nemes, R.-J. M. van Geuns, M. L. Geleijnse, and J. Folkert. Value of assessment of tricuspid annulus: real-time three-dimensional echocardiography and magnetic resonance imaging. The international journal of cardiovascular imaging. 23:701-705, 2007.

3. Badano, L. P., L. P. de Isla, P. Gianfagna, and J. L. Zamorano. Evaluation of the tricuspid valve morphology and function by transthoracic real-time three-dimensional echocardiography. European Heart Journal-Cardiovascular Imaging. 10:477-484, 2009.

4. Badano, L. P., D. Muraru, and M. Enriquez-Sarano. Assessment of functional tricuspid regurgitation. Eur. Heart J. 34:1875-85, 2013.

5. Bai, Y., G.-J. Zong, H.-R. Wang, H.-B. Jiang, H. Wang, H. Wu, X.-X. Zhao, and Y.-W. Qin. An integrated pericardial valved stent special for percutaneous tricuspid implantation: an animal feasibility study. J. Surg. Res. 160:215-221, 2010.

6. Bell, R. M., M. M. Mocanu, and D. M. Yellon. Retrograde heart perfusion: the Langendorff technique of isolated heart perfusion. J. Mol. Cell. Cardiol. 50:940-950, 2011.

7. Bonhoeffer, P., Y. Boudjemline, Z. Saliba, J. Merckx, Y. Aggoun, D. Bonnet, P. Acar, J. Le Bidois, D. Sidi, and J. Kachaner. Percutaneous replacement of pulmonary valve in a right-ventricle to pulmonary-artery prosthetic conduit with valve dysfunction. The Lancet. 356:1403-1405, 2000.

8. Bonow, R. O., B. A. Carabello, K. Chatterjee, A. C. de Leon, D. P. Faxon, M. D. Freed, W. H. Gaasch, B. W. Lytle, R. A. Nishimura, and P. T. O'Gara. ACC/AHA 2006 guidelines for the management of patients with valvular heart disease: a report of the American College of Cardiology/American Heart Association Task Force on Practice Guidelines (writing Committee to Revise the 1998 guidelines for the management of patients with valvular heart disease) developed in collaboration with the Society of Cardiovascular Anesthesiologists endorsed by the Society for Cardiovascular Angiography and Interventions and the Society of Thoracic Surgeons. J. Am. Coll. Cardiol. 48:e1-e148, 2006.

9. Boudjemline, Y., G. Agnoletti, D. Bonnet, L. Behr, N. Borenstein, D. Sidi, and P. Bonhoeffer. Steps toward the percutaneous replacement of atrioventricular valves: an experimental study. J. Am. Coll. Cardiol. 46:360-365, 2005.

10. Calafiore, A. M., S. Gallina, A. L. Iacò, M. Contini, A. Bivona, M. Gagliardi, P. Bosco, and M. Di Mauro. Mitral valve surgery for functional mitral regurgitation: should moderate-or-more tricuspid regurgitation be treated? a propensity score analysis. The Annals of thoracic surgery. 87:698-703, 2009.

11. Calafiore, A. M., A. L. Iacò, A. Romeo, S. Scandura, R. Meduri, E. Varone, and M. Di Mauro. Echocardiographic-based treatment of functional tricuspid regurgitation. The Journal of thoracic and cardiovascular surgery. 142:308-313, 2011.

12. Carpentier, A., A. Deloche, G. Hanania, J. Forman, P. H. Sellier, A. Piwnica, C. H. Dubost, and D. C. McGoon. Surgical management of acquired tricuspid valve disease. The Journal of thoracic and cardiovascular surgery. 67:53, 1974.

13. Carrier, M., Y. Hébert, M. Pellerin, D. Bouchard, L. P. Perrault, R. Cartier, A. Basmajian, P. Pagé, and N. C. Poirier. Tricuspid valve replacement: an analysis of 25 years of experience at a single center. The Annals of thoracic surgery. 75:47-50, 2003.

14. Chatterjee, K., *Cardiology: An Illustrated Textbook*. 2012: Jaypee Brothers,Medical Publishers Pvt. Limited.

15. Chopra, H. K., N. C. Nanda, P. Fan, K. K. Kapur, R. Goyal, D. Daruwalla, and A. Pacifico. Can two-dimensional echocardiography and Doppler color flow mapping identify the need for tricuspid valve repair? J. Am. Coll. Cardiol. 14:1266-1274, 1989.

16. Cribier, A., H. Eltchaninoff, A. Bash, N. Borenstein, C. Tron, F. Bauer, G. Derumeaux, F. Anselme, F. Laborde, and M. B. Leon. Percutaneous transcatheter implantation of an aortic valve prosthesis for calcific aortic stenosis first human case description. Circulation. 106:3006-3008, 2002.

17. Dalrymple-Hay, M. J., Y. Leung, S. K. Ohri, M. P. Haw, J. K. Ross, S. A. Livesey, and J. L. Monro. Tricuspid valve replacement: bioprostheses are preferable. The Journal of heart valve disease. 8:644-648, 1999.

18. De Bonis, M., E. Lapenna, G. La Canna, A. Grimaldi, F. Maisano, L. Torracca, A. Caldarola, and O. Alfieri. A novel technique for correction of severe tricuspid valve regurgitation due to complex lesions. Eur. J. Cardiothorac. Surg. 25:760-765, 2004.

19. De Bonis, M., E. Lapenna, F. Sorrentino, G. La Canna, A. Grimaldi, F. Maisano, L. Torracca, and O. Alfieri. Evolution of tricuspid regurgitation after mitral valve repair for functional mitral regurgitation in dilated cardiomyopathy. Eur. J. Cardiothorac. Surg. 33:600-6, 2008.

20. Depace, N. L. , J. Ross, A. S. Iskandrian, P. F. Nestico, M. N. Kotler, G. S. Mintz, B. L. Segal, A.-H. Hakki, and J. Morganroth. Tricuspid Regurgitation: Noninvasive Techniques for Determining Causes and Severity JACC. 3, 1984.

21. Desai, R. R., L. M. Vargas Abello, A. L. Klein, T. H. Marwick, R. A. Krasuski, Y. Ye, E. R. Nowicki, J. Rajeswaran, E. H. Blackstone, and G. B. Pettersson. Tricuspid regurgitation and right ventricular function after mitral valve surgery with or without concomitant tricuspid valve procedure. J. Thorac. Cardiovasc. Surg. 146:1126-1132 e10, 2013.

22. DeVega, N. G. Selective adjustable and permanent annuloplasty: An original technique for the treatment of tricuspid insufficiency. Rev. Esp. Cardiol. 2:555-556, 1972.

23. Di Mauro, M., G. P. Bezante, A. Di Baldassarre, D. Clemente, A. Cardinali, A. Acitelli, S. Salerni, M. Penco, A. M. Calafiore, S. Gallina, and Cardiology Italian Study Group on Valvular Heart Disease Italian Society of. Functional tricuspid regurgitation: an underestimated issue. Int. J. Cardiol. 168:707-15, 2013.

24. Di Mauro, M., A. Bivona, A. L. Iacò, M. Contini, M. Gagliardi, E. Varone, S. Gallina, and A. M. Calafiore. Mitral valve surgery for functional mitral regurgitation: prognostic role of tricuspid regurgitation. Eur. J. Cardiothorac. Surg. 35:635-640, 2009.

25. Dreyfus, G. D., P. J. Corbi, K. M. Chan, and T. Bahrami. Secondary tricuspid regurgitation or dilatation: which should be the criteria for surgical repair? Ann. Thorac. Surg. 79:127-32, 2005.

26. Dreyfus, G. D., R. P. Martin, K. M. J. Chan, F. Dulguerov, and C. Alexandrescu. Functional tricuspid regurgitation: a need to revise our understanding. J. Am. Coll. Cardiol. 65:2331-2336, 2015.

27. Dubreuil, O., A. Basmadjian, A. Ducharme, B. Thibault, J. Crepeau, J. Y.-T. Lam, and L. Bilodeau. Percutaneous mitral valve annuloplasty for ischemic mitral regurgitation: first in man experience with a temporary implant. Catheter. Cardiovasc. Interv. 69:1053-1061, 2007.

28. Ellis, J. T., B. R. Travis, and A. P. Yoganathan. An in vitro study of the hinge and near-field forward flow dynamics of the St. Jude medical® regent™ bileaflet mechanical heart valve. Ann. Biomed. Eng. 28:524-532, 2000.

29. Ellis, J. T. and A. P. Yoganathan. A comparison of the hinge and near-hinge flow fields of the St Jude medical hemodynamic plus and regent bileaflet mechanical heart valves. The Journal of thoracic and cardiovascular surgery. 119:83-93, 2000.

30. Filsoufi, F., A. C. Anyanwu, S. P. Salzberg, T. Frankel, L. H. Cohn, and D. H. Adams. Long-term outcomes of tricuspid valve replacement in the current era. Ann. Thorac. Surg. 80:845-50, 2005.

31. Filsoufi, F., S. P. Salzberg, M. Coutu, and D. H. Adams. A three-dimensional ring annuloplasty for the treatment of tricuspid regurgitation. Ann. Thorac. Surg. 81:2273-7, 2006.

32. Fukuda, S., A. M. Gillinov, P. M. McCarthy, W. J. Stewart, J.-M. Song, T. Kihara, M. Daimon, M.-S. Shin, J. D. Thomas, and T. Shiota. Determinants of recurrent or residual functional tricuspid regurgitation after tricuspid annuloplasty. Circulation. 114:I-582-I-587, 2006.

33. Fukuda, S., A. M. Gillinov, J.-M. Song, M. Daimon, V. Kongsaerepong, J. D. Thomas, and T. Shiota. Echocardiographic insights into atrial and ventricular mechanisms of functional tricuspid regurgitation. Am. Heart J. 152:1208-1214, 2006.

34. Fukuda, S., G. Saracino, Y. Matsumura, M. Daimon, H. Tran, N. L. Greenberg, T. Hozumi, J. Yoshikawa, J. D. Thomas, and T. Shiota. Three-dimensional geometry of the tricuspid annulus in healthy subjects and in patients with functional tricuspid regurgitation a real-time, 3-dimensional echocardiographic study. Circulation. 114:I-492-I-498, 2006.

35. Ghanta, R. K., R. Chen, N. Narayanasamy, S. McGurk, S. Lipsitz, F. Y. Chen, and L. H. Cohn. Suture bicuspidization of the tricuspid valve versus ring annuloplasty for repair of functional tricuspid regurgitation: midterm results of 237 consecutive patients. The Journal of thoracic and cardiovascular surgery. 133:117-126, 2007.

36. Grigioni, M., C. Daniele, G. D'Avenio, and V. Barbaro. A discussion on the threshold limit for hemolysis related to Reynolds shear stress. J. Biomech. 32:1107-1112, 1999.

37. Ismail, M., F. Kabinejadian, Y. N. Nguyen, E. Tay, K. Sangho, and H. L. Leo. In Vitro Investigation of the Hemodynamics of Transcatheter Heterotopic Valves Implantation in the Cavo-Atrial Junction. Artif. Organs. 39:803-814, 2015.

38. Jesty, J., W. Yin, P. Perrotta, and D. Bluestein. Platelet activation in a circulating flow loop: combined effects of shear stress and exposure time. Platelets, 2009.

39. Kaplan, M., M. S. Kut, M. M. Demirtas, S. Cimen, and A. Ozler. Prosthetic replacement of tricuspid valve: bioprosthetic or mechanical. The Annals of thoracic surgery. 73:467-473, 2002.

40. Kay, J. H., G. Maselli-Campagna, and H. K. Tsuji. Surgical treatment of tricuspid insufficiency. Ann. Surg. 162:53, 1965.

41. Khambadkone, S., L. Coats, A. Taylor, Y. Boudjemline, G. Derrick, V. Tsang, J. Cooper, V. Muthurangu, S. R. Hegde, and R. S. Razavi. Percutaneous pulmonary valve implantation in humans results in 59 consecutive patients. Circulation. 112:1189-1197, 2005.

42. Kress, J. P. Hemodynamic Monitoring. ACCP Critical Care Medicine Board Review: 21st Edition, 2012.

43. Kuwaki, K., K. Morishita, M. Tsukamoto, and T. Abe. Tricuspid valve surgery for functional tricuspid valve regurgitation associated with left-sided valvular disease. Eur. J. Cardiothorac. Surg. 20:577-582, 2001.

44. Lancellotti, P., L. Moura, L. A. Pierard, B. A. Popescu, C. Tribouilloy, A. Hagendorff, J.-L. Monin, L. Badano, J. L. Zamorano, and R. Sicari. European Association of Echocardiography recommendations for the assessment of valvular regurgitation. Part 2: mitral and tricuspid regurgitation (native valve disease). European Heart Journal-Cardiovascular Imaging. 11:307-332, 2010.

45. Latib, A., A. Pozzoli, P. Denti, M. Taramasso, P. Spagnolo, J.-M. Juliard, E. Brochet, P. Ou, M. Enriquez-Sarano, and F. Grigioni. First-in-man implantation of a tricuspid annular remodeling device for functional tricuspid regurgitation. JACC Cardiovasc. Interv. 8:e211-e214, 2015.

46. Laule, M., V. Stangl, W. Sanad, A. Lembcke, G. Baumann, and K. Stangl. Percutaneous transfemoral management of severe secondary tricuspid regurgitation with Edwards

Sapien XT bioprosthesis: first-in-man experience. J. Am. Coll. Cardiol. 61:1929-1931, 2013.

47. Lauten, A., T. Doenst, A. Hamadanchi, M. Franz, and H. R. Figulla. Percutaneous Bicaval Valve Implantation for Transcatheter Treatment of Tricuspid Regurgitation Clinical Observations and 12-Month Follow-Up. Circ. Cardiovasc. Interv. 7:268-272, 2014.

48. Lauten, A., M. Ferrari, K. Hekmat, R. Pfeifer, G. Dannberg, A. Ragoschke-Schumm, and H. R. Figulla. Heterotopic transcatheter tricuspid valve implantation: first-in-man application of a novel approach to tricuspid regurgitation. Eur. Heart J. 32:1207-13, 2011.

49. Lauten, A., H. R. Figulla, C. Willich, A. Laube, W. Rademacher, H. Schubert, S. Bischoff, and M. Ferrari. Percutaneous caval stent valve implantation: investigation of an interventional approach for treatment of tricuspid regurgitation. Eur. Heart J. 31:1274-81, 2010.

50. Leo, H. L., Z. He, J. T. Ellis, and A. P. Yoganathan. Microflow fields in the hinge region of the CarboMedics bileaflet mechanical heart valve design. The Journal of thoracic and cardiovascular surgery. 124:561-574, 2002.

51. Little, S. H. Is it really getting easier to assess mitral regurgitation using the proximal isovelocity surface area? J. Am. Soc. Echocardiogr. 25:824-826, 2012.

52. Matsuyama, K. , M. Matsumoto, T. Sugita, J. Nishizawa, Y. Tokuda, and T. Matsuo. Predictors of Residual Tricuspid Regurgitation After Mitral Valve Surgery. The Society of Thoracic Surgeons, 2002.

53. Matsuyama, K., M. Matsumoto, T. Sugita, J. Nishizawa, Y. Tokuda, and T. Matsuo. Predictors of residual tricuspid regurgitation after mitral valve surgery. The Annals of Thoracic Surgery. 75:1826-1828, 2003.

54. Matsuyama, K., M. Matsumoto, T. Sugita, J. Nishizawa, Y. Tokuda, T. Matsuo, and Y. Ueda. De Vega annuloplasty and Carpentier-Edwards ring annuloplasty for secondary tricuspid regurgitation. The Journal of heart valve disease. 10:520-524, 2001.

55. McCarthy, P. M., S. K. Bhudia, J. Rajeswaran, K. J. Hoercher, B. W. Lytle, D. M. Cosgrove, and E. H. Blackstone. Tricuspid valve repair: durability and risk factors for failure. The Journal of thoracic and cardiovascular surgery. 127:674-685, 2004.

56. Munro, A. I., W. R. E. Jamieson, G. Frank, O. Tyers, and E. Germann. Tricuspid valve replacement: porcine bioprostheses and mechanical prostheses. The Annals of thoracic surgery. 60:S470-S474, 1995.

57. Mutlak, D., D. Aronson, J. Lessick, S. A. Reisner, S. Dabbah, and Y. Agmon. Functional tricuspid regurgitation in patients with pulmonary hypertension: is pulmonary artery pressure the only determinant of regurgitation severity? CHEST Journal. 135:115-121, 2009.

58. Mutlak, D., J. Lessick, S. A. Reisner, D. Aronson, S. Dabbah, and Y. Agmon. Echocardiography-based spectrum of severe tricuspid regurgitation: the frequency of apparently idiopathic tricuspid regurgitation. J. Am. Soc. Echocardiogr. 20:405-408, 2007.

59. Nanthakumar, K., J. Jalife, S. Massé, E. Downar, M. Pop, J. Asta, H. Ross, V. Rao, S. Mironov, and E. Sevaptsidis. Optical mapping of Langendorff-perfused human hearts: establishing a model for the study of ventricular fibrillation in humans. American Journal of Physiology-Heart and Circulatory Physiology. 293:H875-H880, 2007.

60. Nath, J., E. Foster, and P. A. Heidenreich. Impact of tricuspid regurgitation on long-term survival. J. Am. Coll. Cardiol. 43:405-9, 2004.

61. Navia, J. L., E. R. Nowicki, E. H. Blackstone, N. A. Brozzi, D. E. Nento, F. A. Atik, J. Rajeswaran, A. M. Gillinov, L. G. Svensson, and B. W. Lytle. Surgical management of secondary tricuspid valve regurgitation: annulus, commissure, or leaflet procedure? The Journal of Thoracic and Cardiovascular Surgery. 139:1473-1482. e5, 2010.

62. Oh, J. K., C. P. Appleton, L. K. Hatle, R. A. Nishimura, J. B. Seward, and A. J. Tajik. The noninvasive assessment of left ventricular diastolic function with two-dimensional and Doppler echocardiography. J. Am. Soc. Echocardiogr. 10:246-270, 1997.

63. Onoda, K., F. Yasuda, M. Takao, T. Shimono, K. Tanaka, H. Shimpo, and I. Yada. Long-term follow-up after Carpentier-Edwards ring annuloplasty for tricuspid regurgitation. The Annals of thoracic surgery. 70:796-799, 2000.

64. Otto, C. M., W. H. Gaasch, and S. B. Yeon, *Management and prognosis of tricuspid regurgitation*. 2014.

65. Raine-Fenning, N. J., N. M. Nordin, K. V. Ramnarine, B. K. Campbell, J. S. Clewes, A. Perkins, and I. R. Johnson. Evaluation of the effect of machine settings on quantitative

three-dimensional power Doppler angiography: an in-vitro flow phantom experiment. Ultrasound Obstet. Gynecol. 32:551-559, 2008.

66. Ratnatunga, C. P., M.-B. Edwards, C. J. Dore, and K. M. Taylor. Tricuspid valve replacement: UK Heart Valve Registry mid-term results comparing mechanical and biological prostheses. The Annals of thoracic surgery. 66:1940-1947, 1998.

67. Rizzoli, G., L. De Perini, T. Bottio, G. Minutolo, G. Thiene, and D. Casarotto. Prosthetic replacement of the tricuspid valve: biological or mechanical? The Annals of thoracic surgery. 66:S62-S67, 1998.

68. Rizzoli, G., I. Vendramin, G. Nesseris, T. Bottio, C. Guglielmi, and L. Schiavon. Biological or mechanical prostheses in tricuspid position? A meta-analysis of intra-institutional results. The Annals of thoracic surgery. 77:1607-1614, 2004.

69. Sadeghi, H. M., B. J. Kimura, A. Raisinghani, D. G. Blanchard, E. Mahmud, P. F. Fedullo, S. W. Jamieson, and A. N. DeMaria. Does lowering pulmonary arterial pressure eliminate severe functional tricuspid regurgitation?: Insights from pulmonary thromboendarterectomy. J. Am. Coll. Cardiol. 44:126-132, 2004.

70. Sallam, A. M. and N. H. Hwang. Human red blood cell hemolysis in a turbulent shear flow: contribution of Reynolds shear stresses. Biorheology. 21:783-797, 1983.

71. Samstad, SO, HG Torp, David T Linker, O Rossvoll, T Skjaerpe, E Johansen, K Kristoffersen, BA Angelsen, and L Hatle. Cross sectional early mitral flow velocity profiles from colour Doppler. Br. Heart J. 62:177-184, 1989.

72. Sarnoff, S. J., E. Braunwald, G. H. Welch, R. B. Case, W. N. Stainsby, and R. Macruz. Hemodynamic determinants of oxygen consumption of the heart with special reference to the tension-time index. American Journal of Physiology--Legacy Content. 192:148-156, 1957.

73. Schnabel, R., A. V. Khaw, R. S. Von Bardeleben, C. Strasser, T. Kramm, J. Meyer, and S. Mohr-Kahaly. Assessment of the tricuspid valve morphology by transthoracic real-time-3D-echocardiography. Echocardiography. 22:15-23, 2005.

74. Schofer, J., K. Bijuklic, C. Tiburtius, L. Hansen, A. Groothuis, and R. T. Hahn. First-in-human transcatheter tricuspid valve repair in a patient with severely regurgitant tricuspid valve. J. Am. Coll. Cardiol. 65:1190-1195, 2015.

75. Siminiak, T., R. Dankowski, A. Baszko, C. Lee, L. Firek, P. Kalmucki, A. Szyszka, and A. Groothuis. Percutaneous direct mitral annuloplasty using the Mitralign Bident system: description of the method and a case report. Kardiol. Pol. 71:1287-92, 2013.

76. Tan, S. G.-D., S. Kim, J. K. F. Hon, and H. L. Leo. A D-Shaped Bileaflet Bioprosthesis which Replicates Physiological Left Ventricular Flow Patterns. PLoS One. 11:e0156580, 2016.

77. Tang, G. H.-L., T. E. David, S. K. Singh, M. D. Maganti, S. Armstrong, and M. A. Borger. Tricuspid valve repair with an annuloplasty ring results in improved long-term outcomes. Circulation. 114:I-577-I-581, 2006.

78. Taramasso, M., A. Pozzoli, A. Guidotti, F. Nietlispach, D. T. Inderbitzin, S. Benussi, O. Alfieri, and F. Maisano. Percutaneous tricuspid valve therapies: the new frontier. Eur. Heart J., 2016.

79. Taramasso, M., H. Vanermen, F. Maisano, A. Guidotti, G. La Canna, and O. Alfieri. The growing clinical importance of secondary tricuspid regurgitation. J. Am. Coll. Cardiol. 59:703-10, 2012.

80. Ton-Nu, T. T., R. A. Levine, M. D. Handschumacher, D. J. Dorer, C. Yosefy, D. Fan, L. Hua, L. Jiang, and J. Hung. Geometric determinants of functional tricuspid regurgitation: insights from 3-dimensional echocardiography. Circulation. 114:143-9, 2006.

81. Topilsky, Y., C. Tribouilloy, H. I. Michelena, S. Pislaru, D. W. Mahoney, and M. Enriquez-Sarano. Pathophysiology of Tricuspid Regurgitation Quantitative Doppler Echocardiographic Assessment of Respiratory Dependence. Circulation. 122:1505-1513, 2010.

82. Tribouilloy, C. M., M. Enriquez-Sarano, K. R. Bailey, A. J. Tajik, and J. B. Seward. Quantification of tricuspid regurgitation by measuring the width of the vena contracta with Doppler color flow imaging: a clinical study. J. Am. Coll. Cardiol. 36:472-478, 2000.

83. Webb, J. G., J. Harnek, B. I. Munt, P. O. Kimblad, M. Chandavimol, C. R. Thompson, J. R. Mayo, and J. O. Solem. Percutaneous transvenous mitral annuloplasty initial human experience with device implantation in the coronary sinus. Circulation. 113:851-855, 2006.

84. Yoganathan, A. P. Cardiac valve prostheses. The Biomedical Engineering Handbook. 1, 1995.

85. Yoganathan, A. P., Z. He, and S. Casey Jones. Fluid mechanics of heart valves. Annu Rev Biomed Eng. 6:331-62, 2004.

86. Yong Kim, W., T. Bisgaard, S. T. Nielsen, J. K. Poulsen, E. M. Pendersen, M. Hasenkam, and A. P. Yoganathan. Two-Dimensional Mitral Flow Velocity Profiles in Pig Models Using Epicardial Doppler Echocardiography. JACC. 24, 1994.

APPENDIX A: MATLAB CODE

```
function Master_Post_Processing
```

```
% This function will plot the data extacted from the pressure catheter and
% the flow meter. The function will plot the 4 cycles and determine the
% maximum pressure of the average of the 4 peaks and the flow rate.
%
% Author: Karthic
% Institution: National University of Singapore
% ------------------------------------------------------------------------
clear all;
clc;
```

Cardiac Output

Regurgitation flow in the PA (IVC Run), the time step is 0.01s and the vertical axis is in litres per min

Divide by 60 to change it to litres per second rather than per min

```
% Data
% Regurgitant
%Cardiac_Output_IVC_run = xlsread('Regurgitant_Data.xlsx','B2:B401')/60;
Cardiac_Output_IVC_run = xlsread('Regurgitant_Data_2.xlsx','B2:B402')/60;
%Cardiac_Output_IVC_time = xlsread('Regurgitant_Data.xlsx','A2:A401');
Cardiac_Output_IVC_time = xlsread('Regurgitant_Data_2.xlsx','A2:A402');

% Ventricularized
Cardiac_Output_V_IVC_run = xlsread('Ventricularization_1.xlsx','B2:B406')/60;
%Cardiac_Output_V_IVC_run = xlsread('Ventricularization_2.xlsx','B2:B406')/60;
Cardiac_Output_V_IVC_time = xlsread('Ventricularization_1.xlsx','A2:A406');
%Cardiac_Output_V_IVC_time = xlsread('Ventricularization_2.xlsx','A2:A406');

x_CO_IVC = length(Cardiac_Output_IVC_time);
Cardiac_Output_IVC_time = (1:x_CO_IVC) * 0.01;

x_CO_V_IVC = length(Cardiac_Output_V_IVC_time);
Cardiac_Output_V_IVC_time = (1:x_CO_V_IVC) * 0.01;

% Plot for the Regurgitation CO in IVC run
% figure(1);

[curveIVC, goodness, output] = fit(Cardiac_Output_IVC_time',...
```

```
    Cardiac_Output_IVC_run,'Smoothingspline');

% subplot(2,1,1)
% plot(curveIVC,Cardiac_Output_IVC_time,Cardiac_Output_IVC_run);
% title('\fontsize{16} Regurgitant Cardiac Output_1 Flow Waveform',...
% 'fontweight','bold','fontname','Monotype Corsiva');
% xlabel('\fontsize{10} Seconds [s]','fontweight','bold');
% ylabel('\fontsize{10} Litres per second [L/s]','fontweight','bold');
% legend('Data points','CO','location','best');

% subplot(2,1,2)
int_IVC_run = integrate(curveIVC,Cardiac_Output_IVC_time,0);
CO_flowrate_IVC = int_IVC_run(end)*(60/Cardiac_Output_IVC_time(end));
% plot(Cardiac_Output_IVC_time,int_IVC_run);
% title('\fontsize{16} Integral of Regurgitant Cardiac Output over 4 seconds',...
% 'fontweight','bold','fontname','Monotype Corsiva');
% xlabel('\fontsize{10} Seconds [s]','fontweight','bold');
% ylabel('\fontsize{10} Litres per min [L/s]','fontweight','bold');
% text(2,0,['Cardiac Output per min = ',num2str(CO_flowrate_IVC), ' L/min']);


% Regurgitation flow in the PA (SVC Run) , the time step is 0.01s and the vertical
% axis is in litres per min
% Divided by 60 to convert the units to litres per second

% Data
% Regurgitation
%Cardiac_Output_SVC_run = xlsread('Regurgitant_Data.xlsx','H2:H408')/60;
Cardiac_Output_SVC_run = xlsread('Regurgitant_Data_2.xlsx','H2:H405')/60;
%Cardiac_Output_SVC_time = xlsread('Regurgitant_Data.xlsx','G2:G408');
Cardiac_Output_SVC_time = xlsread('Regurgitant_Data_2.xlsx','G2:G405');

% Ventriculrized
Cardiac_Output_V_SVC_run = xlsread('Ventricularization_1.xlsx','H2:H398')/60;
%Cardiac_Output_V_SVC_run = xlsread('Ventricularization_2.xlsx','H2:H404')/60;
Cardiac_Output_V_SVC_time = xlsread('Ventricularization_1.xlsx','G2:G398');
%Cardiac_Output_V_SVC_time = xlsread('Ventricularization_2.xlsx','G2:G404');

x_CO_SVC = length(Cardiac_Output_SVC_time);
Cardiac_Output_SVC_time = (1:x_CO_SVC) * 0.01;

x_CO_V_SVC = length(Cardiac_Output_V_SVC_time);
Cardiac_Output_V_SVC_time = (1:x_CO_V_SVC) * 0.01;

% Plot for the Regurgitation CO in the SVC run
% figure(2);

[curveSVC, goodness, output] = fit(Cardiac_Output_SVC_time',...
    Cardiac_Output_SVC_run,'Smoothingspline');

% subplot(2,1,1)
% plot(curveSVC,Cardiac_Output_SVC_time,Cardiac_Output_SVC_run);
% title('\fontsize{16} Regurgitant Cardiac Output_2 Flow Waveform',...
```

```
% 'fontweight','bold','fontname','Monotype Corsiva');
% xlabel('\fontsize{10} Seconds [s]','fontweight','bold');
% ylabel('\fontsize{10} Litres per second [L/s]','fontweight','bold');
% legend('Data points','CO','location','best');

% subplot(2,1,2)
int_SVC_run = integrate(curveSVC,Cardiac_Output_SVC_time,0);
CO_flowrate_SVC = int_SVC_run(end)*(60/Cardiac_Output_SVC_time(end));
% plot(Cardiac_Output_SVC_time, int_SVC_run);
% title('\fontsize{16} Integral of Regurgitant Cardiac Output over ~4 seconds',...
% 'fontweight','bold','fontname','Monotype Corsiva');
% xlabel('\fontsize{10} Seconds [s]','fontweight','bold');
% ylabel('\fontsize{10} Litres per min [L/s]','fontweight','bold');
% text(2,0,['Cardiac Output per min = ',num2str(CO_flowrate_SVC),' L/min']);


% Plotting the Flow for the Reurgitation both in the IVC and SVC in both
% cases of ventricularization and regurgitation

% Ventricularization plotting details
[curve_V_IVC, goodness, output] = fit(Cardiac_Output_V_IVC_time',...
    Cardiac_Output_V_IVC_run,'Smoothingspline');
int_V_IVC_run = integrate(curve_V_IVC,Cardiac_Output_V_IVC_time,0);
CO_flowrate_V_IVC = int_V_IVC_run(end)*(60/Cardiac_Output_V_IVC_time(end));

[curve_V_SVC, goodness, output] = fit(Cardiac_Output_V_SVC_time',...
    Cardiac_Output_V_SVC_run,'Smoothingspline');
int_V_SVC_run = integrate(curve_V_SVC,Cardiac_Output_V_SVC_time,0);
CO_flowrate_V_SVC = int_V_SVC_run(end)*(60/Cardiac_Output_V_SVC_time(end));

% Comparative analysis between Regurgitation and Ventricularization
Average_regurgitant_flow = (CO_flowrate_IVC + CO_flowrate_SVC)/2;
Average_ventricularization_flow = (CO_flowrate_V_SVC+CO_flowrate_V_IVC)/2;

figure(1)
% Regurgitation; red is used to represent the dieseased state
subplot(2,1,1)
[curveIVC, goodness, output] = fit(Cardiac_Output_IVC_time',...
    Cardiac_Output_IVC_run,'Smoothingspline');

plot(curveIVC,'r',Cardiac_Output_IVC_time,Cardiac_Output_IVC_run,'k.');
title(...
'\fontsize{16} Cardiac Flow Output Waveforms: Regurgitant Vs Ventricularized',...
'fontname','Times New Roman');
hold on;
[curveSVC, goodness, output] = fit(Cardiac_Output_SVC_time',...
    Cardiac_Output_SVC_run,'Smoothingspline');

plot(curveSVC,'r',Cardiac_Output_SVC_time,Cardiac_Output_SVC_run,'k.');
% Ventricularization; blue is used to represent the corrected state
plot(curve_V_IVC,'b',Cardiac_Output_V_IVC_time,Cardiac_Output_V_IVC_run,'k.');
plot(curve_V_SVC,'b',Cardiac_Output_V_SVC_time,Cardiac_Output_V_SVC_run,'k.');
legend('Data points for Regurgitant State',...
```

```
    'CO for 1st Regurgitant State','Data points for Regurgitant State',...
'CO for 2nd Regurgitant State','Data points for Ventricularized State',...
'CO for 1st Ventricularised State','Date points for Ventricularized State',...
'CO for 2nd Ventricularized State','location','northeast');
xlabel('\fontsize{14} Seconds [s]','fontname','Times New Roman');
ylabel('\fontsize{14} Litres per min [L/min]','fontname','Times New Roman');
hold off;


subplot(2,1,2)
plot(Cardiac_Output_IVC_time,int_IVC_run,'r');
title(...
'\fontsize{16} Integral of Cardiac Flow Output: Regurgitant vs Ventricularized',...
    'fontname','Times New Roman');
hold on;
plot(Cardiac_Output_SVC_time, int_SVC_run,'r');
plot(Cardiac_Output_V_IVC_time, int_V_IVC_run,'b');
plot(Cardiac_Output_V_SVC_time, int_V_SVC_run,'b');
xlabel('\fontsize{14} Seconds [s]','fontname','Times New Roman');
ylabel('\fontsize{14} Litres per min [L/s]','fontname','Times New Roman');
text(1.65,0,['\fontsize{12} Average Cardiac Output during Regurgitation per min = ',...
    num2str(Average_regurgitant_flow),' L/min']);
text(2.5,0.0725,[...
    '\fontsize{12} Average Cardiac Output after Ventricularization per min = ',...
    num2str(Average_ventricularization_flow),' L/min']);
hold off;
```

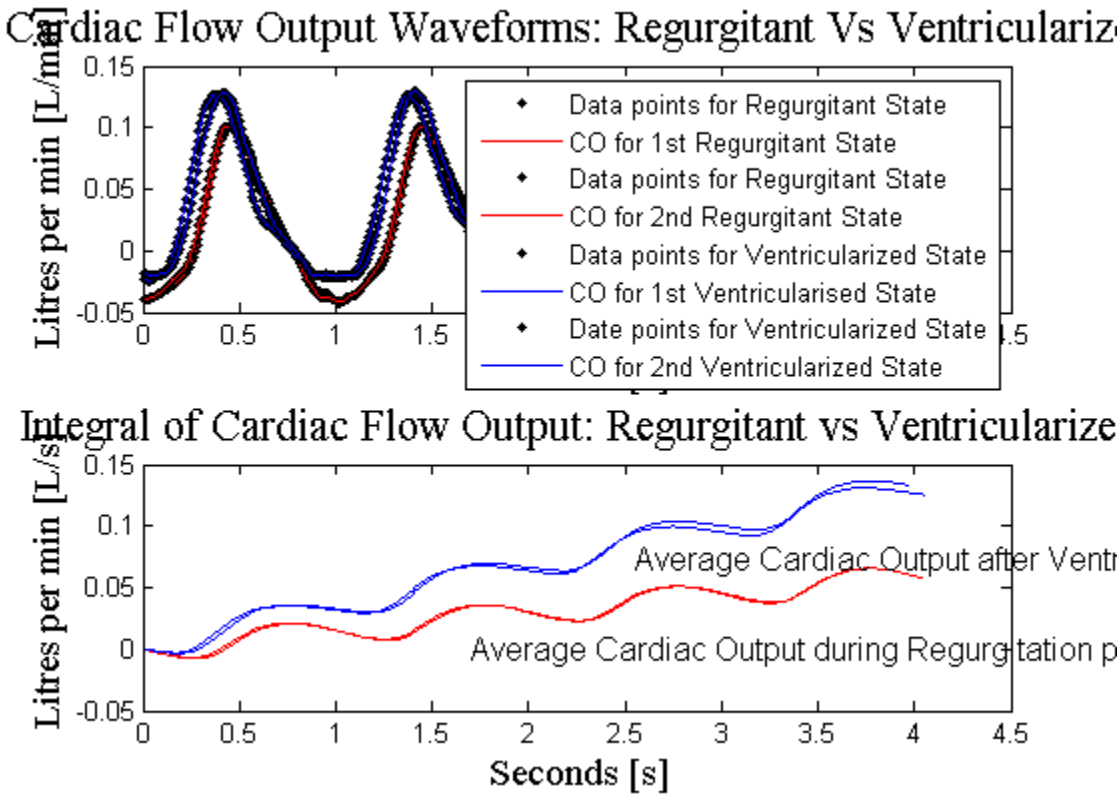

Pressure Waveform

Pressure for the IVC

```
%IVC_Pressure = xlsread('Regurgitant_Data.xlsx','E2:E406');
IVC_Pressure = xlsread('Regurgitant_Data_2.xlsx','E2:E404');
%V_IVC_Pressure = xlsread('Ventricularization_1','E2:E401');
V_IVC_Pressure = xlsread('Ventricularization_2','E2:E403');

xpivc = length(IVC_Pressure);
time_ivc = (1:xpivc)*0.01;

Vxpivc = length(V_IVC_Pressure);
time_V_ivc = (1:Vxpivc)*0.01;

% Plot of pressure in the IVC
% figure(4);
% plot(time_ivc,IVC_Pressure);
% title('\fontsize{16} Regurgitant Pressure Profile in IVC','fontweight',...
%     'bold','fontname','Monotype Corsiva');
% xlabel('\fontsize{10} Seconds [s]','fontweight','bold');
% ylabel('\fontsize{10} Pressure [mmHg]','fontweight','bold');
%
% index_P_IVC_min = find(min(IVC_Pressure) == IVC_Pressure);
% time_min = time_ivc(index_P_IVC_min);
% P_IVC_min = IVC_Pressure(index_P_IVC_min);
%
% index_P_IVC_max = find(max(IVC_Pressure) == IVC_Pressure);
% time_max = time_ivc(index_P_IVC_max);
% P_IVC_max = IVC_Pressure(index_P_IVC_max);
%
% strminivc = ['Minimum = ',num2str(P_IVC_min)];
% text(time_min,P_IVC_min,strminivc,'HorizontalAlignment','left');
%
% strmaxivc = ['Maximum = ',num2str(P_IVC_max)];
% text(time_max,P_IVC_max,strmaxivc,'HorizontalAlignment','right');


% Pressure for SVC
%SVC_Pressure = xlsread('Regurgitant_Data.xlsx','K2:K405');
SVC_Pressure = xlsread('Regurgitant_Data_2.xlsx','K2:K403');
%V_SVC_Pressure = xlsread('Ventricularization_1','K2:K401');
V_SVC_Pressure = xlsread('Ventricularization_2','K2:K401');

xpsvc = length(SVC_Pressure);
time_svc = (1:xpsvc)*0.01;

Vxpsvc = length(V_SVC_Pressure);
time_V_svc = (1:Vxpsvc)*0.01;

% Plot of pressure in the SVC
```

```
% figure(5);
% plot(time_svc,SVC_Pressure);
% title('\fontsize{16} Regurgitant Pressure Profile in SVC','fontweight',...
%     'bold','fontname','Monotype Corsiva');
% xlabel('\fontsize{10} Seconds [s]','fontweight','bold');
% ylabel('\fontsize{10} Pressure [mmHg]','fontweight','bold');
%
% index_P_SVC_min = find(min(SVC_Pressure) == SVC_Pressure);
% time_min = time_svc(index_P_SVC_min);
% P_SVC_min = SVC_Pressure(index_P_SVC_min);
%
% index_P_SVC_max = find(max(SVC_Pressure) == SVC_Pressure);
% time_max = time_svc(index_P_SVC_max);
% P_SVC_max = SVC_Pressure(index_P_SVC_max);
%
% strminsvc = ['Minimum = ',num2str(P_SVC_min)];
% text(time_min,P_SVC_min,strminsvc,'HorizontalAlignment','left');
%
% strmaxsvc = ['Maximum = ',num2str(P_SVC_max)];
% text(time_max,P_SVC_max,strmaxsvc,'HorizontalAlignment','right');


% Comparing the values of the IVC and SVC Pressure Profiles
figure(2)
plot(time_ivc,IVC_Pressure,'r',time_svc,SVC_Pressure,'r--');
title('\fontsize{16} Regurgitant vs Ventricularized Pressure Profiles',...
    'fontname','Times New Roman');

% Find Min and Max Regurgitant
index_P_IVC_min = find(min(IVC_Pressure) == IVC_Pressure);
time_min = time_ivc(index_P_IVC_min);
P_IVC_min = IVC_Pressure(index_P_IVC_min);

index_P_IVC_max = find(max(IVC_Pressure) == IVC_Pressure);
time_max = time_ivc(index_P_IVC_max);
P_IVC_max = IVC_Pressure(index_P_IVC_max);

index_P_SVC_min = find(min(SVC_Pressure) == SVC_Pressure);
time_min = time_svc(index_P_SVC_min);
P_SVC_min = SVC_Pressure(index_P_SVC_min);

index_P_SVC_max = find(max(SVC_Pressure) == SVC_Pressure);
time_max = time_svc(index_P_SVC_max);
P_SVC_max = SVC_Pressure(index_P_SVC_max);

% Find Min and Max Ventricularization
index_P_V_IVC_min = find(min(V_IVC_Pressure) == V_IVC_Pressure);
V_time_min = time_V_ivc(index_P_V_IVC_min);
P_V_IVC_min = V_IVC_Pressure(index_P_V_IVC_min);

index_P_V_IVC_max = find(max(V_IVC_Pressure) == V_IVC_Pressure);
V_time_max = time_V_ivc(index_P_V_IVC_max);
P_V_IVC_max = V_IVC_Pressure(index_P_V_IVC_max);
```

```
index_P_V_SVC_min = find(min(V_SVC_Pressure) == V_SVC_Pressure);
V_time_min = time_V_svc(index_P_V_SVC_min);
P_V_SVC_min = V_SVC_Pressure(index_P_V_SVC_min);

index_P_V_SVC_max = find(max(V_SVC_Pressure) == V_SVC_Pressure);
V_time_max = time_V_svc(index_P_V_SVC_max);
P_V_SVC_max = V_SVC_Pressure(index_P_V_SVC_max);

% Plotting the texts for Regurgitation
strminivc = ['\fontsize{12}Min = ',num2str(P_IVC_min)];
text(2.45,P_IVC_min,strminivc,'HorizontalAlignment','right');
%text(time_min,P_IVC_min,strminivc,'HorizontalAlignment','left');

strmaxivc = ['\fontsize{12}Max = ',num2str(P_IVC_max)];
text(4.0,P_IVC_max,strmaxivc,'HorizontalAlignment','right');
%text(time_max,P_IVC_max,strmaxivc,'HorizontalAlignment','right');

strminsvc = ['\fontsize{12}Min = ',num2str(P_SVC_min)];
text(2.45,P_SVC_min,strminsvc,'HorizontalAlignment','right');
%text(time_min,P_SVC_min,strminsvc,'HorizontalAlignment','left');

strmaxsvc = ['\fontsize{12}Max = ',num2str(P_SVC_max)];
text(4.0,P_SVC_max,strmaxsvc,'HorizontalAlignment','right');
%text(time_max,P_SVC_max,strmaxsvc,'HorizontalAlignment','right');

hold on;
plot(time_V_ivc,V_IVC_Pressure,'b',time_V_svc,V_SVC_Pressure,'b--');

% Plotting the texts for Ventricularization
strminVivc = ['\fontsize{12}Min = ',num2str(P_V_IVC_min)];
text(3.35,P_V_IVC_min,strminVivc,'HorizontalAlignment','left');
%text(V_time_min,P_V_IVC_min,strminVivc,'HorizontalAlignment','left');

strmaxVivc = ['\fontsize{12}Max = ',num2str(P_V_IVC_max)];
text(3.55,P_V_IVC_max,strmaxVivc,'HorizontalAlignment','right');
%text(V_time_max,P_V_IVC_max,strmaxVivc,'HorizontalAlignment','right');

strminVsvc = ['\fontsize{12}Min = ',num2str(P_V_SVC_min)];
text(3.35,1.5,strminVsvc,'HorizontalAlignment','left');
%text(V_time_min,P_V_SVC_min,strminVsvc,'HorizontalAlignment','left');

strmaxVsvc = ['\fontsize{12}Max = ',num2str(P_V_SVC_max)];
text(3.55,P_V_SVC_max,strmaxVsvc,'HorizontalAlignment','right');
%text(V_time_max,P_V_SVC_max,strmaxVsvc,'HorizontalAlignment','right');

xlabel('\fontsize{14} Seconds [s]','fontname','Times New Roman');
ylabel('\fontsize{14} Pressure [mmHg]','fontname','Times New Roman');
legend('IVC Regur','SVC Regur','IVC Ventr','SVC Ventr','location','best');
hold off;
```

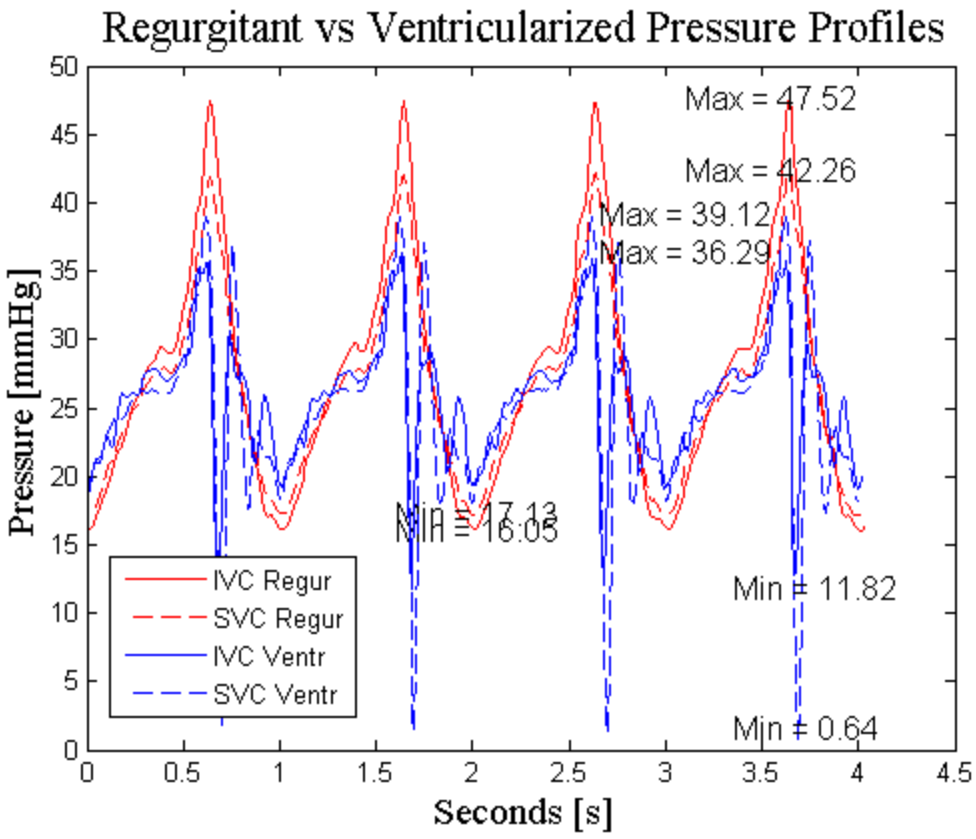

One Cycle with Echocardiographic Time ppoints

```
% x-axis
t_ivc_onecycle = (0.01:0.01:1);
t_ivc_V_onecycle = (0.01:0.01:1);

t_svc_onecycle = (0.01:0.01:1);
t_svc_V_onecycle = (0.01:0.01:1);


% y-axis
ivc = zeros(100,1);
v_ivc = zeros(100,1);
svc = zeros(100,1);
v_svc = zeros(100,1);

c = 1;
for c = 1:100
    ivc(c,1) = IVC_Pressure(c,1);
    v_ivc(c,1) = V_IVC_Pressure(c,1);
    svc(c,1) = SVC_Pressure(c,1);
    v_svc(c,1) = V_SVC_Pressure(c,1);
    c+1;
```

```
end
% Plot of one cycle of each waveform
figure (3);
plot(t_ivc_onecycle,ivc,'r',t_svc_onecycle,svc,'r--');
title('\fontsize{16} Regurgitant Pressure Profiles Over One Second',...
    'fontname','Times New Roman');
xlabel('\fontsize{14} Seconds [s]','fontname','Times New Roman');
ylabel('\fontsize{14} Pressure [mmHg]','fontname','Times New Roman');
legend('IVC Regur','SVC Regur','location','best');

figure (4);
plot(t_ivc_V_onecycle,v_ivc,'b',t_svc_V_onecycle,v_svc,'b--');
title('\fontsize{16} Ventricularized Pressure Profiles Over One Cycle',...
    'fontname','Times New Roman');
xlabel('\fontsize{14} Seconds [s]','fontname','Times New Roman');
ylabel('\fontsize{14} Pressure [mmHg]','fontname','Times New Roman');
legend('IVC Ventricularized','SVC Ventricularized','location','best');
```

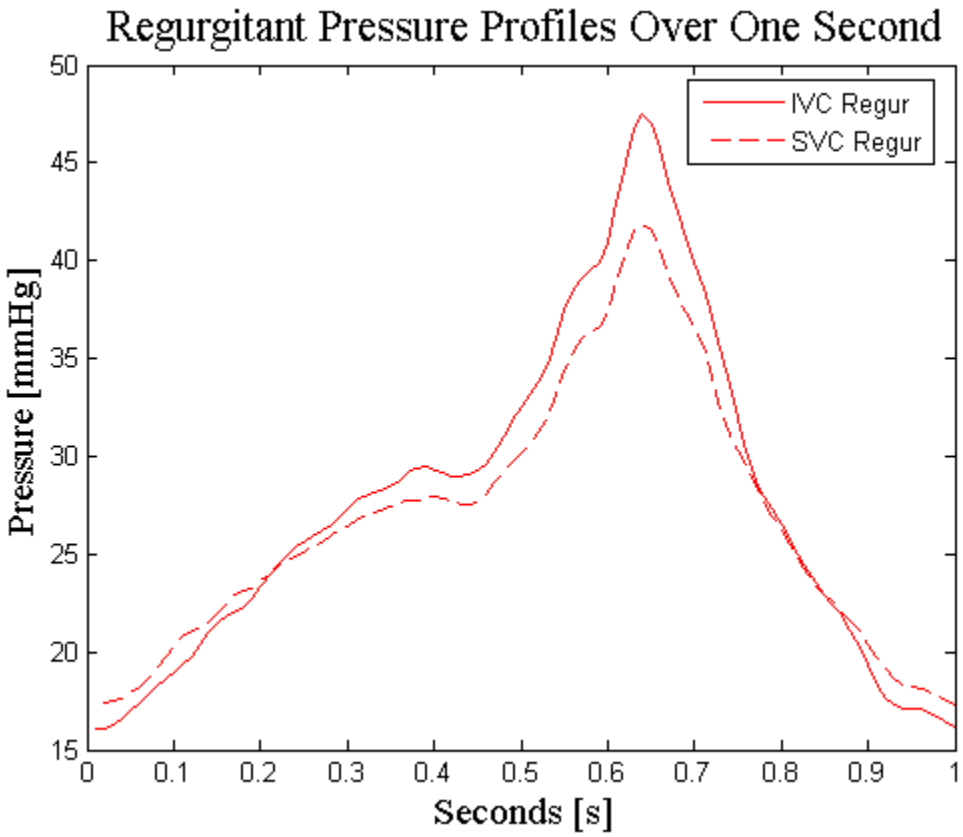

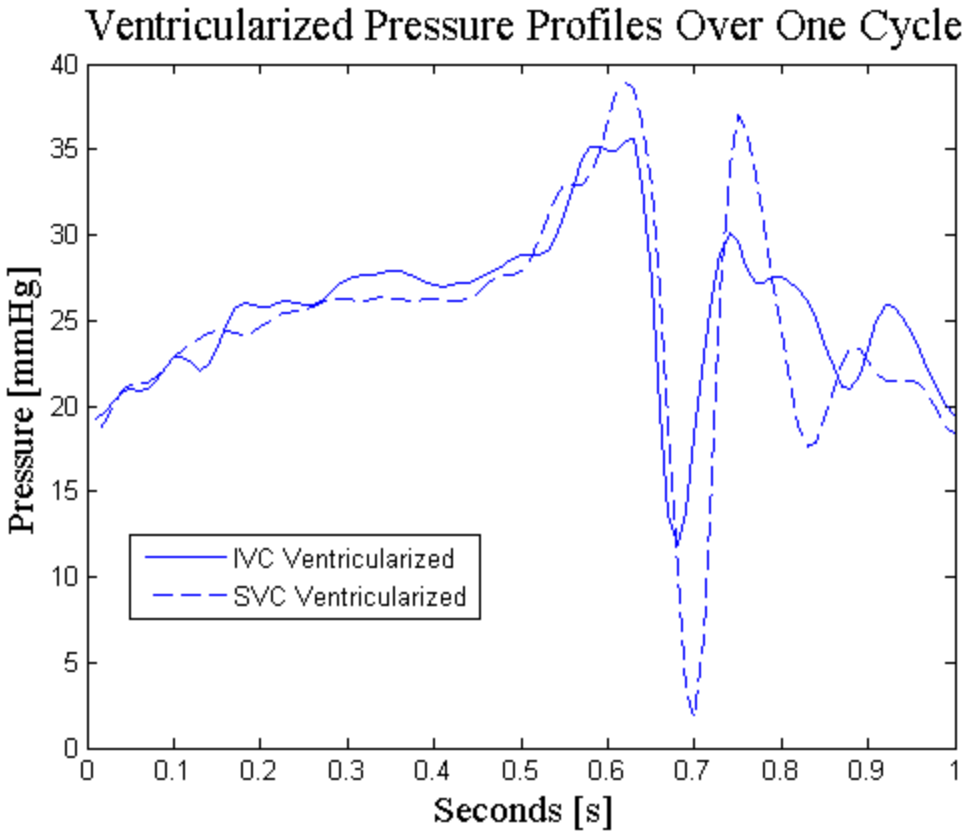

Published with MATLAB® R2013b

APPENDIX B: SOLIDWORKS DESIGN

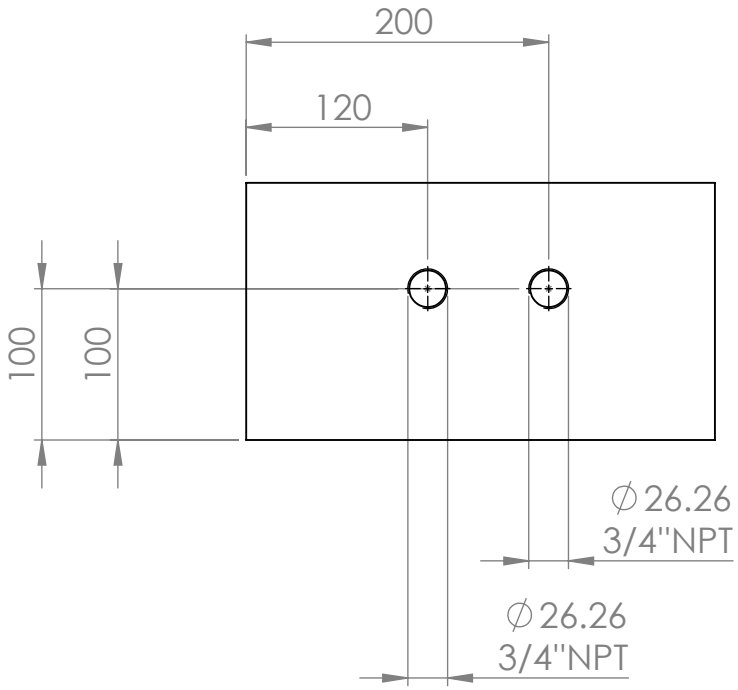

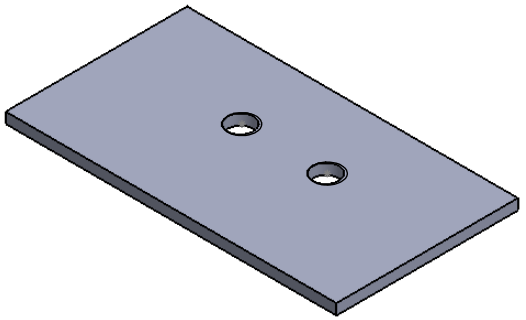

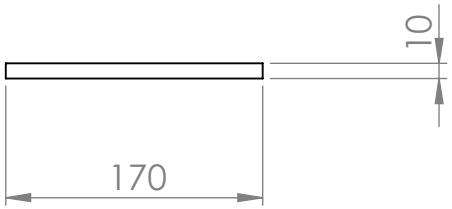

UNLESS OTHERWISE SPECIFIED: DIMENSIONS ARE IN MILLIMETERS SURFACE FINISH: TOLERANCES: LINEAR: ANGULAR:	FINISH: **Smooth**		DEBUR AND BREAK SHARP EDGES	DO NOT SCALE DRAWING	REVISION	
				National University of Singapore (NUS) - Confidential		
	NAME	SIGNATURE	DATE	TITLE: **Heart Chamber**		
DRAWN	**Karthic A**		**9/1/2015**			
CHK'D						
APPV'D						
MFG						
Q.A				MATERIAL: **Acrylic**	DWG NO. Back_Plate	A4
				WEIGHT:	SCALE:1:5	SHEET 1 OF 1

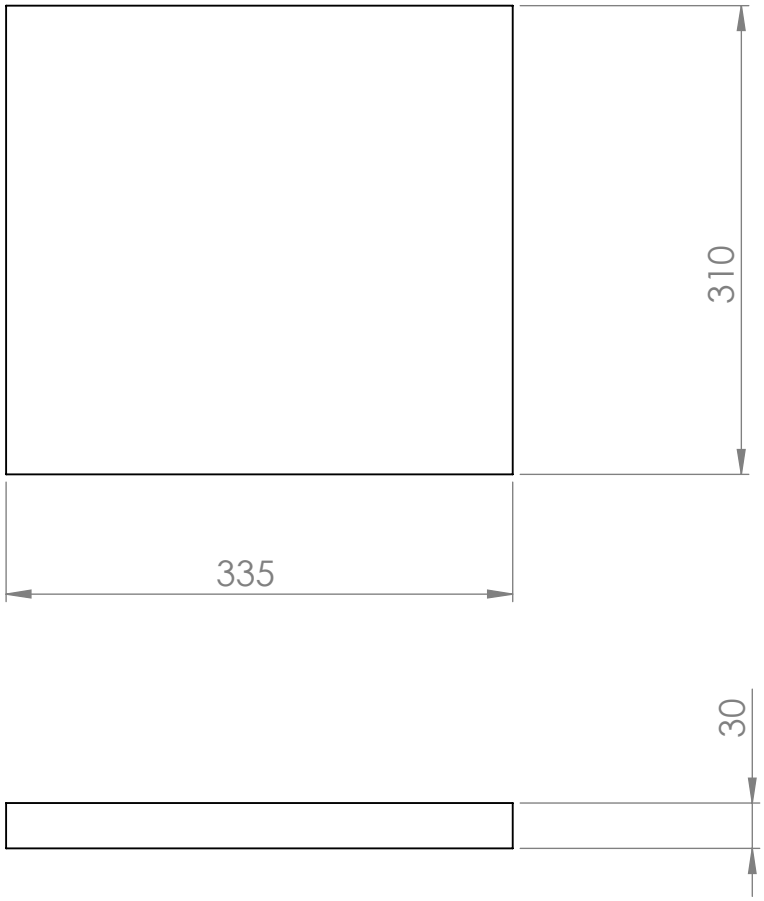

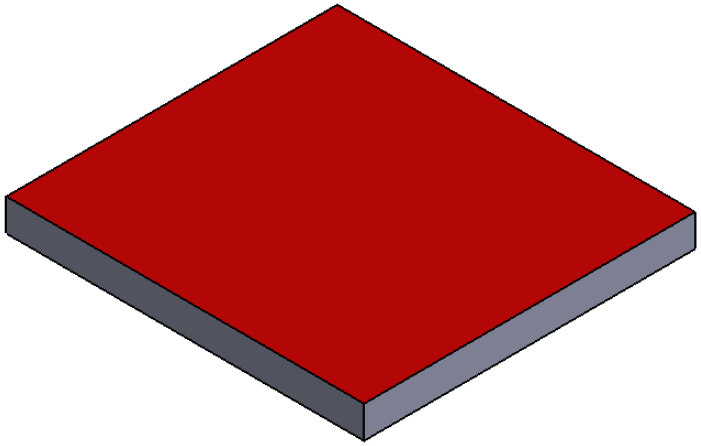

UNLESS OTHERWISE SPECIFIED: DIMENSIONS ARE IN MILLIMETERS SURFACE FINISH: TOLERANCES: LINEAR: ANGULAR:	FINISH: **Smooth**		DEBUR AND BREAK SHARP EDGES	DO NOT SCALE DRAWING	REVISION	
				National University of Singapore (NUS) - Confidential		
	NAME	SIGNATURE	DATE	TITLE: **Heart Chamber**		
DRAWN	**Karthic A**		**9/1/2015**			
CHK'D						
APPV'D						
MFG						
Q.A				MATERIAL: **Acrylic**	DWG NO. Bottom_Plate	A4
				WEIGHT:	SCALE:1:5	SHEET 1 OF 1

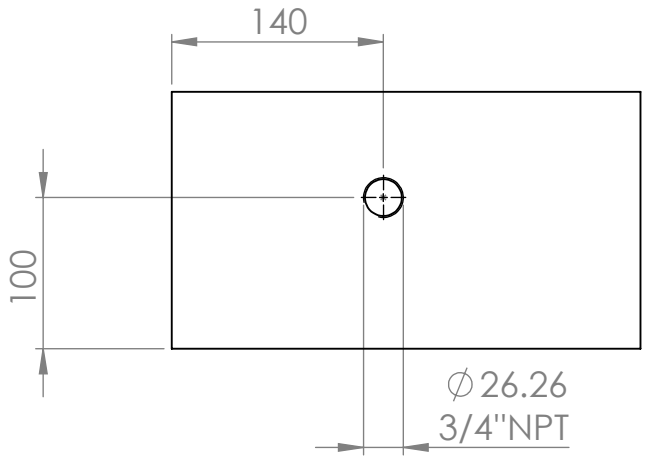

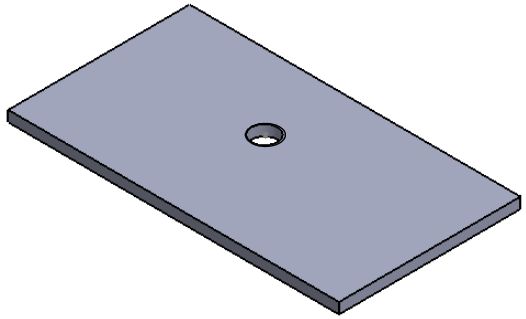

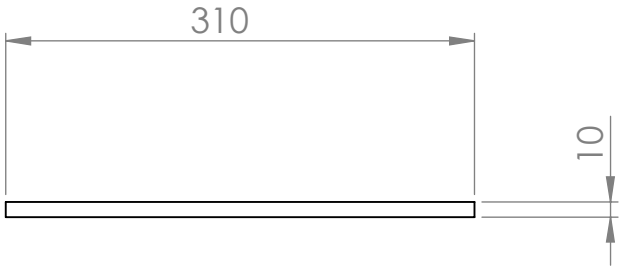

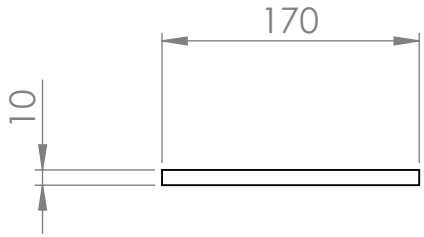

UNLESS OTHERWISE SPECIFIED: DIMENSIONS ARE IN MILLIMETERS SURFACE FINISH: TOLERANCES: LINEAR: ANGULAR:	FINISH: **Smooth**				DEBUR AND BREAK SHARP EDGES	DO NOT SCALE DRAWING / REVISION
	NAME	SIGNATURE	DATE			**National University of Singapore (NUS) - Confidential**
DRAWN	**Karthic A**		**9/1/2015**			TITLE: **Heart Chamber**
CHK'D						
APPV'D						
MFG						
Q.A				MATERIAL: **Acrylic**		DWG NO. Front_Plate / A4
				WEIGHT:		SCALE:1:5 / SHEET 1 OF 1

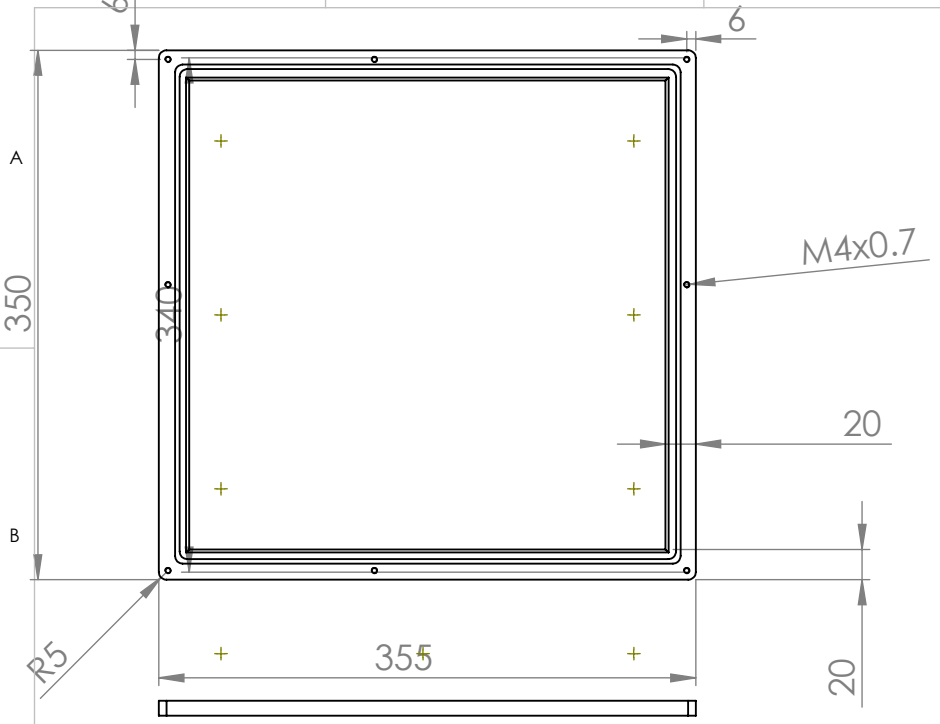

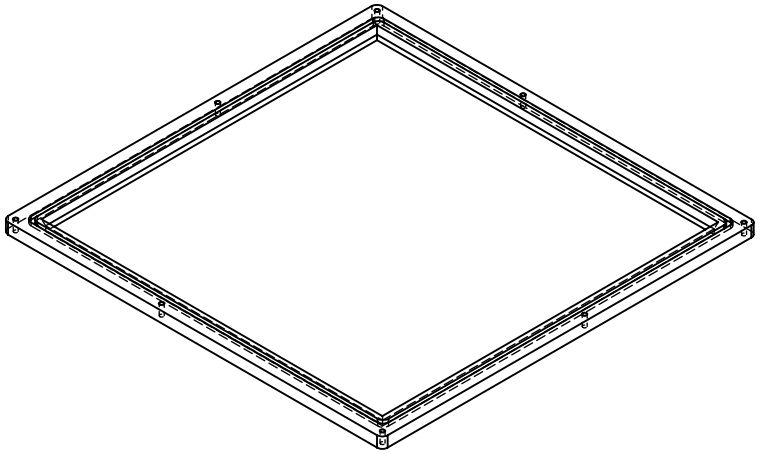

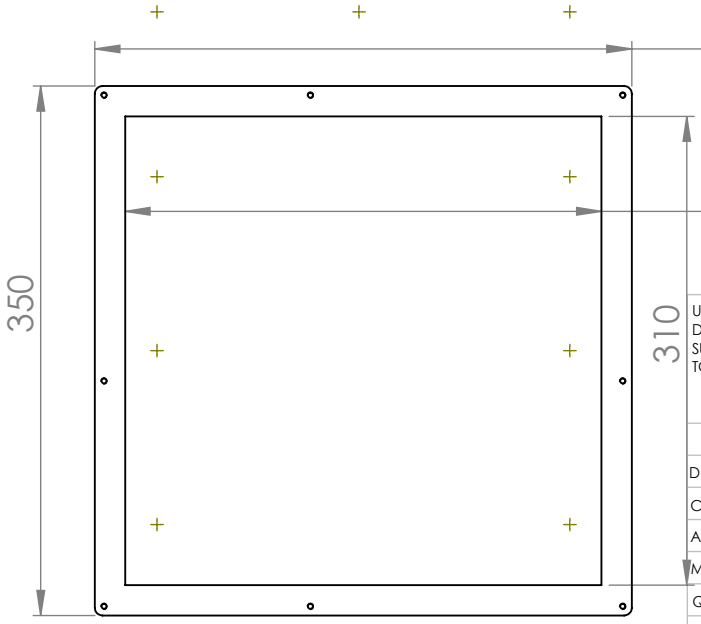

UNLESS OTHERWISE SPECIFIED: DIMENSIONS ARE IN MILLIMETERS SURFACE FINISH: TOLERANCES: LINEAR: ANGULAR:	FINISH: **Smooth**		DEBUR AND BREAK SHARP EDGES	DO NOT SCALE DRAWING	REVISION	
				National University of Singapore (NUS) - Confidential		
	NAME	SIGNATURE	DATE	TITLE: **Heart Chamber**		
DRAWN	**Karthic A**		**9/1/2015**			
CHK'D						
APPV'D						
MFG						
Q.A				MATERIAL: **Acrylic**	DWG NO. Gasket_Cover	A4
				WEIGHT:	SCALE:1:5	SHEET 1 OF 1

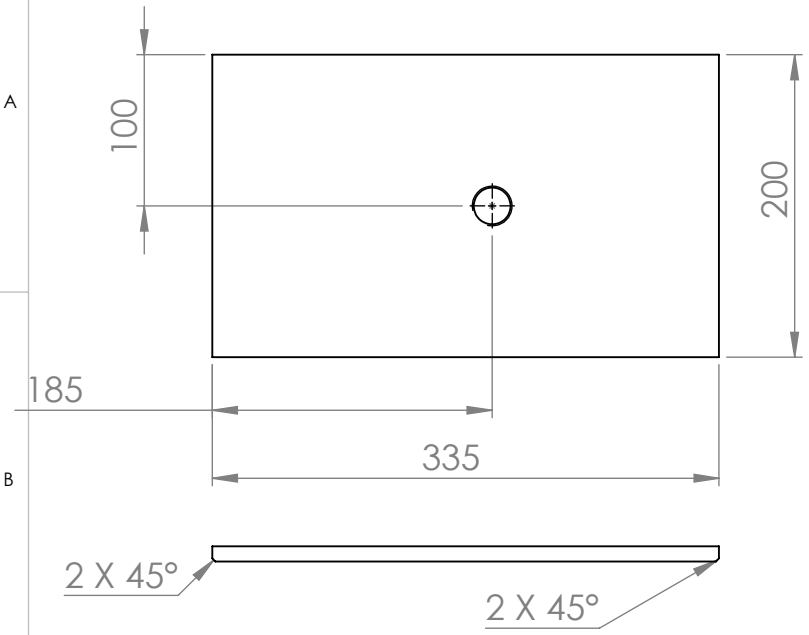

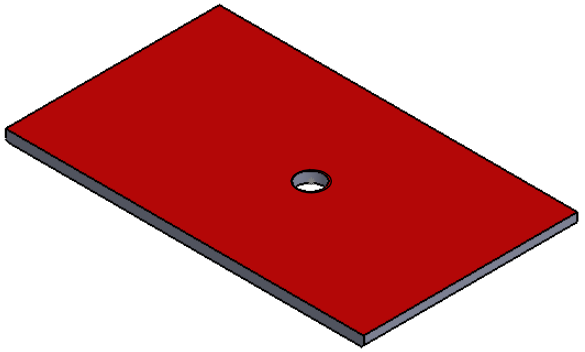

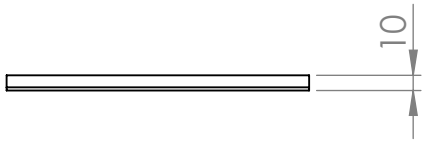

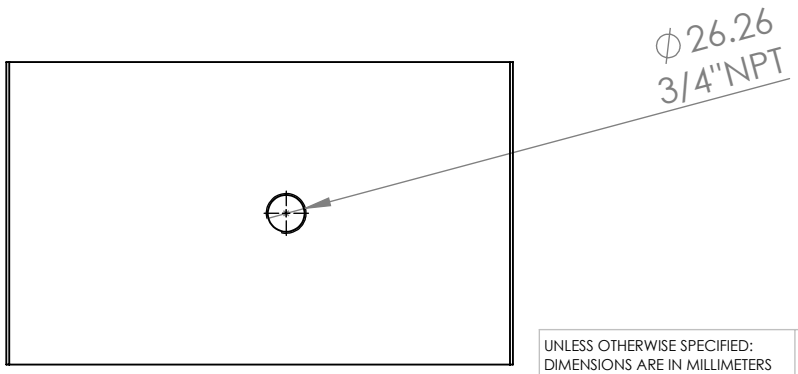

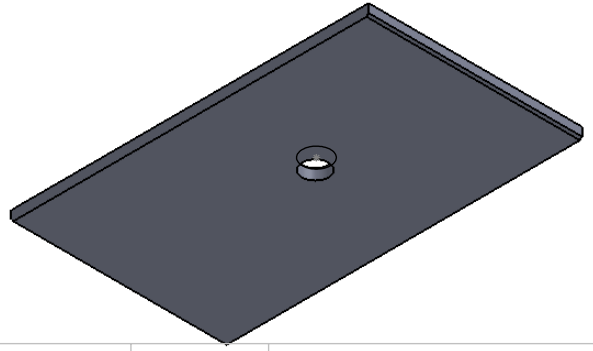

UNLESS OTHERWISE SPECIFIED: DIMENSIONS ARE IN MILLIMETERS SURFACE FINISH: TOLERANCES: LINEAR: ANGULAR:	FINISH: **Smooth**		DEBUR AND BREAK SHARP EDGES	DO NOT SCALE DRAWING	REVISION	
				National University of Singapore (NUS) - Confidential		
	NAME	SIGNATURE	DATE	TITLE: **Heart Chamber**		
DRAWN	**Karthic A**		**9/1/2015**			
CHK'D						
APPV'D						
MFG						
Q.A				MATERIAL: **Acrylic**	DWG NO. Left_Plate	A4
				WEIGHT:	SCALE:1:5	SHEET 1 OF 1

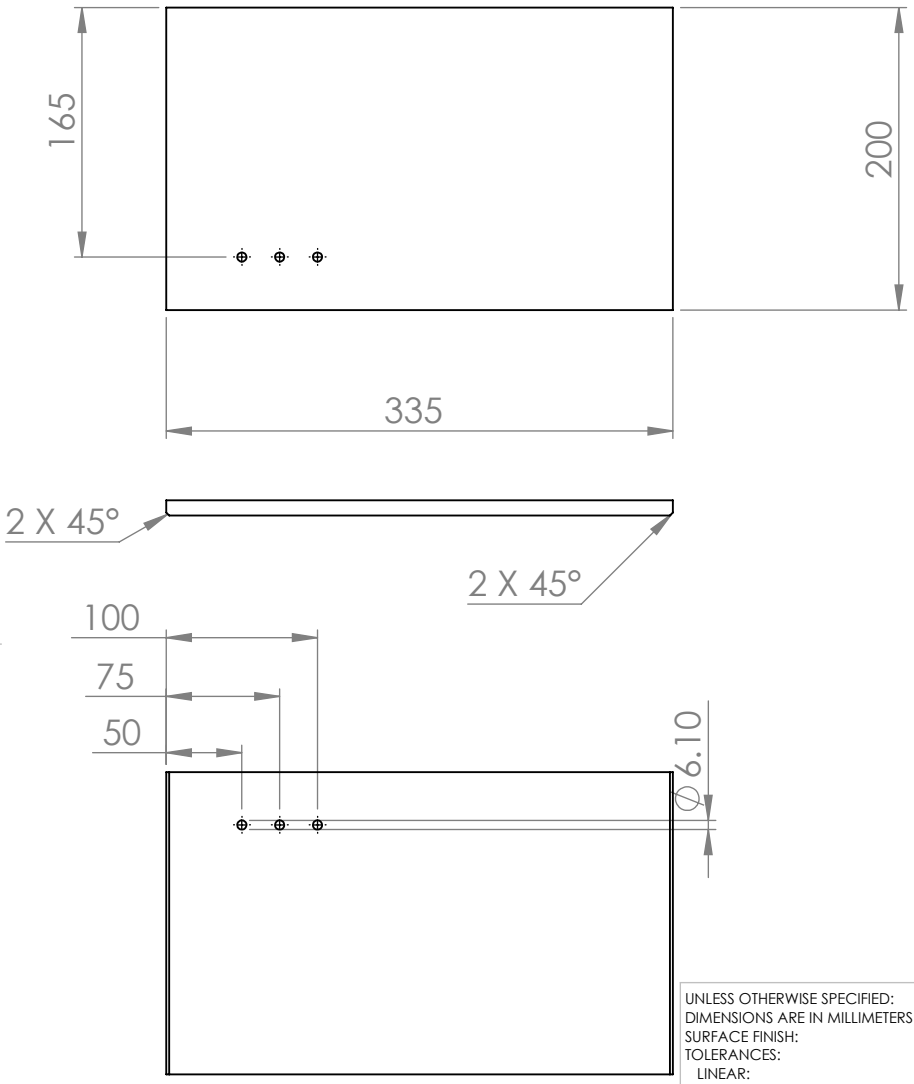

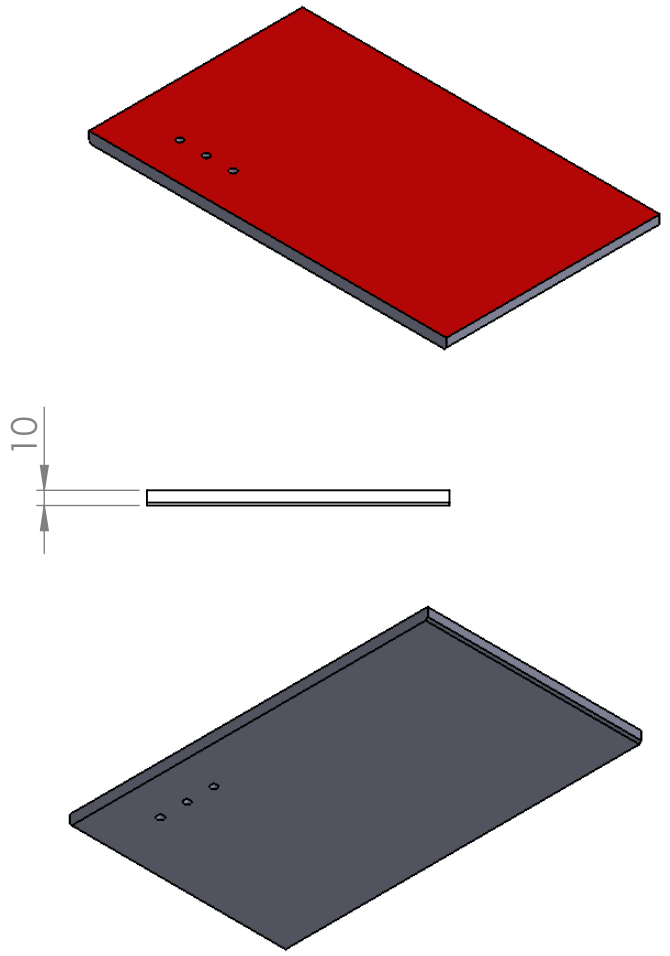

UNLESS OTHERWISE SPECIFIED: DIMENSIONS ARE IN MILLIMETERS SURFACE FINISH: TOLERANCES: LINEAR: ANGULAR:	FINISH: **Smooth**	DEBUR AND BREAK SHARP EDGES	DO NOT SCALE DRAWING	REVISION		
			National University of Singapore (NUS) - Confidential			
	NAME	SIGNATURE	DATE			
DRAWN	**Karthic A**		**9/1/2015**	TITLE: **Heart Chamber**		
CHK'D						
APPV'D						
MFG						
Q.A				MATERIAL: **Acrylic**	DWG NO. Right_Plate	A4
				WEIGHT:	SCALE:1:5	SHEET 1 OF 1

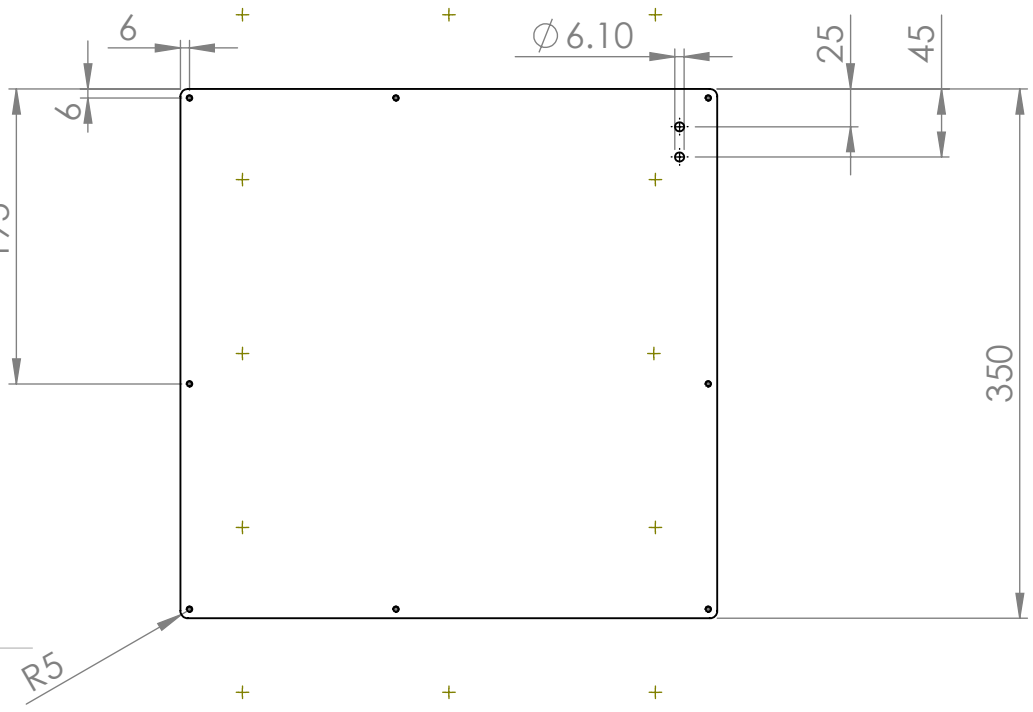

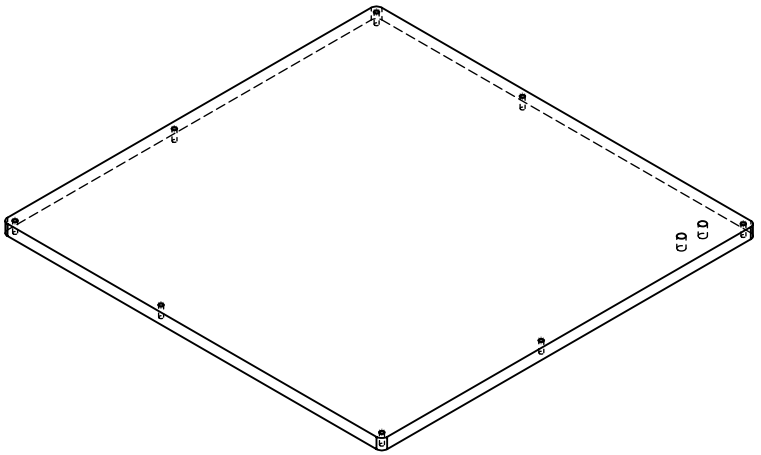

UNLESS OTHERWISE SPECIFIED: DIMENSIONS ARE IN MILLIMETERS SURFACE FINISH: TOLERANCES: LINEAR: ANGULAR:	FINISH: **Smooth**		DEBUR AND BREAK SHARP EDGES	DO NOT SCALE DRAWING	REVISION	
				National University of Singapore (NUS) - Confidential		
	NAME	SIGNATURE	DATE	TITLE: **Heart Chamber**		
DRAWN	**Karthic A**		**9/1/2015**			
CHK'D						
APPV'D						
MFG						
Q.A				MATERIAL: **Acrylic**	DWG NO. Top_Cover	A4
				WEIGHT:	SCALE:1:5	SHEET 1 OF 1

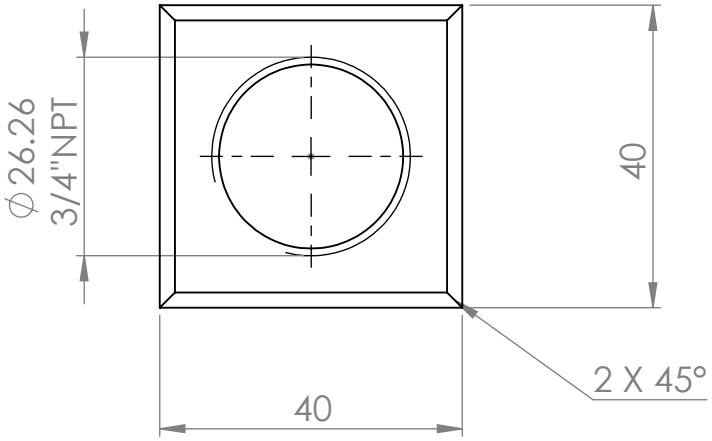

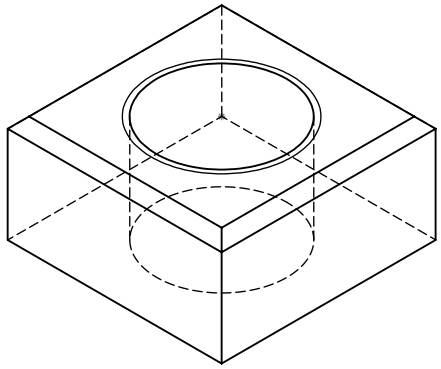

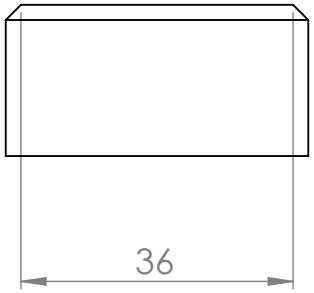

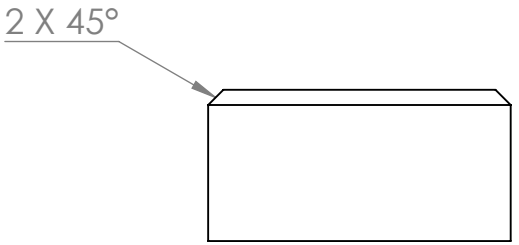

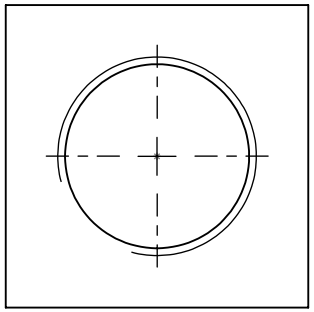

UNLESS OTHERWISE SPECIFIED: DIMENSIONS ARE IN MILLIMETERS SURFACE FINISH: TOLERANCES: LINEAR: ANGULAR:	FINISH: **Smooth**		DEBUR AND BREAK SHARP EDGES	DO NOT SCALE DRAWING	REVISION	
	NAME	SIGNATURE	DATE	**National University of Singapore (NUS) - Confidential**		
DRAWN	**Karthic A**		**9/1/2015**	TITLE: **Heart Chamber**		
CHK'D						
APPV'D						
MFG						
Q.A				MATERIAL: **Acrylic**	DWG NO. Nozzle Connector	A4
				WEIGHT:	SCALE:1:1	SHEET 1 OF 1

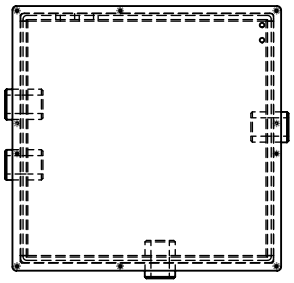

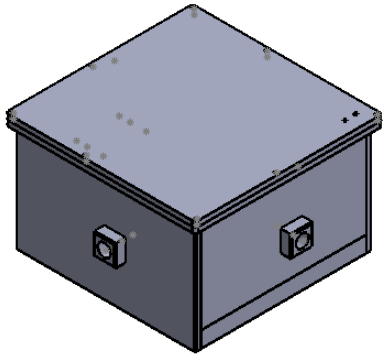

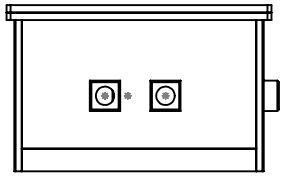

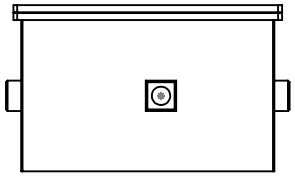

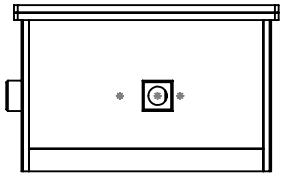

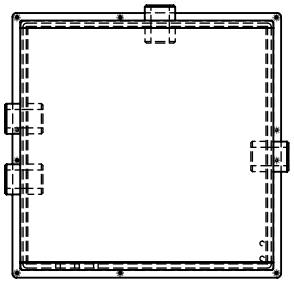

UNLESS OTHERWISE SPECIFIED: DIMENSIONS ARE IN MILLIMETERS SURFACE FINISH: TOLERANCES: LINEAR: ANGULAR:	FINISH: **Smooth**				DEBUR AND BREAK SHARP EDGES	DO NOT SCALE DRAWING / REVISION
	NAME	SIGNATURE	DATE			**National University of Singapore (NUS) - Confidential**
DRAWN	**Karthic A**		**11/16/2015**			TITLE: **Heart Chamber**
CHK'D						
APPV'D						
MFG						
Q.A				MATERIAL: **Acrylic**		DWG NO. Full_Heart_Chamber_Small / A4
				WEIGHT:		SCALE:1:10 / SHEET 1 OF 1